Pontifícia Universidade Católica
do Rio de Janeiro

Daniel Henrique Braz de Sousa

Nonlinear system identification of hybrid machine learning and physical models for mechanical systems

Tese de Doutorado

Thesis presented to the Programa de Pós–graduação em Engenharia Mecânica, do Departamento de Engenharia Mecânica da PUC-Rio in partial fulfillment of the requirements for the degree of Doutor em Engenharia Mecânica.

Advisor: Prof. Helon Vicente Hultmann Ayala

Rio de Janeiro
March 2023

Pontifícia Universidade Católica
do Rio de Janeiro

Daniel Henrique Braz de Sousa

Nonlinear system identification of hybrid machine learning and physical models for mechanical systems

Thesis presented to the Programa de Pós–graduação em Engenharia Mecânica da PUC-Rio in partial fulfillment of the requirements for the degree of Doutor em Engenharia Mecânica. Approved by the Examination Committee:

Prof. Helon Vicente Hultmann Ayala
Advisor
Departamento de Engenharia Mecânica – PUC-Rio

Prof. Marco Antônio Meggiolaro
Departamento de Engenharia Mecânica – PUC-Rio

Prof. Leandro dos Santos Coelho
PUCPR / UFPR

Prof. Gustavo Simão Rodrigues
IME

Prof. Elias Dias Rossi Lopes
IME

Rio de Janeiro, March 6th, 2023

Daniel Henrique Braz de Sousa

Holds a Master's degree in Mechanical Engineering (2017) and a Bachelor's degree in Mechanical and Weaponry Engineering (2012), both from the Military Institute of Engineering.

Bibliographic data

Sousa, Daniel Henrique Braz

Nonlinear system identification of hybrid machine learning and physical models for mechanical systems / Daniel Henrique Braz de Sousa; advisor: Helon Vicente Hultmann Ayala. – 2023.

101 f: il. color. ; 30 cm

Tese (doutorado) - Pontifícia Universidade Católica do Rio de Janeiro, Departamento de Engenharia Mecânica, 2023.

Inclui bibliografia

1. Engenharia Mecânica – Teses. 2. Identificação de Sistemas. 3. Sistemas Não-lineares. 4. Redes Neurais Artificiais. 5. Modelos Híbridos. I. Ayala, Helon V. H.. II. Pontifícia Universidade Católica do Rio de Janeiro. Departamento de Engenharia Mecânica. III. Título.

CDD: 621

To my wife Camila, who encouraged me throughout this research.

Acknowledgments

To God, for all the strength, health and inspiration to carry out this work, specially in the difficult times imposed by the global pandemic.

To my beloved wife Camila, for her company over the last 8 years and for her patience and understanding during the development of this thesis.

To my parents Helio and Elaine, and my sister Thais, whose support and love are essential throughout my life.

To my advisor Prof. Helon Ayala, for the precise and pragmatic guidance, which was crucial for the conclusion of this thesis under the conditions that I had to fulfill.

To the Brazilian Army, for the opportunity of this course and to my colleagues at the Military Institute of Engineering, for their friendship and support over these years.

To PUC-Rio and the Department of Mechanical Engineering, for all administrative and technical support.

This study was financed in part by the Coordenação de Aperfeiçoamento de Pessoal de Nível Superior - Brasil (CAPES) - Finance Code 001

Abstract

Sousa, Daniel Henrique Braz; Ayala, Helon V. H. (Advisor). **Nonlinear system identification of hybrid machine learning and physical models for mechanical systems**. Rio de Janeiro, 2023. 101p. Tese de Doutorado – Departamento de Engenharia Mecânica, Pontifícia Universidade Católica do Rio de Janeiro.

There is a growing demand for accurate dynamic models, driven by the Industry 4.0 paradigm that introduces, among others, the concept of the digital twin in which dynamic models play an important role. Ideally, a dynamic model presents a compromise between complexity and accuracy, while providing physical insight into the system. To improve a model accuracy while keeping interpretability, the usual approach is to mathematically model all the nonlinearities, which ultimately leads to an overcomplex model. Another approach involves a black-box identification, a data-driven approach where a mathematical model is adjusted to describe the system's input-output relation, which may provide an accurate model, but it does not provide interpretability. The developments in computational processing capacity have allowed the flourishing of the field of machine learning, which has shown interesting results in different fields of knowledge. One of these applications is black-box identification, where machine learning has successfully been employed in the modeling of nonlinear systems, which has inspired research on the topic. Even though the machine-learning-based models present enhanced accuracy, which for several applications is sufficient, they do not provide interpretability. Aiming at providing both accuracy and interpretability while keeping a compromise with model complexity, this work proposes a hybrid identification methodology that combines a gray-box phenomenological model with a black-box model based on artificial neural networks. The proposed methodology is applied in three case studies of nonlinear systems with experimental data, namely, the vertical dynamics of a vehicle, an elastomer-based series elastic actuator, and an electromechanical positioning system. The results show that the proposed hybrid model is up to 60% more accurate while providing the physical interpretability of the system, without significantly increasing the complexity of the model.

Keywords

System Identification; Nonlinear Systems; Artificial Neural Networks; Hybrid Models.

Resumo

Sousa, Daniel Henrique Braz; Ayala, Helon V. H.. **Identificação não linear híbrida de sistemas mecânicos com modelos físicos e de aprendizado de máquina**. Rio de Janeiro, 2023. 101p. Tese de Doutorado – Departamento de Engenharia Mecânica, Pontifícia Universidade Católica do Rio de Janeiro.

Existe uma crescente demanda por modelos dinâmicos precisos, parte impulsionada pelo paradigma da indústria 4.0 que introduz, dentre outros, o conceito de gêmeo digital no qual modelos dinâmicos possuem um papel importante. Idealmente, um modelo dinâmico apresenta um compromisso entre complexidade e precisão, enquanto proporciona informações sobre a física do sistema. Para melhorar a precisão de um modelo mantendo a interpretabilidade, a abordagem usual é modelar matematicamente todas não-linearidades, o que leva a um modelo muito complexo. Outra abordagem envolve identificação caixa-preta, uma abordagem onde um modelo matemático é ajustado para descrever a relação de entrada e saída do sistema, a qual pode fornecer um modelo preciso, porém não interpretável. Os avanços na capacidade de processamento computacional permitiram o florescimento da area de aprendizado de máquinas, a qual tem mostrado resultados interessantes em diferentes campos do conhecimento. Uma dessas aplicações é em identificação caixa-preta, onde o aprendizado de máquinas tem sido empregado com sucesso na modelagem de sistemas não-lineares, o que tem inspirado pesquisas sobre o tema. Apesar dos modelos baseados em aprendizado de máquina apresentarem elevada precisão, o que é suficiente para diversas aplicações, eles não são interpretáveis. Dessa forma, visando obter modelos que possuem ambas as características de precisão e interpretabilidade, enquanto mantém um compromisso com a complexidade, esta tese propõe uma metodologia de identificação híbrida que combina um modelo fenomenológico caixa cinza com um modelo caixa preta baseado em redes neurais artificiais. A metodologia proposta é aplicada em três casos de estudo de sistemas não lineares com dados experimentais, a saber, a dinâmica vertical de um veículo, um atuador com junta flexível baseado em elastômero e um sistema de posicionamento eletromecânico. Os resultados mostram que o modelo híbrido proposto é até 60% mais preciso enquanto proporciona a interpretabilidade física do sistema, sem aumentar significativamente a complexidade do modelo.

Palavras-chave

Identificação de Sistemas; Sistemas Não-lineares; Redes Neurais Artificiais; Modelos Híbridos.

Table of Contents

List of Figures

List of Tables

List of Abreviations

ADAM – Adaptive Momentum

ANN – Artificial Neural Network

DKF – Dual Kalman Filter

DOF – Degrees of Freedom

DT – Digital Twins

EKF – Extended Kalman Filter

eSEA – Elastomer based Series Elastic Actuator

GR – Gaussian Regression

IMU - Inertial Measurement Unit

KF – Kalman Filter

LQR – Linear Quadratic Regulator

LS – Least Squares

MPC – Model-based Predictive Control

NARMAX – Nonlinear Auto-Regressive Moving Average models with eXogenous input

NARX – Nonlinear Auto-Regressive models with eXogenous input

NN – Neural Network

NNOE – Neural Network based on Output Error

PD – Proportional–Derivative

PSO – Particle Swarm Optimization

R^2 – Multiple Correlation Coefficient

RBFNN – Radial Basis Function Neural Network

RLS – Recursive Least Squares

SEA – Series Elastic Actuator

SVM – Support Vector Machine

UKF – Unscented Kalman Filter

WKF – Weighted Kalman Filter

FEM – Finite Element Models

TOP – Test Operations Procedure

It is not enough to have faith; we must also work towards the realization of our ideals.

Allan Kardec

Part I

Preliminaries

1
Introduction

Models of real systems are of fundamental importance in almost all disciplines, especially in engineering, where they are required for the design of new processes and the analysis of the existing ones [1]. Recently, the current stage of technology development is characterized by arising new paradigms for the construction of anthropogenic systems, such as cyber-physical systems and sociocybernetic systems [2]. One of these new concepts is the Digital Twin (DT), which can be defined as a scale, physic, unified, stochastic simulation of an as-built system, permitted by the use of a digital thread, which employs the best accessible models (physical, behavioral, etc.), as well as the updated information to emulate the life cycle, actions, and operation of its real twin [3]. In the paradigm of Industry 4.0, DT is a hot topic of research and an urgent problem to be solved [4]. Moreover, as an emergent technology, the DT widespread implementation is increasing in other domains than the industrial, such as medical, automotive, and smart-cities [5].

In the construction of DT, the system's dynamic model plays an important role in considering the requirements of accurate real-time simulations, which not only allow for improvements in design and usability, but also a comprehensive understanding of the system [4]. These requirements demand a model that holds the characteristics of accuracy, simplicity, and interpretability. Concerning obtaining a dynamic model for the system there are numerous approaches in the literature, which can be divided into two main groups: physics-based modeling, and system identification, where data-driven modeling is included. The physics-based modeling approach has been the workhorse throughout time in many engineering applications [6] and relies on the physics theory and properties of the materials to obtain the dynamic models. Even though these approaches generate models that allow a physical insight into the system and, therefore, the desired interpretability, depending on the complexity of the system, the obtained models can be complex and computationally expensive in order to achieve the desired level of accuracy. Moreover, the accuracy is affected by parameter uncertainties and unmodelled nonlinearities.

The system identification approach can be considered the science of obtaining models of dynamic systems from observed input-output data [7]. The

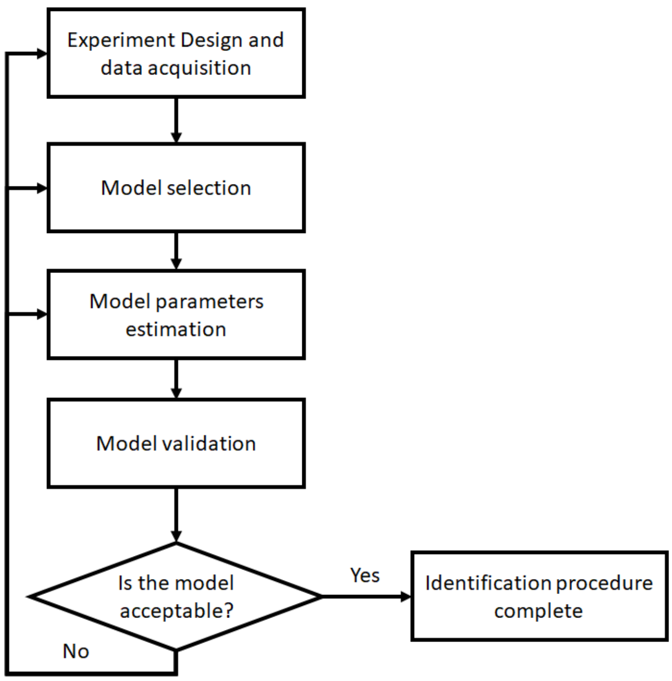

Figure 1.1: System identification procedure.

system identification procedure includes not only the model estimation but also the experiment design and data, considering that system data should carry the necessary information to adjust the model. Figure 1.1 shows the general flow chart for an identification procedure. Through system identification, it is possible to adjust the uncertain parameters of a model, known as gray-box identification, or obtain an empirical model that predicts the system's behavior, known as black-box identification. For parameter and states estimation Recursive Least Squares (RLS) and Kalman filter (KF) and its variations for nonlinear systems such as Extended Kalman Filter (EKF) and Unscented Kalman Filters (UKF) have been largely used as one can see in [8–11]. Even though the nonlinear filters present good results in real-time applications, computational complexity to achieve a given estimation accuracy is still a key issue [12]. Additionally, the gray-box identification problem can also be interpreted as an optimization problem where the parameters are adjusted in order to obtain the best fit between the model response and the system data. Several works use that interpretation and employ optimization methods [13, 14], including swarm and evolutionary methods such as genetic algorithm [15] and particle swarm [16], to estimate the models' parameters. In fact, metaheuristic and nature/bio-inspired algorithms are research topics of great importance for the solution of complex optimization problems and recently have experienced major advances as one can see in the surveys presented in [17–19].

The gray-box identification approach allows the adjustment of a model in order to fit the system's dynamics data, however, it still depends on the choice of a suitable model, which may present a complex formulation in order to properly predict the system's dynamics. Therefore, the model accuracy is affected by unmodeled nonlinearities. Alternatively, the black-box identification approach is focused on obtaining data-driven mathematical abstractions of dynamic systems with little or no information about their intrinsic properties [20, 21]. Due to the advances in processing capacity and parallel computing, the machine learning approach, which includes kernel-based methods, such as Support Vector Machines (SVM) and Gaussian Regression (GR), and Neural Networks (NN) have been extensively employed [22]. Machine learning black-box models usually are accurate models, nonetheless, they do not provide any interpretability about the system. A broad review of recent developments in the field of complex dynamical systems with an emphasis on data-driven, data-assisted, and artificial intelligence-based discovery of dynamical systems is presented in [23].

For the specific case of systems whose dynamics are defined by partial differential equations, which is the case of fluid dynamics and mechanics of materials, several works have been developed in order to insert physics-driven or physics-based constraints during artificial neural network training. Generally, there are three distinct neural network frameworks that enforce the underlying physics: physics-guided neural networks, physics-informed neural networks, and physics-encoded neural networks [24]. Each framework has its own advantages and drawbacks. For a critical review of the recent developments and research in that subject, one can recall to [24, 25].

In machine learning, ensemble learning models are commonly used since it was noticed that an ensemble of predictors performs better than a single predictor in the average [26]. Ensemble modeling is a process where multiple models are used to predict an outcome, whose objective is to reduce the generalization error [27]. This fact urges the research of new architectures that combine different model approaches in order to obtain models for nonlinear systems that are interpretable, more accurate, and yet mathematically simple, all ideal characteristics for modern engineering applications.

1.1 Objectives

This thesis proposes a novel architecture of hybrid models that combines a phenomenological gray-box model and an Artificial Neural Network black-box model to be applied in the modeling of nonlinear systems. The proposed hybrid model provides the desired combination of interpretability and accuracy without increasing mathematical complexity significantly. Therefore, the general objective of this thesis is to present three contributions regarding the modeling of nonlinear systems using the proposed approach. The contributions are:

- Contribution 1: Modeling of the vertical dynamics of a Toyota Hilux RWD using the data from the vehicle acquired during the transposition of a type-A bump described in the Test Operations Procedure (TOP) 01-1-011B of the Vehicle Test Facilities at Aberdeen Test Center and Yuma Test Center [28]. The hybrid model used combines a linear half-car vertical model with two Nonlinear Auto-Regressive models with exogenous input (NARX) adjusted using a neural network.
- Contribution 2: Modeling of an elastomer-based Series Elastic Actuator (eSEA) using its experimental data. The eSEA is an inherent nonlinear system because of its elastomer-based compliant element. Several hybrid models, which combine a phenomenological gray-box model with a NARX neural network model, are used.
- Contribution 3: Modeling of a Electromechanical Positioning System, a system extensively used in the manufacture of robotic manipulators and machine tool, which has challenging friction characteristics. The hybrid model proposed combines an phenomenological model with a Radial Basis Function Neural Network (RBFNN) model.

1.2 Document Organization

The remainder of this thesis is organized as follows. The first part is dedicated to exposing the literature review, motivation, and contribution of the thesis. The second part presents the theoretical background that includes the gray-box and black-box algorithms used in the proposed methodology. In the third part, the contributions of the thesis are exposed, with the details inherent to each one, including the specific problem definition, the results, and a discussion about them. In the last part, the conclusions of the thesis are discussed, as well as the possible future research that may be developed using the theory basis herein presented.

2
Related Works and Originality Claims

This chapter is dedicated to presenting and discussing recent works whose subject is related to this work. A literature review is presented, containing a critical analysis of the research gaps, for the objectives mentioned in section 1.1. Then, the original contributions are presented regarding each of the objectives.

2.1
Critical Literature Review

The critical literature review is divided according to the objectives presented in Section 1.1. However, bearing in mind that Objectives 2 and 3 are related to modeling of robotics, a single literature review encompass both objectives.

2.1.1
Vehicle vertical dynamics modeling

In the context of vehicle vertical dynamics, a dynamical model can be used in the design of an active suspension system and in the analysis of comfort and performance, for instance. Therefore, several physics-based dynamic models were developed and their use depends on the intended applications

The quarter-car model is the simplest suspension model and various works are focused on improving its accuracy. In Sandu and Andersen [29] a quarter-car test rig McPherson structure suspension is identified using a multi-body quarter-car suspension model. The identified multi-body model presented better results when compared with a linear quarter-car suspension identified using the same data A similar approach is addressed in Fallah et al. [30] where a nonlinear quarter-car model for a McPherson suspension is proposed for riding control applications. The model simulations showed good results compared with an ADAMS McPherson suspension model. In Hurel et al. [31], equivalent stiffness and damper parameters for a quarter-car suspension model are analytically derived considering the suspension kinematics. Simulation results were compared with an ADAMS multi-body model showing an increase in accuracy when compared to the conventional quarter-car linear model. Niu et al. [32] derived a whole-range nonlinear dynamic model for a double wish bone suspension for geometric optimization purposes, which was validated using an ADAMS model of the suspension. Gonçalves et al. [33] used a similar dynamic model for a double-wishbone suspension to study the interaction of asymmetrical damping and geometrical nonlinearity and the effects on comfort. A test rig was specially designed to validate the simulations results. Chiang and Lee [34] proposed an optimized virtual model reference control synthesis method for semi-active suspension based on a quarter-car McPherson suspension model. The simulations results of the proposed architecture presented better results when compared to a linear quadratic regulator (LQR) control. All the aforementioned work aimed to improve the accuracy of a quarter-car suspension model taking into consideration the kinematics and dynamics of the suspension elements and, therefore, increasing the complexity of the models. Furthermore, the quarter-car model only considers the dynamics of the suspension, neglecting the vehicle's pitch dynamics.

A more complex model is the full-car model, which considers the chassis' pitch and row dynamics, as well as each suspension dynamics. Zhou et al. [35] proposed a new method to obtain the equivalent suspension and damping rates for different suspension geometries to be applied in a full vehicle model. The model's performance is then compared with a multi-body ADAMS model showing a minimal error between simulations for several scenarios. Kanchwala [36] obtained a full-car model using test track data. A frequency-domain identification was employed to adjust the model. Reiterer et al. [37] combined three identification techniques to adjust a full-car model using experimental data from a sensored vehicle. The proposed approach allowed the identification of all the model's parameters based only on the vehicle sensor's measurements. Attia et al. [38] proposed an observer/controller method to estimate the states and improve stability and riding comfort using the measurements of a single IMU. The state observer is based on a full-car model with active suspension. Those works are focused on a full-car suspension model, which is a more accurate model, but also mathematically complex.

A model between the above models in terms of complexity is the half-car model, which considers the chassis' pitch dynamics and the front and rear suspensions sets. In Cui et al. [39] three nonlinear empirical damper models were adjusted using test rig data. Afterward, the influence of the damper model on the parameter identification of a half-car model was analyzed. In this case, for the identification process, simulated data was used. The results obtained showed that the damper models previously adjusted have no significant impact on the parameters identification when simulated data is used. A continuous system identification approach is used in Thaller et al. [40] to identify the damper coefficient of a vehicle's suspension using a half-car linear model. The identification is performed using simulated data obtained with *CarMaker* software package. The results showed that the employed methodology was able to identify the damper coefficients for several different simulated data scenarios. Pedro et al. [41] used a half-car model with active suspension to implement a model predictive control whose parameters were optimized using a Particle Swarm Optimization algorithm. Simulations showed the superior performance of the proposed control in rejecting the deterministic road disturbance when compared to the passive vehicle suspension system and the non-optimized Model-based Predictive Control (MPC). The half-car model, the focus of the previously mentioned works, is the simplest suspension model that takes into consideration the influence of the vehicle's body.

Several of the aforementioned works are based on data-driven modeling techniques to adjust the parameters of a model. Other works use state estimators to obtain the vehicle states and the suspension parameters. Imine and Madani [42] used the sliding mode observer approach to estimate the vertical forces and to identify dynamic parameters, such as damper coefficient and unsprung masses, based on a half-car model for roll dynamics of a heavy vehicle. Experimental data were measured from an instrumented semi-truck performing a double-lane change maneuver at different speeds. The results showed that the sliding mode observer has a quick convergence and presented minimal error. The state observer approach can also be applied in fault detection on suspension systems. Alcantara et al. [43] compare two different techniques of fault detection for semi-active suspensions. One is based on state observers and the other on system identification. Both techniques use a quarter-car model of a semi-active suspension. The techniques are compared through simulations, and results show that the approaches have complementary characteristics, although the state observer technique presented better qualitative and quantitative performance. In fact, state observer and Kalman-filters techniques are largely used for vehicle states and parameter estimation, for instance one can refer to Antonov et al. [44], Wenzel et al. [45], Hong et al [46], Liu et al. [47], Reina and Messina [48], among others.

The neural-network approach has been extensively employed in the study of vehicle systems as seen in the following. In Yao and Xu [49] a progressive neural network is used to identify the suspension parameters of a tracked vehicle. In this case, the suspension damping is modeled as a cubic polynomial and the neural network is employed to determine the polynomial coefficients. The neural network is trained using simulated data from a vehicle model implemented in ADAMS. Results show that the application of the progressive neural network in the identification of suspension parameters is feasible. A neural network approach is also employed by Witters and Swevers [50] where a nonlinear black box model for a semi-active damper is obtained using a neural network based on output error (NNOE). The neural network was adjusted using a set of experimental data obtained from a test rig. The experimental data was optimally designed for that purpose. The results showed that the NNOE black-box model was able to describe the dynamics of the semi-active damper with minimal error, except at very low damper velocities. Liu and Cui [51] employed a Nonlinear Auto-regressive model with eXogenous input (NARX) neural-network method to identify the road roughness. The data for the training and identification process were generated using a full-car suspension model. In fact, the neural-network approach is commonly used in the identification of nonlinear damper models as can be seen in [52–55].

When the accuracy of a vehicle dynamic model needs to be improved, the general approach is to mathematically model the nonlinearities, which inevitably increases the model complexity, or employ a black-box identification technique that generates a model which does not allow any physical interpretation.

2.1.2 Robotic systems modeling

In the case of robotic systems, obtaining an accurate model can be a particularly challenging task given that they are inherently nonlinear systems not only because of their dynamics but also because of joint friction and gear/chain backlash [56–59], for example. For robots with SEA, the compliant element can add another source of nonlinearity. Furthermore, besides the system nonlinearities, parameter uncertainties represent an additional difficulty in obtaining an accurate model.

For Series Elastic Actuators (SEA), one of the ways to reduce the parameter uncertainties about the compliant element is by optimizing its design to present desired characteristics of weight, dimension, and stiffness. Yildirim et al. [60] designed and developed an SEA with optimized spring topology, which was submitted to numerous experimental tests to validate the design. The stiffness test showed that the spring can be used as a torque sensor, presenting a 5% nonlinearity error in most of the specified torque range. However, near the maximum torque, the nonlinearity error reaches its maximum value of 13%. Irmscher et al. [61] develop a similar work, but focuses only on the design and optimization of the compliant element. In this case, experimental data and simulation results showed discrepancies that can be attributed to fabrication imperfections and differences in the material properties. A similar explanation can be found in Liu et al. [62], where the compliant element presented a stiffness 32.6% larger than the simulations. In these works, the compliant element had its design optimized, however, the optimization algorithms were based on finite element models (FEM), which require a compromise between accuracy and complexity to be computationally cost-effective. Therefore, the discrepancies between simulations and experimental data are common, especially when material property mismatches are present. This urges a data-driven modeling to obtain more accurate dynamic models.

Through gray-box identification it is possible adjust a model to fit a dynamic system data, but it is still depends on the choice of a suitable model to describe the system behavior. In fact, a gray-box identification can be addressed as an optimization problem and, therefore, there are many methods to obtain a solution. Because of its simplicity and good performance in ill-posed problems, some works use evolutionary algorithms in the identification of models that consider nonlinear friction [63, 64] or other nonlinearities including elasticity and hysteresis [65]. Most parameter estimation methods are based on Maximum Likelihood Estimation (MLE) [66], least squares algorithm [67–69] and its expansion such as weighted least squares (WLS) [70], recursive least squares [66, 71], and nonlinear least squares (LS) [68, 69, 72]. Jia et al. [73] propose a method that integrates MLE and WLS to identify the dynamic parameters of a SEA manipulator. Other alternative estimation approaches commonly used are based on state observers, mainly to estimate disturbances [74–76], Kalman Filter (KF) [77, 78], and other filter architectures [79]. For a more extensive survey about parameter identification in robotics, one can recall to Leboutet et. al. [80].

There are several machine learning approaches used in robotics black-box identification, for instance, Banka et al. [81] use a complex-valued Gaussian Process Regression (cGPR) technique to estimate a linearized local system model to reduce position tracking errors. However, one of the most used approaches is Neural Networks (NN) due to their simplicity and performance in modeling nonlinear systems. Mukhopadhyay et al. [82] compare 3 types of recursive neural networks in the modeling of two robotic manipulators with 7 DoF. Zhang et al. [83] use a recurrent fuzzy Neural Network to adjust a nonlinear autoregressive moving average with an exogenous input model to describe the load-dependent dynamic behavior of a pneumatic artificial muscle. Shao et al. [84] use a RBFNN to model the nonlinear behavior of a series elastic drive joint, while Wang et al. [85] uses to model static friction in robotic manipulator joint.

Regarding eSEA, Seo et al. [86] use a MATLAB parameter estimation toolbox to adjust a Bouc-Wen hysteresis model for an eSEA. Sun et al. [87] and Kim et al. [88] also model the hysteresis of a eSEA, the first adjusts the parameters of a proposed hysteresis model, and the last uses a Gaussian process to adjust a nonlinear auto-regressive moving average with exogenous inputs (NARMAX) model. Austin et al. [89] use a Zener model to describe the compliant element of eSEA in order to implement a nonlinear observer-based control. A Zener model was also used in Wei et al. [90] combined with a nonlinear friction model to build an eSEA model used in the implementation of a dual Kalman filter (DKF) for torque estimations. As it can be seen, those works approach the nonlinearities of the eSEA by either employing a gray-box identification method to adjust the parameters of a model, or by employing a black-box approach.

A gray-box model still relies on a mathematical model, which may become excessively complex to reach the desired level of accuracy; on the other hand, a black-box model may reach the desired level of accuracy but does not offer any phenomenological insight about the system, which is crucial to optimize the system. In fact, for a DT, a dynamic model must have a compromise between complexity and accuracy, but also must be interpretable, an important characteristic that allows the proper study of the system.

2.2 Contributions

The machine learning approach has been successfully employed in the modeling of nonlinear systems [49–55, 81–90], however, despite its ability to accurately model nonlinear systems, it does not provide interpretable models, except for specific cases [91]. Alternatively, physics-based modeling and gray-box identification approaches [29–48, 60–80] do provide interpretability about the system, but in order to achieve accuracy the system nonlinearity has to be mathematically modeled, which ultimately may lead to a computationally expensive model. Thus, this work aims at filling this gap, by proposing different methods to construct hybrid models that would provide interpretable and accurate models.

In the following, we establish the contributions of this thesis, which are divided into three groups:

- Vehicle vertical dynamics modeling (presented in Chapter 4):
  - Propose and test a novel nonlinear hybrid half-vehicle model for vertical dynamics, which to date has not been explored in the literature;
  - Validate the method using experimental track data acquired from a TOYOTA HILUX RWD.

  This chapter has been submitted for review:

  SOUSA, D. H. B.; AYALA, H. V. H. **A Novel ensemble model approach applied to vehicle vertical dynamics modeling**. Under Review in *Vehicle System Dynamics*, 2022.
- Elastomer-based Series Elastic Actuator Modeling (presented in Chapter 5):
  - Propose a hybrid model approach to be applied in the modeling of an 1-DOF eSEA which combines a phenomenologycal model with a NARX neural network;
  - Compare with original data several hybrid models which use different phenomenological models.

  This chapter has been submitted for review:

  SOUSA, D. H. B.; LOPES, F. L.; LAGO, A. W. C.; MEGGIOLARO, M. A.; AYALA, H. V. H. **Hybrid Grey and Black-box Nonlinear System Identification of an Elastomer Joint Flexible Robotic Manipulator**. Under Review in *Mechanical System and Signal Processing*, 2022.
- Modeling of a Electromechanical Positioning System (presented in Chapter 6):
  - Propose a nonlinear hybrid model approach the combines a phenomenological model with a RBFNN black-box model;
  - The RBFNN is used to model a nonlinear friction model which is inserted in the model state-space equations;

  This chapter has been submitted for review:

  SOUSA, D. H. B.; SOUSA, L. C.; AYALA, H. V. H. **An hybrid gray and black-box artificial neural network friction identification of an Electromechanical Positioning System**. To be submitted, 2023.

Additionally, the following papers have been published in conference proceedings as a result of collaboration throughout the completion of the present thesis:

- PEREIRA, C. L.; DE SOUSA, D. H. B. ; AYALA, H. V. H.. **Three-axle vehicle lateral dynamics identification using double lane change maneuvers data**. In: 2021 29^{th} MEDITERRANEAN CONFERENCE ON CONTROL AND AUTOMATION (MED), p. 910–915. Puglia, Italy, 2021. IEEE.
- LAGO, A. W. C. ; SOUSA, L. C. ; SOUSA, D. H. B. ; LOPES, F. R. ; MEGGIOLARO, M. A. ; AYALA, H. V. H.. **Identificação usando método não linear de um sistema de posicionamento**. In: 2022 XXIV CONGRESSO BRASILEIRO DE AUTOMÁTICA. Fortaleza, Brazil, 2022. SBA.
- LAGO, A. W. C. ; CAMERINI, I. G. ; SOUSA, L. C. ; SOUSA, D. H. B. ; LOPES, F. R. ; MEGGIOLARO, M. A. ; AYALA, H. V. H.. **Black-Box Identification with Static Neural Networks of Non-linearities of an Elastomer-Based Elastic Joint Manipulator**. In: 2023 INTERNATIONAL JOINT CONFERENCE ON NEURAL NETWORKS. Queensland, Australia, 2023. IEEE.

3
Identification Methods

This chapter deals with the identification methods employed in the contributions presented in Part II. First, the gray-box identification method, which is common to all contribution, is presented. Then, it is presented two different black-box identification methods based on artificial neural networks.

3.1
Gray-box Identification Method

Given a suitable dynamic model of a system, the gray-box identification consists in tuning the unknown parameters from the model in order to make its simulations fit the system available data. Therefore, the gray-box identification can be considered an optimization problem whose objective is to minimize a cost function defined as the error between the system data and the model simulations, and the control variables are the model's unknown parameters.

In order to carry on the models simulations and, consequently the optimization problem, the dynamic models are discretized in this thesis with 4^{th}-order Runge-Kutta algorithm.

Generally, a discrete-time nonlinear state space model may be defined as:

$$\begin{cases} x(k+1) = f(x(k), u(k)) \\ z(k+1) = h(x(k+1), u(k+1)) + \xi_n \end{cases} \tag{3-1}$$

where the index k denotes discrete-time dependence, $x(k)$ is the state vector, $u(k)$ is the input vector of the system, and $z(k)$ is the output vector. Functions $f(\cdot)$ and $h(\cdot)$ are called state and measurement equations, respectively, and they are nonlinear mappings, generally.

Therefore, let y be the system output data and p the vector of unknown parameters, and considering the system discrete representation in (3-1), cost function, i.e., the error function is defined as follows:

$$J(p) = \|y - z\|^2 \tag{3-2}$$

The method chosen to solve the referred optimization problem is the multiple-shooting algorithm [92], extensively used in Model-based Predictive Control (MPC) problems [93]. Then, considering N as the size of the optimization window, and X as the set of the possible values of the states x, the following optimization problem is defined:

$$
\begin{aligned}
\min_{x_{k+1,k+N+1},p} \quad & \sum_{i=k}^{k+N-1} \left\| y\left(i\right) - z\left(i\right) \right\|^2 \\
\text{s.t.} \quad & x\left(i+1\right) - f\left(x\left(i\right), u\left(i\right)\right) = 0,\ i = k, k+1, \ldots, k+N-1 \\
& x\left(i\right) \in X,\ i = k, k+1, \ldots, k+N-1 \\
& p_{min} \leq p \leq p_{max}
\end{aligned}
\tag{3-3}
$$

where p_{min} and p_{max} defines the parameters searching space. Thus, in order to perform the gray-box identification, the nonlinear optimization problem defined in (3-3) must be solved.

In this thesis, the algorithm was implemented in MATLAB® using the CasADi optimization tool [94]. The solution to nonlinear optimization problems using CasADi is performed through nonlinear programming (NLP) and in this work is used the plugin Interior Point Optimization (IPOPT), which may be used on higher dimension problems with faster local convergence [95]. The NLP is solved through symbolic variables, using the Lagrange Multipliers method and the Karush-Kuhn-Tucker (KKT) conditions [96]. The implementation of the above optimization problem is similar to the ones for nonlinear MPC, which is presented in detail in [96] and [97].

3.1.1 Constrained Optimization Problem

Constrained optimization problems, such as the one presented for the gray-box identification method used in this thesis, may be formulated as follows:

$$
\begin{aligned}
\arg\min \quad & f_{obj}(x) \\
\text{s.t.} \quad & g_i(x) = 0, \quad i = 1, \cdots, n_g \\
& h_j(x) \geq 0, \quad j = 1, \cdots, n_h
\end{aligned}
\tag{3-4}
$$

The function f_{obj} is the cost or objective function, whose argument is the vector $x \in \mathbb{R}^n$. The problem is constrained by n_g equality constraints $g_i(x)$, and n_h inequality constraints $h_j(x)$. To solve this constrained optimization problem, a Lagrangian function must be defined:

$$
\mathcal{L}(x, \lambda, \mu) = f(x) - \sum_{i=1}^{n_g} \lambda_i g_i(x) - \sum_{j=1}^{n_h} \mu_j h_j(x) \tag{3-5}
$$

where λ_i and μ_j are the Lagrange multipliers related, respectively, to equality and inequality constraints. The feasible set Ω of the optimization problem is:

$$\Omega = \{x| \quad g_i(x) = 0, \quad i = 1, \cdots, n_g; \quad h_j(x) \geq 0, \quad j = 1, \cdots, n_h\} \tag{3-6}$$

The KKT conditions, presented in the following, are the necessary, but not sufficient first-order conditions for the existence of a local solution to the optimization problem. Supposing that f, g_i, h_j are continuously differentiable, for a local solution $x^* \in \Omega$ of the Eq. (3-4), there is a set of Lagrange multipliers (λ^*, μ^*) so that the following conditions are satisfied:

$$\nabla_x \mathcal{L}(x^*, \lambda^*, \mu^*) = 0 \tag{3-7a}$$
$$g_i(x^*) = 0, \quad for \quad i = 1, \cdots, n_g \tag{3-7b}$$
$$h_j(x^*) = 0, \quad for \quad j = 1, \cdots, n_h \tag{3-7c}$$
$$\mu_j{}^* \geq 0, \quad for \quad j = 1, \cdots, n_h \tag{3-7d}$$
$$\lambda_i{}^* g_i(x^*) = 0, \quad for \quad i = 1, \cdots, n_g \tag{3-7e}$$
$$\mu_j{}^* h_j(x^*) = 0, \quad for \quad j = 1, \cdots, n_h \tag{3-7f}$$

The two last ones are known as complementarity conditions, which indicate that if these conditions are active, i.e., equal to zero, the relative Lagrange multipliers are positive. If the conditions are inactive, the Lagrange multipliers are zero. Consequently, the value of each multiplier indicates the application of the condition [98].

The second-order conditions are related to the Lagrangian second derivative, and they are also sufficient conditions. It is possible to prove that a feasible point x^*, for which a set of Lagrange multipliers (λ^*, μ^*) satisfy the KKT conditions, is a strict local solution for the optimization problem if:

$$s^T \nabla^2{}_{xx} \mathcal{L}(x^*, \lambda^*) s > 0, \quad \forall s \in \mathcal{C}(x^*, \lambda^*, \mu^*), \ s \neq \mathbf{0} \tag{3-8}$$

where $\mathcal{C}(x^*, \lambda^*, \mu^*)$ (critical cone) is the set that contains the critical directions w for which it is not possible to define the direction of $\nabla f(x^*)$. Equivalently:

$$s \in \mathcal{C}(x^*, \lambda^*, \mu^*) \Rightarrow s^T \nabla f(x^*) = \sum_{i=1}^{n_g} \lambda_i s^T \nabla g_i(x) + \sum_{j=1}^{n_h} \mu_j s^T \nabla h_j(x) = 0 \tag{3-9}$$

Therefore, the sufficient condition is that the Hessian of the Lagrangian function must be positive-definite for all critical directions [98].

In this thesis, as mentioned before, the IPOPT algorithm is employed to numerically solve the constrained optimization problem. This algorithm uses a point in the interior of the feasible region to approximate the solution.

Consequently, the cost function is replaced by a barrier function that takes into consideration the inequality constraints:

$$P(x, \rho) = f(x) - \rho \sum_{j=1}^{n_h} \log(h_j(x)) \tag{3-10}$$

The barrier function, as defined, prevents the iteration point from leaving the feasible region, considering that the closer the iterate solution of the boundaries of feasible sets, the higher its value, tending to infinity. Furthermore, because the solution is searched inside the feasible region, where the constraints are active, the problem can be solved using unconstrained optimization methods [99].

3.2 NARX Neural Networks

The black-box identification approach is commonly used in the modeling of dynamic systems with undetermined nonlinearities or when there is no previous knowledge about the system physics. A black-box model uses approximation functions to describe the input/output relations of the system [100]. Machine learning and NN approaches have been largely applied in robotics with significant results in black-box modeling [22, 101].

In this thesis, a multi-layer artificial neural network is used to adjust a Nonlinear Auto-regressive model with Exogenous inputs (NARX). A NARX model is mathematically represented in Eq. (3-11), where F is a nonlinear function, $\hat{y}$ is the model output prediction, u is the input, n_y is the output regression order, and n_u is the input regression order. In this case, the nonlinear function is a multi-layer neural network, whose schematic of its application in the identification of the NARX model is presented in Fig. 3.1.

$$\hat{y}(t) = F\left[\hat{y}(t-1), \ldots, \hat{y}(t-n_y), u(t-1), \ldots, u(t-n_u)\right] \tag{3-11}$$

For the NN training, the Adaptive Moment estimation method (ADAM) [102] was chosen as the optimizer, and the Exponential Linear Unit (ELU) function as the activation function. This function is designed for faster and more precise learning in deep neural networks and outperformed other activation functions in several scenarios [103]. The ELU function is defined as follows, where α is a constant with a default value of 1:

$$ELU(x) = \begin{cases} \alpha\left(e^x - 1\right) & \text{if } x < 0 \\ x & \text{if } x > 0 \end{cases} \tag{3-12}$$

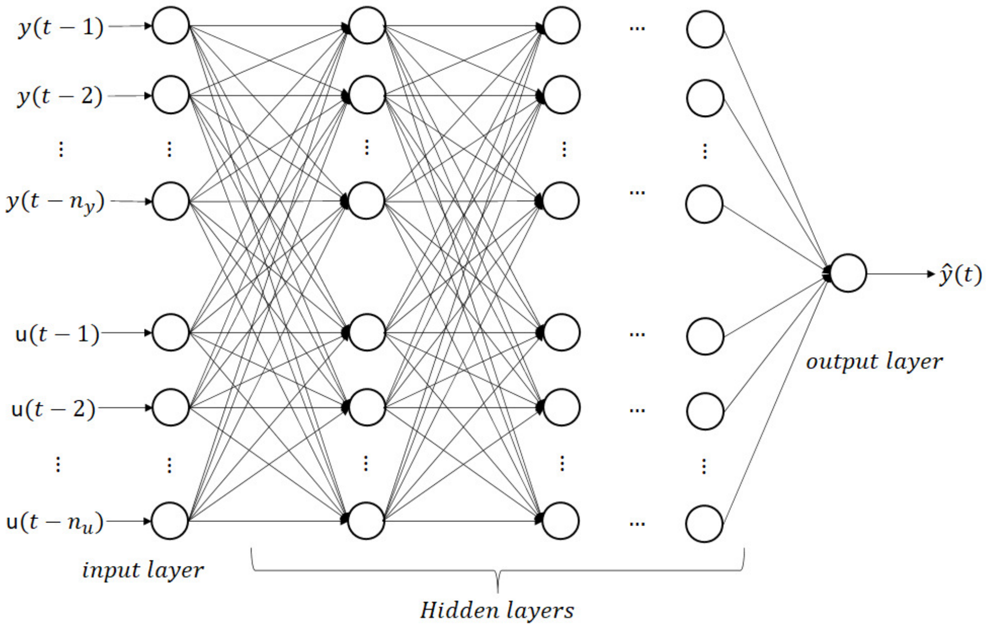

Figure 3.1: Multi-layer artificial neural network schematics

In this thesis, the NARX NN was implemented and trained using the Python programming language using TensorFlow [104]. Due to its extensive usage by the artificial intelligence and machine learning communities, there are several dedicated packages, which facilitate the tasks of implementation and training of the NN.

3.3 Radial Basis Function Neural Networks

Radial Basis Function Neural Networks (RBFNNs) have been extensively used for function approximation purposes, such as in black-box systems identification [105]. An RBFNN is a feedforward network with three layers: the inputs, the hidden/kernel layer, and the output node, whose hidden layer neurons activation function is a radial basis function [106].

In this thesis, the Gaussian radial basis function is used . The Gaussian radial basis function is defined as follows:

$$\phi\left(x\right) = exp\left[-\frac{\left(x-c\right)^2}{2\sigma^2}\right] \tag{3-13}$$

Where c and σ are, respectively, the centers and the width of the Gaussian function. Figure 3.2 show a general schematics of a RBFNN, whose mathematical model is presented in Eq. (3-14).

$$y_{rbf} = \sum_{i=1}^{m} w_i \phi\left(x, c_i, \sigma_i\right) \tag{3-14}$$

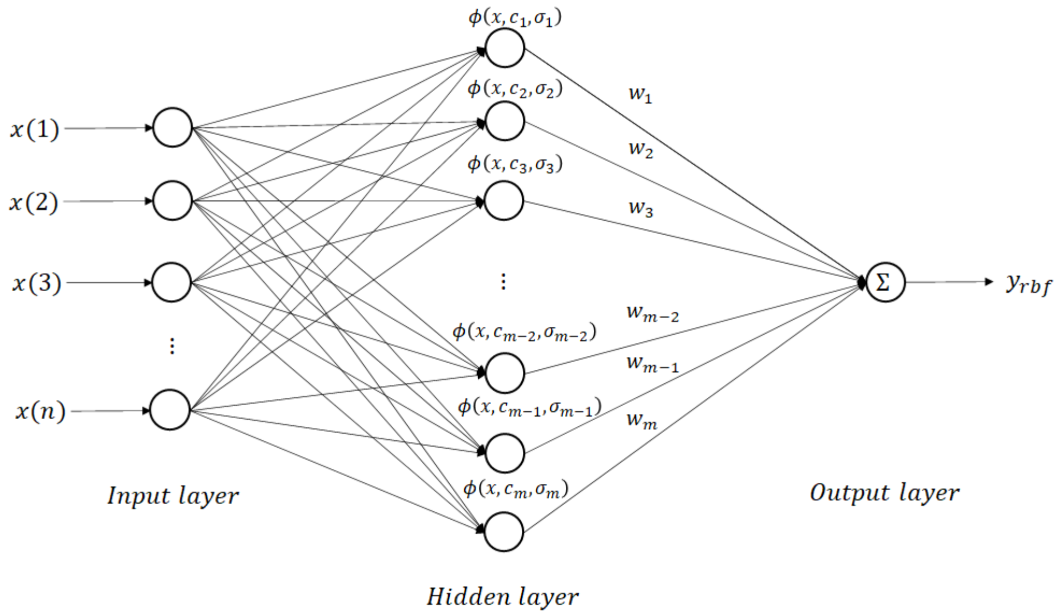

Figure 3.2: Radial basis function artificial neural network schematics

3.4 Validation Metrics

Three metrics were used in this thesis to measure and compare the accuracy of the models: the mean square error (MSE), the root mean square error ($RMSE$), and the multiple correlation coefficient (R^2). Considering y as the measured data, $\overline{y}$ as the measured data mean value, and $\hat{y}$ as the model prediction, both metrics are defined as follows:

$$MSE = \frac{\sum_{i=1}^{n} (y_i - \hat{y}_i)^2}{n} \tag{3-15}$$

$$RMSE = \sqrt{\frac{\sum_{i=1}^{n} (y_i - \hat{y}_i)^2}{n}} \tag{3-16}$$

$$R^2 = 1 - \frac{\sum_{i=1}^{n} (y_i - \hat{y}_i)^2}{\sum_{i=1}^{n} (y_i - \overline{y})^2} \tag{3-17}$$

The more precise model will present a MSE and a $RMSE$ closer to zero and a R^2 closer to one. For most applications, $R^2 > 0.9$ is considered sufficient [107].

Part II

Contributions

4
A Novel hybrid model approach applied to vehicle vertical dynamics modeling

Dynamical models are essential in the engineering field, and depending on the application, they need a compromise between simplicity and accuracy. The usual approach to obtain more accurate models is to increase their mathematical complexity to address the nonlinearities. This contribution proposes a novel approach to vertical dynamics modeling based on hybrid models. To date, there is no research on hybrid models applied to vehicle vertical dynamics. The proposed approach combines a gray-box identification with a black-box identification to obtain a novel nonlinear half-car hybrid model. The methodology is tested and the hybrid model is validated using experimental data. Results indicate that the obtained hybrid model is up to 84% more accurate without significantly increasing model complexity.

4.1
Problem Definition

Dynamical models are essential in many engineering applications, such as control design, parameter optimization, behavior prediction, fault detection, and other simulation purposes. In the case of vertical dynamics, a dynamical model can be used in the design of an active suspension system and in the analysis of comfort and performance, for instance.

Although precision is the primary goal of a dynamical model, an over-complicated model can be time-consuming to simulate and unfeasible to be applied [108]. Therefore, a model needs to have a compromise between precision and complexity.

One of the strategies to obtain a model is through system identification [109]. Not only does the system identification allow us to optimize the parameters of a mathematical model of the system studied, but it also allows us to obtain a model which has no physical interpretation. The first case is known as gray-box identification, and the last is known as black-box identification.

This contribution aims to propose a Hybrid identification technique that combines a gray-box identification, whose purpose is to identify the suspension parameters of a half-car model using field data, with a black-box identification where an artificial neural network is employed in the modeling of the nonlinear error between the half-car model and the data. Using this approach, it is expected to obtain a simple model with enhanced accuracy.

4.2 Case Study and Experiment Description

The case study consists in using experimental data acquired from a four-wheel vehicle transposing an obstacle at a constant speed to obtain a hybrid model that describes the vertical dynamics of the vehicle.

The field measurements are from a Toyota Hilux RWD vehicle transposing a type-A bump described in the Test Operations Procedure (TOP) 01-1-011B of the Vehicle Test Facilities at Aberdeen Test Center and Yuma Test Center [28] at the constant speed of 20 km/h. During the test, the driver was responsible for maintaining the vehicle at the predefined speed. Figure 4.1 shows the dimensions of the type-A bump.

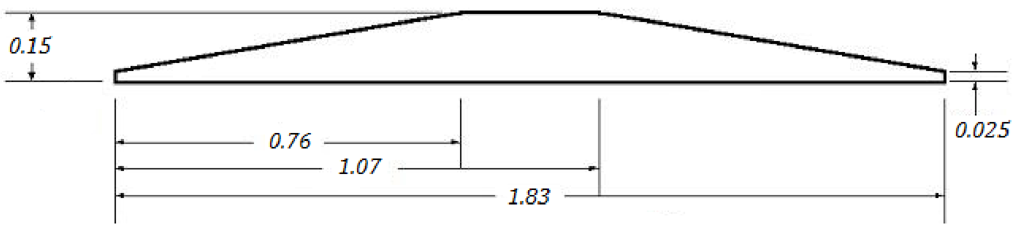

Figure 4.1: Type-A bump dimensions in meters [28].

The measurement data were collected using a VBOX/Racelogic® inertial measurement unit (IMU) positioned on the vehicle's center of gravity (CG) as shown in Figure 4.2. The IMU provides pitch, roll, and yaw rates using three rate gyros, as well as, x, y, and z-axis accelerations from three accelerometers. In this study, only the pitch rate and the z-axis acceleration are used. The data were recorded at 100 Hz sample rate and saved for subsequent analysis.

Due to disturbances mainly caused by vibrations from the running engine and the road roughness, data preprocessing is imperative to ensure good results in the identification process. Therefore, a first-order Butterworth filter with a cutoff frequency of 5 Hz was applied to the pitch rate and z-axis acceleration. The application of this filter intends to remove high-frequency content from the measurements, such as sensor noise and the aforementioned vehicle's vibrations.

Figure 4.3 shows filtered data of pitch angular velocity and vertical acceleration. As can be noticed, the designed filter was capable of filtering the high-frequency noise of both data sets.

Figure 4.2: IMU positioning inside the vehicle.

The proposed method needs the signals of pitch angular velocity and vertical velocity. Therefore, the vertical acceleration signal was integrated to obtain the vertical velocity of the vehicle's center of gravity. Figure 4.4 shows both pitch angular velocity and vertical velocity, which are used in the proposed method.

4.3
Half-car model

The half-car model is the one used in this work. It is a well-known modeling assumption for vertical vehicle dynamics. In this model, the car is assumed to be a two-dimensional object with a front and rear suspension, as shown in Figure 4.5. A more detailed description of the model can be obtained in [110]. In this thesis, for the sake of keeping the model simple, the springs and the dampers were considered to have a linear behavior.

To obtain the equations of motion of the model, the Euler-Lagrange approach was used. Figure 4.5 shows the generalized coordinates used to derive the motion equations, where z_f and z_r are, respectively, the vertical position of the front and rear suspension masses, z_c is the chassis's vertical position, and θ is the chassis's pitch angular position. The entries for the model are the positions of the ground surface at the front wheel contact point u_f and at the rear wheel contact point u_r. The Euler-Lagrange equation is presented as:

$$\frac{d}{dt}\left(\frac{\partial L}{\partial \dot{q}}\right) - \frac{\partial L}{\partial q} + \frac{\partial R}{\partial \dot{q}} = 0 \tag{4-1}$$

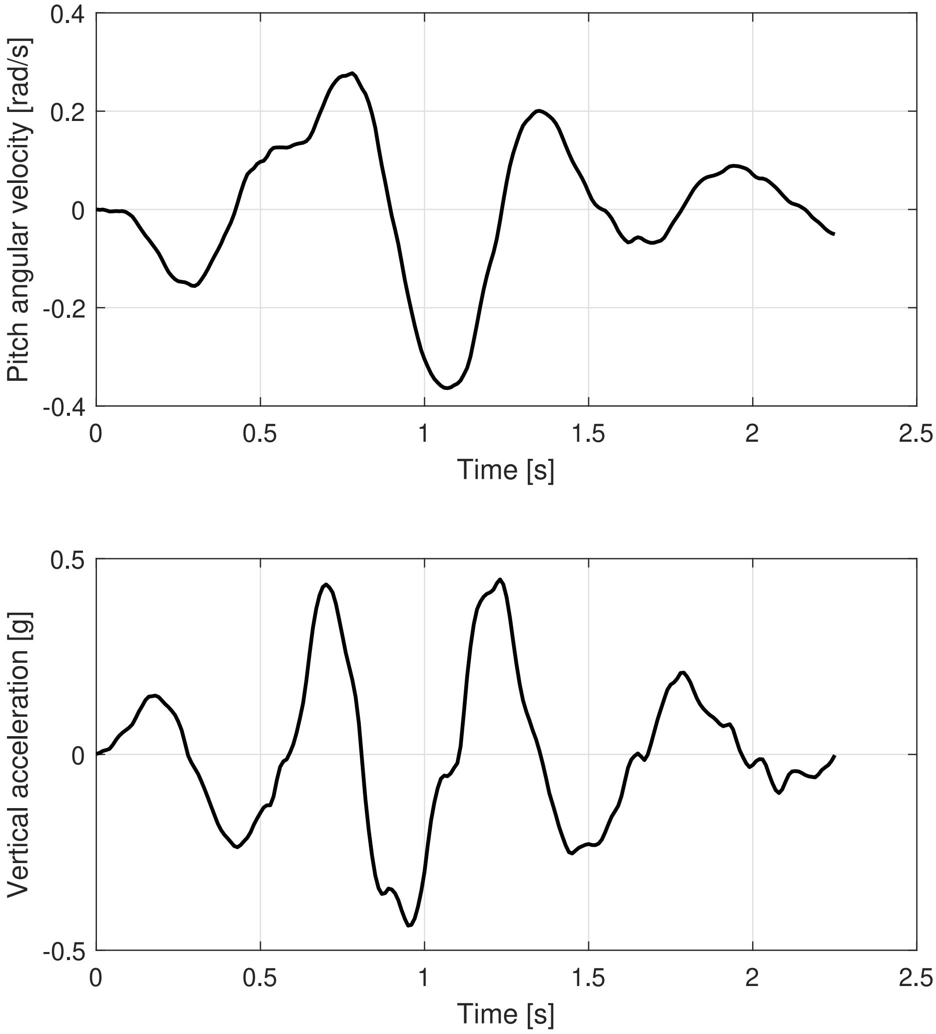

Figure 4.3: Filtered data.

where R is Rayleigh dissipation function for the viscous forces of the dampers and L is the Lagrangian of the system:

$$L = T - V \tag{4-2}$$

In Equation (4-2), T and V are the total kinematic and potential energies, respectively. Therefore, to derive the dynamic equations, the kinematic energy, potential energy, and Rayleigh dissipation function are needed for the chassis, and for the front and rear suspension masses. These terms are calculated as follows, where the subscript c is referring to the chassis, f to the front floating mass, and r to the rear floating mass:

$$T_c = \frac{1}{2}m_c\dot{z}_c^2 + \frac{1}{2}I_{yy}\dot{\theta}^2 \tag{4-3}$$

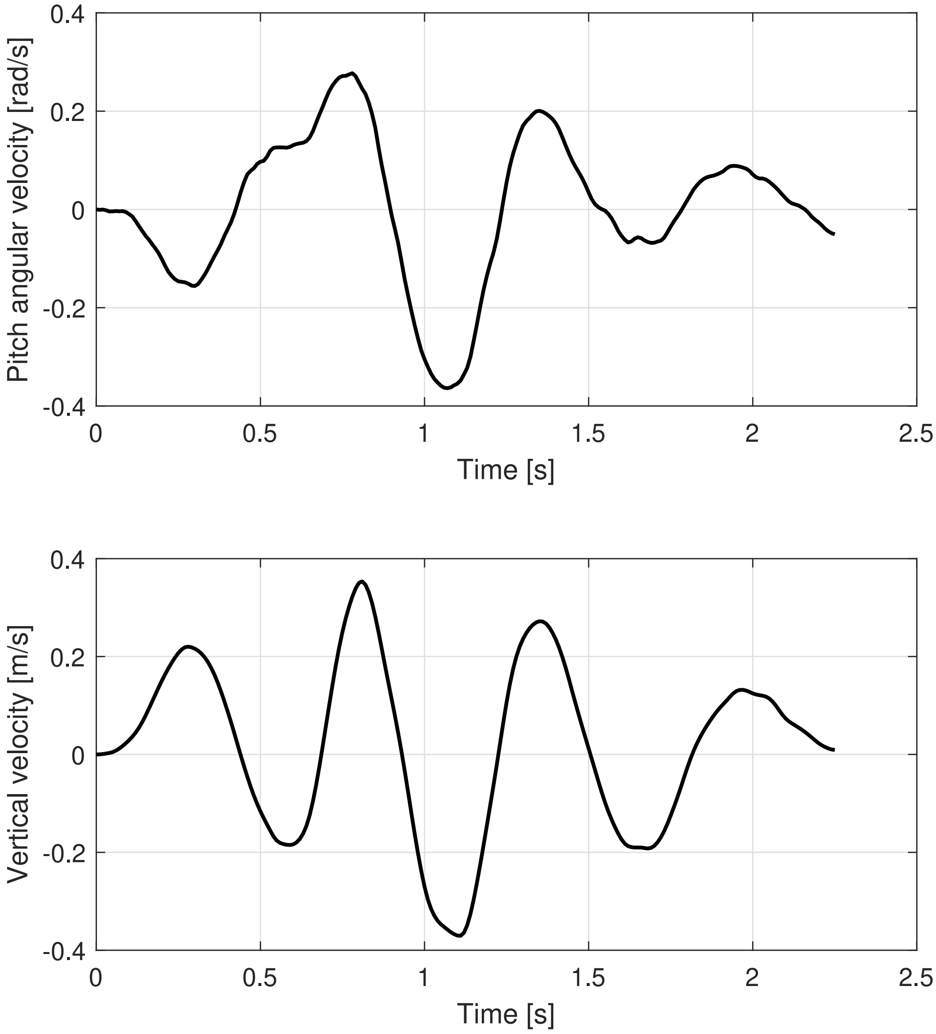

Figure 4.4: Pitch rate and vertical velocity data used in the method.

$$V_c = m_c z_c g \tag{4-4}$$

$$T_f = \frac{1}{2} m_f \dot{z}_f^2 \tag{4-5}$$

$$V_f = m_f z_f g + \frac{1}{2} k_f \left[z_f - (z_c - l_f \theta)\right]^2 + \frac{1}{2} k_p \left(u_f - z_f\right)^2 \tag{4-6}$$

$$R_f = \frac{1}{2} c_f \left[\dot{z}_f - \left(\dot{z}_c - l_f \dot{\theta}\right)\right]^2 \tag{4-7}$$

$$T_r = \frac{1}{2} m_r \dot{z}_r^2 \tag{4-8}$$

$$V_r = m_r z_r g + \frac{1}{2} k_r \left[z_r - (z_c + l_r \theta)\right]^2 + \frac{1}{2} k_p \left(u_r - z_r\right)^2 \tag{4-9}$$

$$R_r = \frac{1}{2} c_r \left[\dot{z}_r - \left(\dot{z}_c + l_r \dot{\theta}\right)\right]^2 \tag{4-10}$$

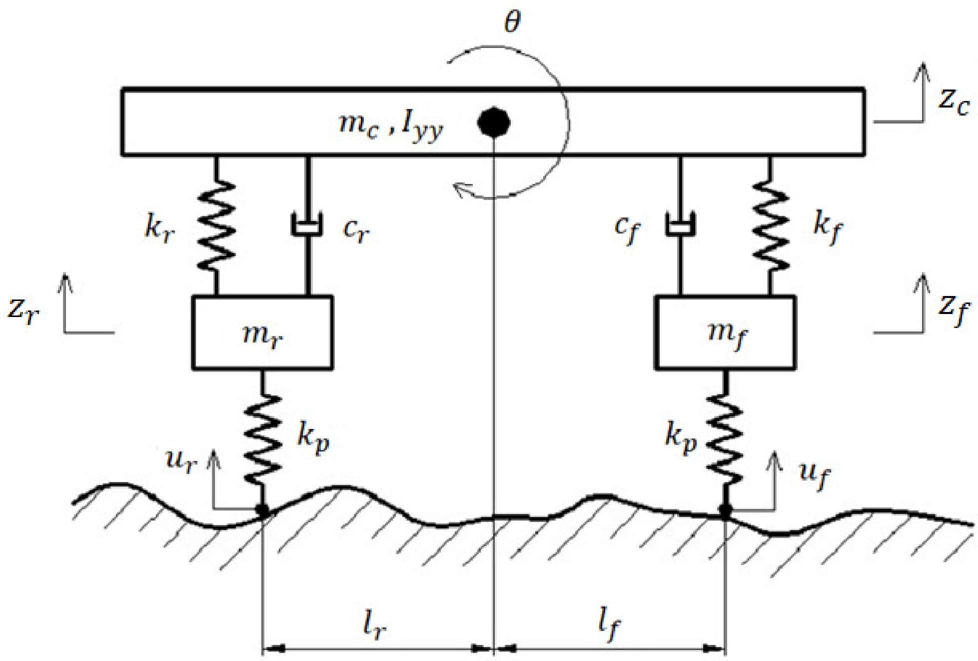

Figure 4.5: Half-car suspension model.

In Eqs. (4-3) – (4-10), I_{yy} is the chassis' moment of inertia with respect to the y-axis; k_f and k_r are, respectively, the front and rear spring stiffness; c_f and c_r are the front and rear damping coefficient; k_p is the tire stiffness; l_f and l_r are the front and the rear axle distance; and m_c, m_f and m_r are the mass of the chassis, the front, and rear floating masses.

Therefore, the total kinematic and potential energies and the Rayleigh term are calculated as follows:

$$T = T_c + T_f + T_r \tag{4-11}$$

$$V = V_c + V_f + V_r \tag{4-12}$$

$$R = R_f + R_r \tag{4-13}$$

With Eqs. (4-11) – (4-13) and the Lagrange equation, the equations of motion of the half-car model are obtained. Defining the vector of states $\mathbf{q}^T = \left[\dot{z}_c \; \dot{\theta} \; \dot{z}_f \; \dot{z}_r \; z_c \; \theta \; z_f \; z_r\right]$ and the vector of inputs as $\mathbf{u}^T = [u_f \; u_r]$, it is possible to write the equations of motion in the form $\dot{\mathbf{q}} = f(\mathbf{q}, \mathbf{u})$. The components of $\dot{\mathbf{q}}$ are shown in Eq. (4-14).

$$
\begin{aligned}
\ddot{z}_c = & -\frac{1}{m_c}[g\,m_c + c_f\,\dot{z}_c - c_f\,\dot{z}_f + c_r\,\dot{z}_c - c_r\,\dot{z}_r + k_f\,z_c - k_f\,z_f + k_r\,z_c - k_r\,z_r - \\
& - c_f\,l_f\,\dot{\theta} + c_r\,l_r\,\dot{\theta} - k_f\,l_f\,\theta + k_r\,l_r\,\theta] \\
\ddot{\theta} = & -\frac{1}{I_{yy}}[c_f\,{l_f}^2\,\dot{\theta} + c_r\,{l_r}^2\,\dot{\theta} + k_f\,{l_f}^2\,\theta + k_r\,{l_r}^2\,\theta - c_f\,l_f\,\dot{z}_c + c_f\,l_f\,\dot{z}_f + c_r\,l_r\,\dot{z}_c - \\
& - c_r\,l_r\,\dot{z}_r - k_f\,l_f\,z_c + k_f\,l_f\,z_f + k_r\,l_r\,z_c - k_r\,l_r\,z_r] \\
\ddot{z}_f = & -\frac{1}{m_f}[g\,m_f - c_f\,\dot{z}_c + c_f\,\dot{z}_f - k_f\,z_c + k_f\,z_f + k_p\,z_f - k_p\,u_f + c_f\,l_f\,\dot{\theta} + \\
& + k_f\,l_f\,\theta] \\
\ddot{z}_r = & \frac{1}{m_r}[c_r\,\dot{z}_c - g\,m_r - c_r\,\dot{z}_r - k_p\,z_r + k_r\,z_c - k_r\,z_r + k_p\,u_r + c_r\,l_r\,\dot{\theta} + k_r\,l_r\,\theta] \\
\dot{z}_c = & \dot{z}_c \\
\dot{\theta} = & \dot{\theta} \\
\dot{z}_f = & \dot{z}_f \\
\dot{z}_r = & \dot{z}_r
\end{aligned}
\tag{4-14}
$$

4.4 Proposed approach

The proposed method is focused on obtaining a hybrid model which consists of the combination of a gray-box model with two black-box models. The gray-box model is a half-car model, and the black-box models are two NARX neural networks, described in Section 3.2.

For the gray-box identification, the model's known parameter and their values are presented in Table 4.1. The vehicle's mass and CG position were obtained using a static weight scale, while the other information was obtained from the vehicle's user manual. Consequently, the unknown parameters are the stiffness (k_f, k_r) and the dumping coefficients (c_f, c_r) of both suspensions, the tires stiffness (k_t) and the moment of inertia (I_{yy}). The gray-box identification was performed using the method described in Section 3.1.

Table 4.1: Model's known parameters.

Parameters	Values
Vehicle's mass m_c	1250 kg
Front axle distance l_f	1.50 m
Rear axle distance l_r	1.60 m
Front floating mass m_f	30 kg
Rear floating mass m_r	30 kg

The black-box identification was performed for each error individually, i.e., one NARX model is obtained for the vertical velocity error, and another for the pitch angular velocity error.Figure 4.6 presents a block-diagram describing the steps of the proposed method for one of the degrees of freedom. Both models consider the tires contact point position inputs u_f and u_r, and the gray-box simulations as inputs. Therefore, the models can be represented as follows:

$$\begin{aligned} \hat{e}_b(t) = F[\hat{e}_b(t-1), \ldots, \hat{e}_b(t-n_e), u_f(t-1), \ldots, u_f\left(t-n_{u_f}\right), \ldots \\ \ldots, u_r(t-1), \ldots, u_r(t-n_{u_r}), \hat{y}_g(t-1), \ldots, \hat{y}_g\left(t-n_{\hat{y}_g}\right)] \end{aligned} \tag{4-15}$$

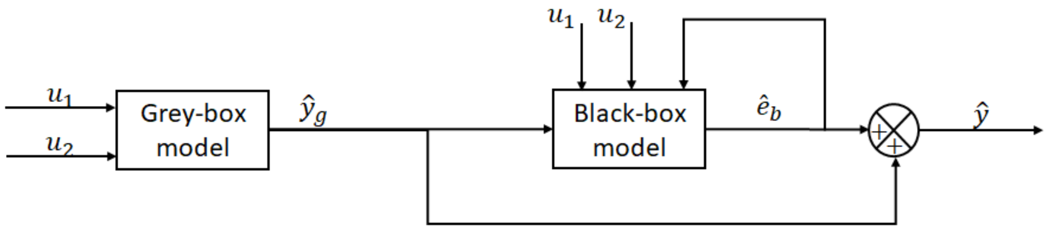

Figure 4.6: Block diagram of the proposed methodology.

Consequently, the combination of the estimated output of the gray-box half-car model $\hat{y}_g$ with the estimated error of the black-box NARX model $\hat{e}_b$ is considered to estimate the vehicle's behavior:

$$y \approx \hat{y} = \hat{y}_g + \hat{e}_b \tag{4-16}$$

4.5 Results

In this section, the proposed method is applied to the vehicle's filtered data shown in Figure 4.4. First, the gray-box identification is performed in order to adjust the half-car model. Therefore, the optimization problem described in Eq. (3-3) is solved. Table 4.2 shows the half-car model's estimated parameters while Figure 4.7 contains the comparison between the experimental data and the model simulation for vertical velocity and pitch angular velocity.

From the analysis of Figure 4.7, it is possible to observe that the half-car model simulations present a curve shape similar to the data. However, they differ in amplitude. A possible explanation for that behavior is the nonlinearities from the suspension components, such as spring stiffness and damping, and from the suspension kinematics, which is not considered in the model. Furthermore, one can notice a slight delay between the curves. This

Table 4.2: Gray-box model estimated parameters.

Parameters	Estimated Values
I_{yy}	$2441.0\ kg.m^4$
k_f	$22223\ N/m$
k_r	$52916\ N/m$
c_f	$2273.6\ N.s/m$
c_r	$1938.6\ N.s/m$
k_t	$5.1148 \cdot 10^6\ N/m$

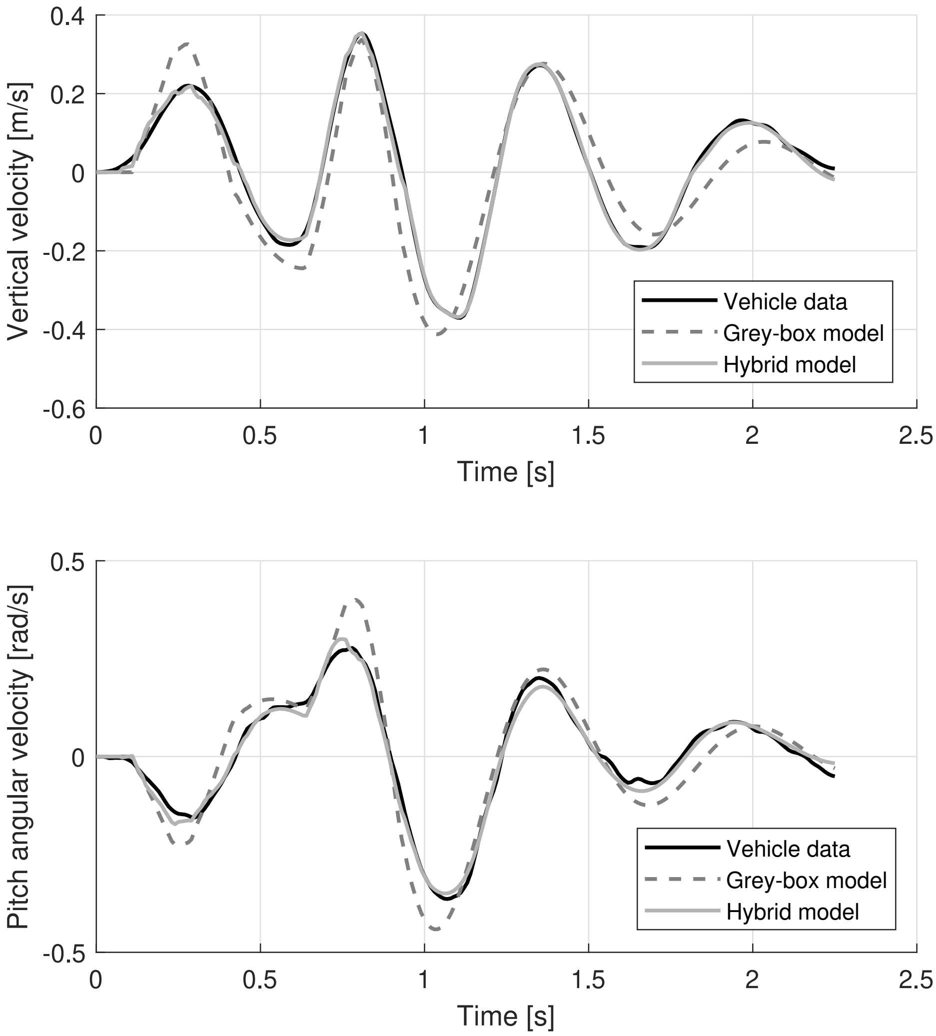

Figure 4.7: Comparison between the data, the gray-box half-car linear model and the hybrid model simulations.

delay is due to the vehicle's speed variations during the test. Those effects reflect in the model's metrics, especially the R^2 coefficient, which has an order of magnitude of 0.8 for both data sets.

Table 4.3: Gray-Box model metrics.

	$RMSE$	R^2
Vertical velocity	0.0678	0.8474
Pitch angular velocity	0.0533	0.8682

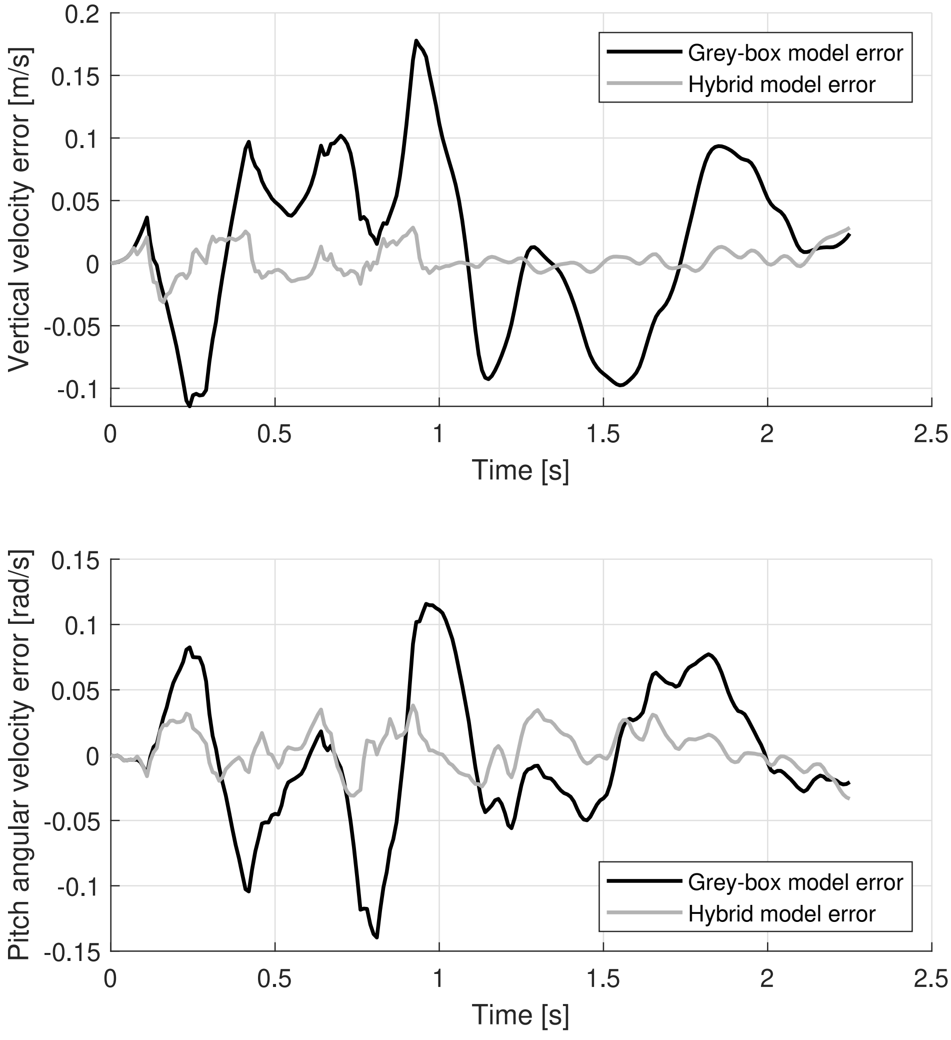

Figure 4.8: Error between the measured data and the gray-box model simulations.

With the error data between the vehicle data and the gray-box model simulations, the NARX models' black-box identification is performed. Figure 4.8 presents the error data for both vertical velocity and pitch angular velocity. As mentioned in section 3.2, two NARX models are identified, one for the vertical velocity error, and another for the pitch angular velocity error.

It is considered that both NARX models have the same regression order. The chosen regression orders were 7 for the error, 2 for both tires inputs u_f

and u_r, and 4 for the gray-box simulation data. Consequently, in Eq. (4-15), $n_e = 7$, $n_{u_f} = n_{u_r} = 2$, and $n_{\hat{y}_b} = 4$ for both NARX models.

The multi-layer neural networks employed in the black-box identification have the same number of neurons per layer for all layers, i.e., the input layer, the hidden layers, and the output layer have all the same number of neurons.

Considering that the parameters of a neural network that have the greater effect on the complexity of the black-box model are the number of neurons per layer and the number of hidden layers, several configurations were tested in order to obtain a model with a compromise between complexity and precision. Tables 4.4 and 4.5 show the configurations tested and the metrics considering the simulations of the hybrid model $\hat{y}$, shown schematically in Figure 4.6, for the vertical velocity and the pitch rate, respectively.

As mentioned before, the model that presents the best fitting will have a $RMSE$ closer to zero and a R^2 closer to one. Therefore, based on the metrics of Tables 4.4 and 4.5, the best model for the vertical velocity is the one with 4 hidden layers and 16 neurons per layer, and for the pitch angular velocity, the one with 3 hidden layers and 16 neurons per layer. Comparing the hybrid model metrics with the metrics of Table 4.3, for the $RMSE$, there is a reduction of 84% for the vertical velocity and a reduction of 70% for the pitch angular velocity. In terms of the R^2 coefficient, for the hybrid model, the magnitude is greater than 0.98 for both data sets, indicating a better fitting when compared with the half-car model.

Figure 4.7 also presents the comparison between the data and the hybrid model simulations for the vertical velocity and the pitch angular velocity. The figure shows the precision of the hybrid model. For both data sets, the curve fitting has increased when compared with the simulations of the gray-box model, in accordance with the model's metrics. In addition, comparing the error graphics of both models, presented in Figure 4.8, it is possible to observe that the amplitude of the error graphics for the hybrid model is smaller than the error graphics of the half-car model.

Figure 4.9 shows the graphic of data vs. model simulations for both data sets. If the model were perfect, the graphic would be a straight line with 45° inclination. Consequently, the closer the simulations are to that line, the more accurate the model is. By comparing the graphics presented in that figure, it is possible to visualize that the hybrid model is more accurate.

Table 4.4: hybrid model results (Vertical velocity).

Neurons per Layer	Hidden Layers	$RMSE$	R^2
8	3	0.0522	0.9093
	4	0.0579	0.8886
	5	0.0289	0.9723
16	3	0.0410	0.9442
	4	0.0108	0.9961
	5	0.0232	0.9821
32	3	0.0607	0.8776
	4	0.0420	0.9415
	5	0.0722	0.8267

Table 4.5: hybrid model results (Pitch rate).

Neurons per Layer	Hidden Layers	$RMSE$	R^2
8	3	0.0247	0.9716
	4	0.0215	0.9786
	5	0.0270	0.9661
16	3	0.0160	0.9881
	4	0.0177	0.9854
	5	0.0181	0.9848
32	3	0.0164	0.9874
	4	0.0231	0.9752
	5	0.0203	0.9809

4.5.1 Results discussion

This contribution used a data set obtained during a test that consisted of a Toyota Hilux RWD vehicle transposing a standardized obstacle at a constant speed. The vehicle was equipped with a single IMU sensor positioned in its center of gravity.

Using the vehicle data, first, a half-car linear model is adjusted using a gray-box identification technique. The results showed that the gray-box model simulations presented a similar curve shape when compared to the vehicle data, although it is clear that the model cannot explain some nonlinearities present in the data set, hence the amplitude divergence between simulations and data. One could address this issue by modifying the suspension model in order to consider its geometry and kinematics [29–33], or consider a nonlinear dumping model [39]. Both approaches or their combination would result in a mathematically complex model whose applications in model-based control

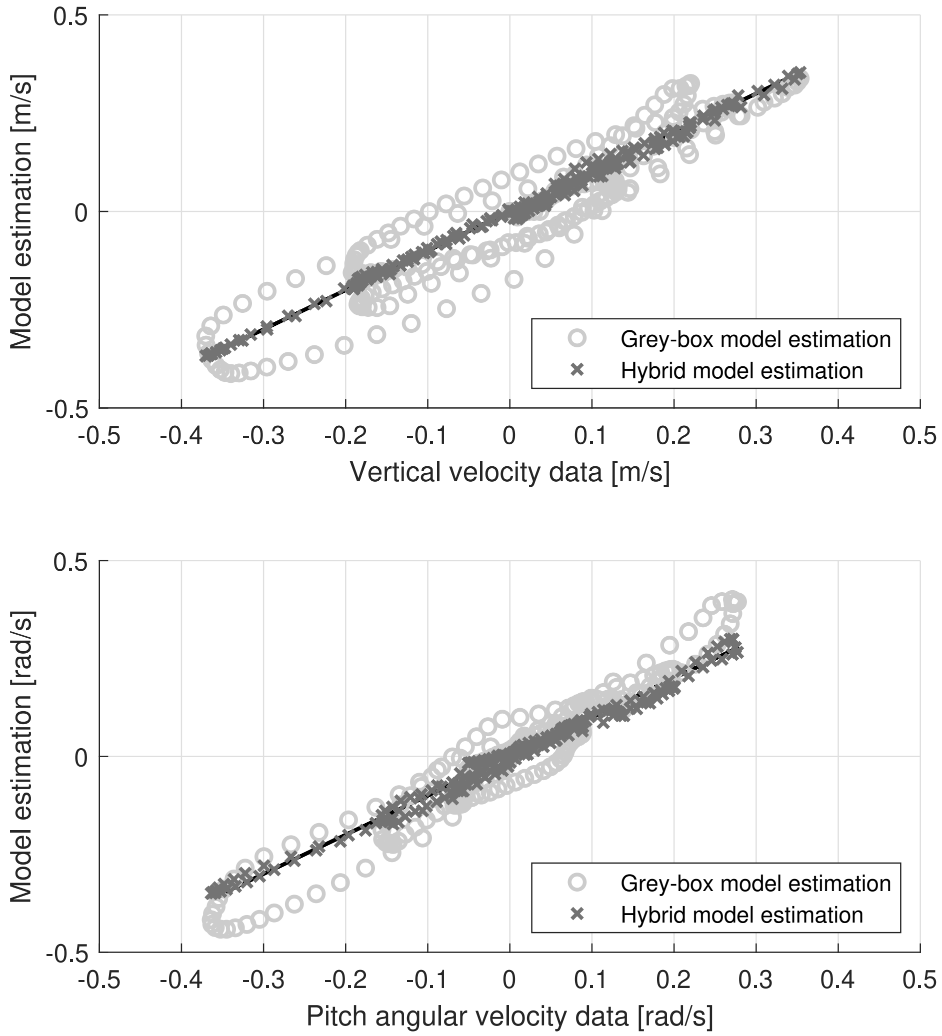

Figure 4.9: Data versus models estimation comparison graphic.

synthesis and real-time simulations would be limited or infeasible.

In the sequence, the proposed methodology is applied to obtain the nonlinear hybrid model. In the proposed approach, the gray-box model is combined with two NARX models of the error between gray-box model simulations and the vehicle data. The results showed that the hybrid model is up to 84% more accurate when compared with the gray-box model, a significant improvement considering the simplicity of the hybrid model. In the hybrid model, the nonlinearities of the system are addressed by the NARX models, which in combination with the linear half-car are capable to describe the vehicle behavior. Furthermore, because the hybrid model uses the gray-box model, it allows us to have some physical insight into the system. It is important to highlight that the aforementioned results were obtained using a single IMU sensor, indicating that it would be possible to obtain an even more accurate model if more information about the other states of the vehicle have been used. This possibility and the results here obtained urge further investigations into the applications of hybrid models on vehicle systems.

Finally, the architecture of the proposed hybrid model combines a linear model and black-box models which, in the case study, were successfully applied to vertical dynamics. However, the same approach can be employed in the study of other subjects such as, but not limited to, lateral dynamics, stability control, active suspensions, and trajectory control.

4.6
Summary

This contribution aimed to propose a hybrid identification technique that combines a gray-box and a black-box identification resulting in a novel nonlinear hybrid half-car model for the vehicle's vertical dynamics. The proposed method consists of three steps. First, a gray-box identification is performed in which a half-car model parameters are adjusted; second, for each of the two chassis' degree of freedom, a black-box identification is performed to obtain NARX model for the nonlinear error of the half-car model; finally, the models are combined in a hybrid model. The proposed method and the resulting hybrid model were validated using experimental data.

Notice that the hybrid model presented an enhanced fitting with the vehicle's data when compared to the linear half-car model. Consequently, the hybrid model is more precise yet simple. In addition, the proposed methodology was able to obtain a simple and precise model for the vehicle's vertical dynamic using data of two chassis' degrees of freedom obtained by a single IMU.

5
Hybrid gray and Black-box Nonlinear System Identification of an Elastomer Joint Flexible Robotic Manipulator

Series elastic actuators possess several properties that make them widely used in collaborative robots which play a major role in the current paradigm of Industry 4.0. However, the compliant element responsible for those desired properties can also be responsible for the addition of unmodelled nonlinearities in the system. Therefore, the aim of this contribution is to propose a novel hybrid model approach and apply it in the modeling of an elastomer-based series elastic joint. The proposed hybrid model combines a phenomenological gray-box model with a black-box Nonlinear Auto-regressive model with Exogenous inputs, which is able to provide the desired physical insight while enhancing accuracy by addressing the unknown nonlinearities. The results showed that the proposed hybrid model is more than 60% more accurate than the phenomenological model, considering the mean square error, and obtained a multiple correlation coefficient up to 0.97 considering the validation data, indicating its capacity to be used in the construction of a digital twin of the system.

5.1
Problem Definition

In the past decades, industrial robots driven by traditional stiff actuators have made remarkable progress due to their precise and fast positioning, as well as large force output, which provides a good performance in structured environments [111]. However, robots with stiff actuators are not suitable to work collaboratively with humans, considering that any unexpected impact represents an injury risk. In this context, the series elastic actuator (SEA) is a type of actuator that has a compliant element between the motor and payload, which brings some properties such as intrinsic safety, low output impedance, passive mechanical energy storage, and accurate force control. Those properties make the SEA suitable for human-robot interactions, showing potential in applications such as collaborative robotics, legged robots, and exoskeleton, for instance [112].

Obtaining an accurate model for robotic systems is particularly challenging due to their inherent nonlinearity. This is not only because of their dynamics, but also due to joint friction, gear/chain backlash, and parameter uncertainties. For robots with SEA, the compliant element can add another source of nonlinearity, thus, posing an additional difficulty in obtaining an accurate model.

In this contribution, a new hybrid identification technique is proposed in the context of eSEA to obtain a hybrid model that combines a phenomenological gray-box model with a black-box model and to apply it in a 1 degree of freedom (DOF) eSEA. The gray-box model is adjusted using experimental data from the eSEA, and the black-box model, consisting of a NARX model, is adjusted to describe the nonlinear error between the gray-box model and the actuator data. The resulting hybrid model is capable of providing the desired phenomenological insight with a compromise between complexity and accuracy. Four cases are considered that differ in the modeling of the friction force.

5.2 Case study

The case study consists of obtaining a dynamic model for an eSEA using experimental data. The system was previously reported in [113] and is herein shown in Figure 5.1a.

The link structure is made of 7075-T6 aluminum, which provides a good relation strength-weight. The system is mounted with two identical CUI AMT 102 encoders with 8192 CPR resolution and a range of 7500 RPM. One is responsible for measuring the motor position and the other for the link position. The motor is a dual-axis DC brushless D5065/270KV with maximum torque of 1.99 $N \cdot m$. The eSEA is controlled using an open-source ODrive Robotics board connected to a computer via a mini USB cable. The system is connected to a Cophert CPS-6005 power supply. The Odrive board was set in the torque control configuration in which the board controller is in closed-loop with the motor. To safely operate the eSEA in order to obtain the experimental data, a PD position controller was implemented, in an external loop, so that closed-loop experiments could be performed. The tests were performed using a 55 Shore A compliant element [113] shown in detail in Figure 5.1b.

The design and development of the system presented in the case study are the results of the research conducted in [114], which is currently in the Laboratório de Desenvolvimento de Sistemas Mecatrônicos - LDSM at Pontifícia Universidade Católica do Rio de Janeiro - PUC-Rio.

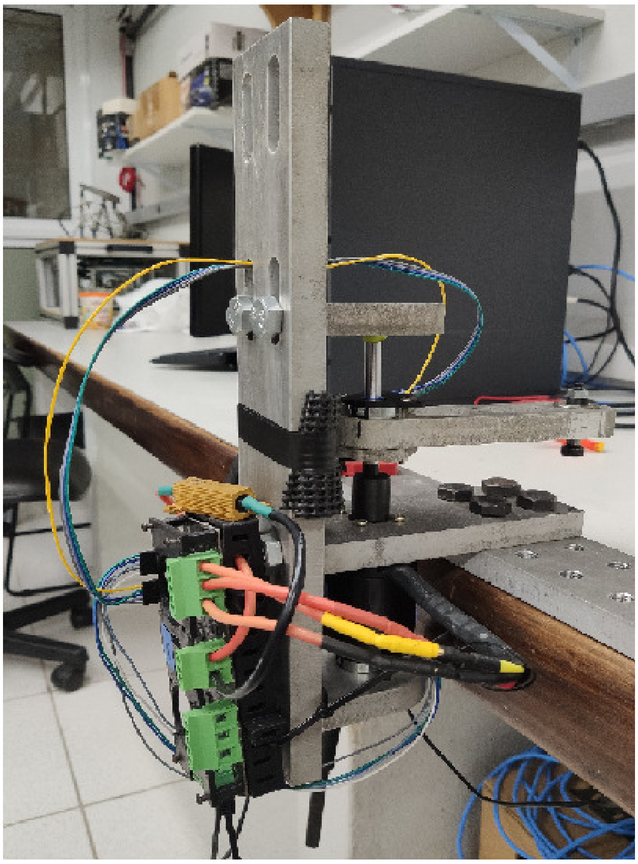

(a) Assembled eSEA.

(b) Detailed view of the 55 Shore A compliant element.

Figure 5.1: Assembled eSEA including a detailed view of the 55 Shore A compliant element.

5.2.1 Data acquisition

Figure 5.2 presents the control flowchart, where τ is the torque signal; δ and $\dot{\delta}$ the motor angular position and angular velocity; and θ and $\dot{\theta}$ the link angular position and angular velocity. The PD position controller was implemented in the computer using the Python programming language. The communication was done throughout the ODrive board, as shown in the figure. By defining a trajectory, i.e. an excitation signal to be followed by the link of the eSEA, the controller generates the torque signal τ for the motor.

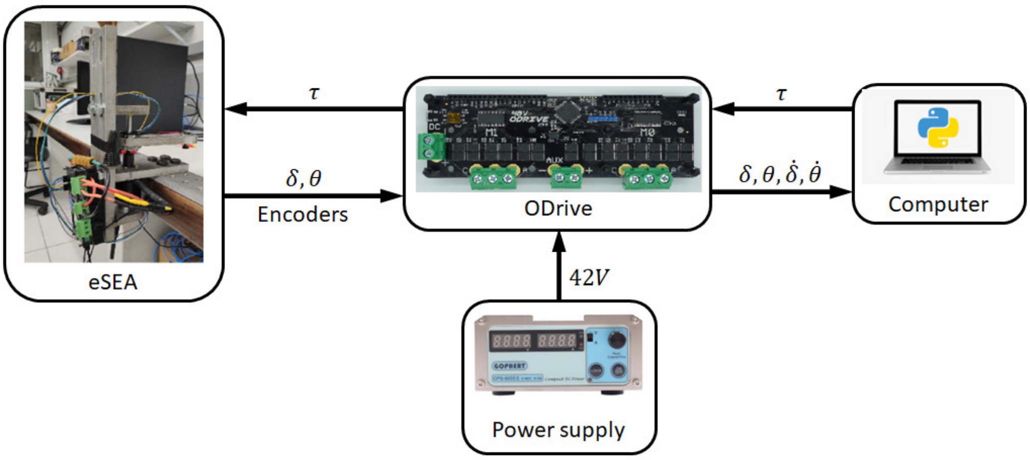

Figure 5.2: System control flowchart showing the signal flow between components.

To perform the identification, the swept-sine signal was chosen as the excitation signal. The swept-sine signal allows to excite the system with a specified range of frequencies, and, therefore, to have a better picture of the system's dynamic behavior. Furthermore, for the validation process, due to hardware limitations, a swept-sine signal was also used, but with a different frequency range and amplitude. The swept-sine used in the identification process has a frequency range varying linearly from 0.1 to 5 Hz, while the validation data set frequency range varies linearly from 0.1 to 3.5 Hz. Furthermore, the validation signal presents an initial phase shift of 180° in relation to the identification signal.

The system input signal is the motor torque and the output is the link angular velocity. The experimental data were recorded at a 500 Hz sample rate and are presented in Figures 5.3 and 5.4, which contain the identification and validation data, respectively. These figures not only do include the input and output signal, but also their frequency spectrum showing the frequencies that were excited during the experiment. In both, $|\mathcal{F}|$ represents the amplitude of the signal's discrete Fourier transform.

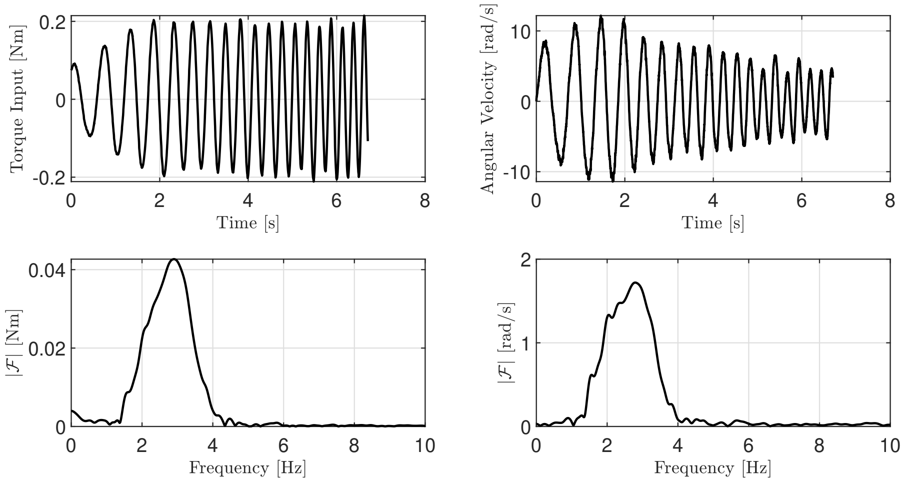

Figure 5.3: Input and output signals used in the identification process and their respective frequency spectrum showing the frequency range that was excited.

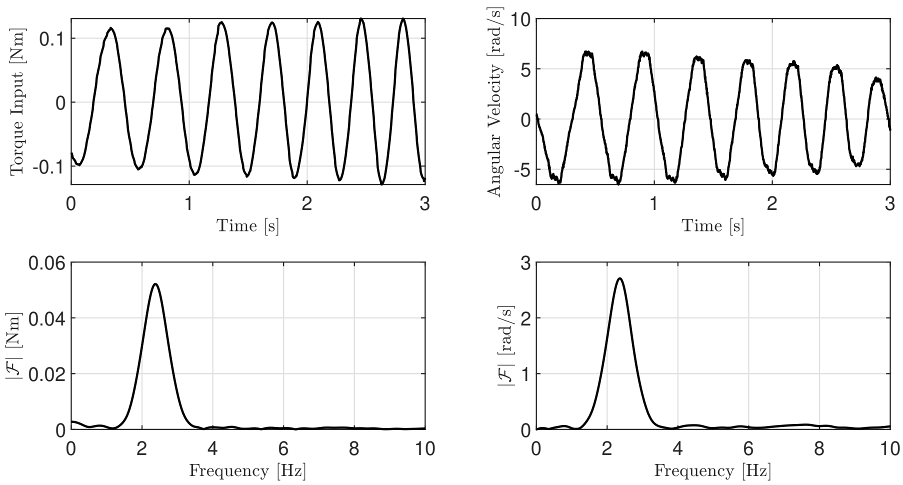

Figure 5.4: Input and output signals used in the validation process and their respective frequency spectrum showing the frequency range that was excited.

5.2.2 eSEA modeling

The series elastic actuator (SEA) is a type of actuator that has a compliant element between the motor and payload, which brings some properties such as intrinsic safety, low output impedance, passive mechanical energy storage, and accurate force control. Figure 5.5 presents a schematic representation of a SEA.

In this work, for the phenomenological model, it is considered that the eSEA compliant element has linear elastic behavior. Furthermore, in order to model the friction acting in the system, several friction models are considered, including linear and nonlinear models.

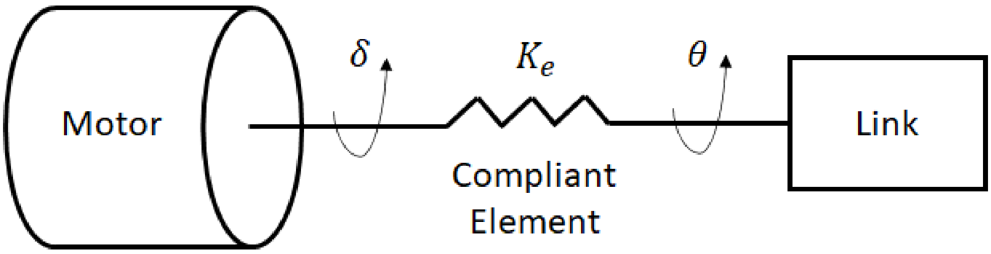

Figure 5.5: Series elastic actuator schematics.

Applying the Euler-Lagrange equations, the system's equation of motion in the matrix form in Eq. (5-1) is obtained, where K_e is the eSEA elastic constant, J is the motor moment of inertia, I is the link moment of inertia about the joint position, $F_f\left(\dot{\delta}\right)$ is the friction force, δ is the motor angular position, θ is the link angular position, and τ is the motor torque.

$$\begin{bmatrix} J & 0 \\ 0 & I \end{bmatrix} \cdot \begin{bmatrix} \ddot{\delta} \\ \ddot{\theta} \end{bmatrix} + \begin{bmatrix} K_e & -K_e \\ -K_e & K_e \end{bmatrix} \cdot \begin{bmatrix} \delta \\ \theta \end{bmatrix} + \begin{bmatrix} F_f\left(\dot{\delta}\right) \\ 0 \end{bmatrix} = \begin{bmatrix} \tau \\ 0 \end{bmatrix} \tag{5-1}$$

Separating Eq. (5-1) in relation to the generalized coordinates, it is possible to obtain the equations of motion from the motor side, Eq. (5-2), and from the load side, Eq. (5-3).

$$\ddot{\delta} = \frac{\tau}{J} + \frac{K_e\theta}{J} - \frac{K_e\delta}{J} - \frac{F_f\left(\dot{\delta}\right)}{J} \tag{5-2}$$

$$\ddot{\theta} = \frac{K_e\delta}{I} - \frac{K_e\theta}{I} \tag{5-3}$$

Defining the state vector as $\alpha = \left[\dot{\delta}\ \dot{\theta}\ \delta\ \theta\right]^T$ and the input as $\tau_{in} = [\tau]$, Eqs. (5-2) and (5-3) can be written in the form $\dot{\alpha} = f\left(\alpha, \tau_{in}\right)$ as follows:

$$\dot{\alpha} = \begin{bmatrix} \frac{\tau + K_e\theta - K_e\delta - F_f\left(\dot{\delta}\right)}{J} \\ \frac{K_e\delta - K_e\theta}{I} \\ \dot{\delta} \\ \dot{\theta} \end{bmatrix} \tag{5-4}$$

5.2.3 Friction models

Throughout the years, many mathematical models were developed to describe the friction phenomenon. For instance, in Marques et al. [115] a survey and comparison are conducted on the friction models commonly employed in dynamical systems. This work uses four different models to describe the friction force $F_f\left(\dot{\delta}\right)$. The selected models are: Linear viscous friction; Coulomb friction with stribeck effect; Dahl friction model [116]; and LuGre friction model [117].

The simplest model is the Linear viscous friction model, represented by Eq. (5-5), where f_v is the viscous friction coefficient. This model assumes that friction and angular velocity are linearly related.

$$F_{f_{viscous}} = f_v \dot{\delta} \tag{5-5}$$

In this contribution, the Coulomb friction model is complemented by taking into consideration the stribeck effect. The model is presented in Eq. (5-6), where f_c is the Coulomb coefficient, f_s is the static friction coefficient, and $\dot{\delta}_s$ is the stribeck velocity.

$$F_{f_{Coulomb}} = f_v \dot{\delta} + \left[f_c + (f_s - f_c)\, e^{\left(\dot{\delta}/\dot{\delta}_s\right)^2} \right] sign\left(\dot{\delta}\right) \tag{5-6}$$

The Dahl friction model considers the Coulomb friction with a delay due to the pre-sliding stage. The friction force is defined by Eqs. (5-7) and (5-8), where σ_0 is the rigidity coefficient and z is an auxiliary variable that represents the displacement in the pre-sliding stage.

$$F_{f_{Dahl}} = \sigma_0 z \tag{5-7}$$

$$\dot{z} = \dot{\delta} \left[1 - \frac{\sigma_0 z}{f_c} sign\left(\dot{\delta}\right) \right] \tag{5-8}$$

The LuGre friction model is an extension of Dahl's model, which better describes both static and dynamic friction characteristics [118]. The model is described by Eqs. (5-9) and (5-10), where σ_1 is the damping coefficient.

$$F_{f_{LuGre}} = \sigma_0 z + \sigma_1 \dot{z} + f_v \dot{\delta} \tag{5-9}$$

$$\dot{z} = \dot{\delta} \left[1 - \frac{\sigma_0 z}{f_c + (f_s - f_c)\, e^{\left(\dot{\delta}/\dot{\delta}_s\right)^2}} sign\left(\dot{\delta}\right) \right] \tag{5-10}$$

5.3 Proposed approach

This contribution proposes a novel hybrid model that combines a phenomenological model, i.e., a gray-box model, with a NARX model, which is described in Section 3.2. The hybrid is represented as a block diagram in Figure 5.6.

Four different friction models, described in Section 5.2.3, were tested. Therefore, four gray-box models and four hybrid models were obtained, differing by the friction model employed in the eSEA modeling. The model known parameters are presented in Table 5.1 and the unknown parameters are those related to the friction models. The gray-box identification was performed using the methodology described in Section 3.1.

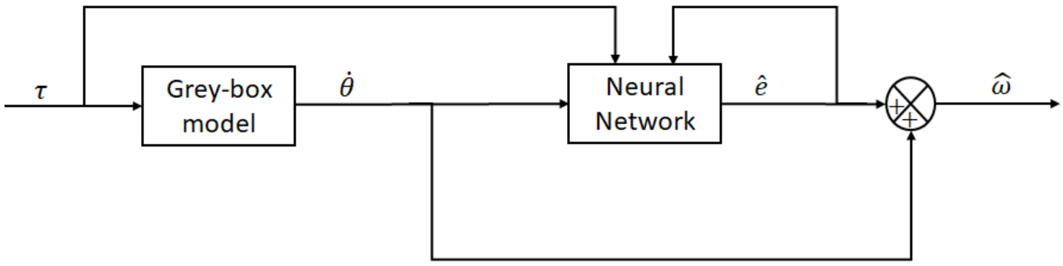

Figure 5.6: Block diagram of the proposed hybrid model.

Table 5.1: eSEA model parameters.

Parameter	Value
I	0.0014 m^4
J	0.0001 m^4
K_e	8.459 $N \cdot m/rad$

The identification of the NARX model was performed to predict the error between the measured data and the gray-box model, as mentioned before. The model considers the motor torque τ and the gray-box angular velocity simulations $\dot{\theta}$ as inputs. Consequently, the NARX model can be represented by the following equation:

$$\begin{aligned} \hat{e}\,(t) = F[&\hat{e}\,(t-1)\,, \ldots, \hat{e}\,(t-n_{\hat{e}})\,, \tau\,(t-1)\,, \ldots, \tau\,(t-n_{\tau})\,, \\ &\dot{\theta}\,(t-1)\,, \ldots, \dot{\theta}\,(t-n_{\dot{\theta}})] \end{aligned} \tag{5-11}$$

where $n_{\hat{e}}$, n_{τ}, and $n_{\dot{\theta}}$ are, respectively, the model regression orders of the error, the motor input torque, and the link angular velocity data.

The hybrid model output $\hat{\omega}$ is, then, the combination of the estimated output of the gray-box model $\dot{\theta}$ with the estimated error of the NARX model $\hat{e}$, as represented in Eq. (5-12):

$$\hat{\omega} = \dot{\theta} + \hat{e} \tag{5-12}$$

5.4 Results

In the following, the results obtained in the application of the proposed hybrid identification technique in the eSEA are presented. The first step is the gray-box identification to obtain the phenomenological models of the system. In the sequence, the black-box identification is performed to obtain a model that describes the error between the gray-box model simulations and the system data. A black-box model is identified for each gray-box model. The combination of both identified models results in the proposed hybrid model, whose results are compared with the gray-box model. Finally, the models are tested using the validation data in order to evaluate their performance with a different dataset.

5.4.1 Gray-box identification

The gray-box identification was performed as described in Section 3.2 to obtain the phenomenological models of the eSEA. By this process, the unknown parameters from the models are obtained, whose values are shown in Table 5.2. Figure 5.7 contains the comparison between the gray-box models and the experimental data.

Table 5.2: Estimated parameter values.

	Linear	Coulomb with Stribeck	Dahl	Lugre
f_v	0.0100	0.0098		0.0046
f_c		0.0089	0.0280	0.0089
f_s		0.0011		0.4987
$\dot{\delta}_s$		0.0075		$1.0201 \cdot 10^{-4}$
σ_0			5.520	0.2263
σ_1				0.0017

From the analysis of Figure 5.7 it is observed that the models followed the system behavior with amplitude errors. Furthermore, the frequency spectrum comparison shown in Figure 5.8 presents the range of frequencies in which the gray-box models have the best fit and the offset error of the models indicated by the difference of amplitude at 0 Hz frequency. The analysis of this figure shows that the Dahl model has a higher offset error. This behavior affects the model metrics presented in Table 5.4.

5.4.2 Hybrid gray and black-box identification approach

The black-box identification was performed in order to predict the gray-box error, which is shown in Figure 5.9. It is possible to observe that the error contains a high-frequency oscillation component. This high-frequency component occurs because of the high-frequency oscillations presented in the link angular velocity data, as shown in Figure 5.3, when the acceleration changes its direction, i.e., the oscillations on the peaks and the valleys of the graphic.

Several NARX models were tested, differing in the model order, the number of hidden layers, and the number of neurons per layer. The range

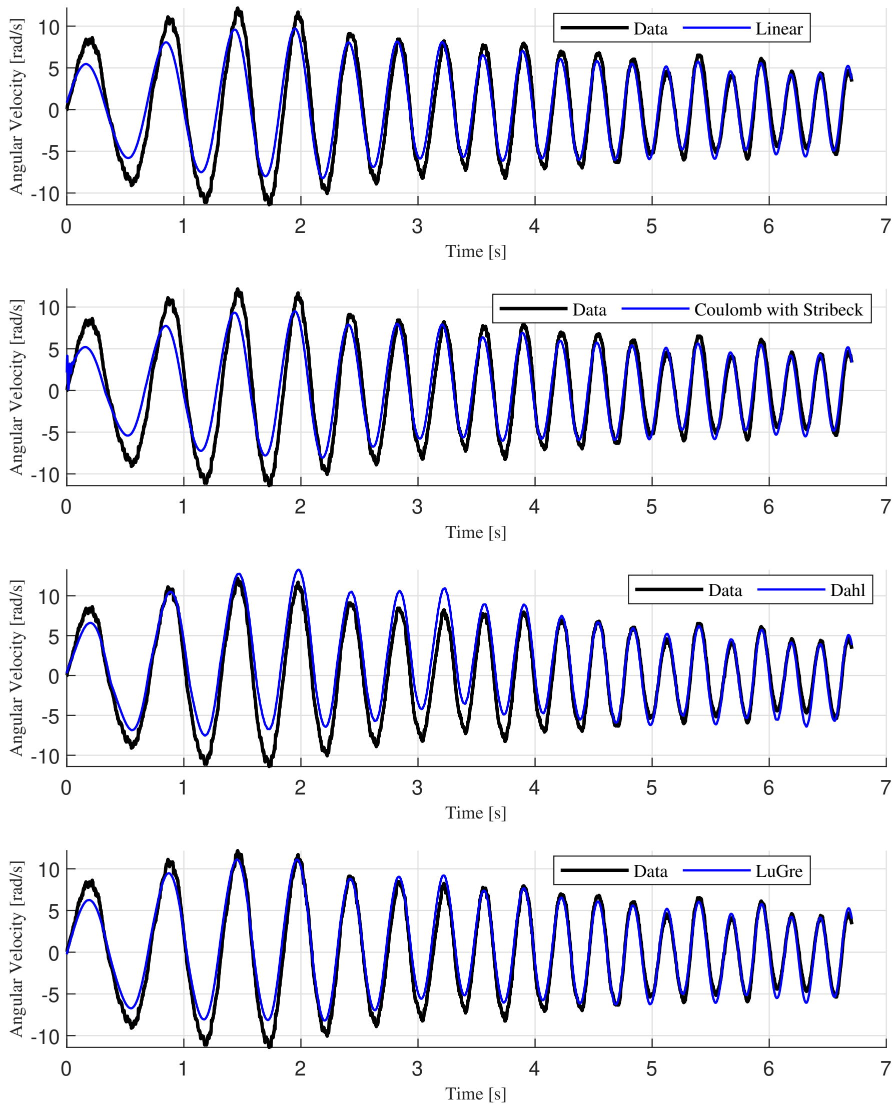

Figure 5.7: Result comparisons between the gray-box simulations and the identification data showing that the models are capable of describing the system behavior satisfactorily.

of parameter values tested is presented in Table 5.3. For all the cases, the best results were obtained by the model with 4 hidden layers, 256 neurons per layer, and model orders $n_{\hat{e}} = 9$, $n_{\tau} = 6$, and $n_{\dot{\theta}} = 8$, according to R^2 metrics. Figure 5.9 contains the comparison between the obtained NARX model free-run prediction and the error data. As seen in the Figure, the NARX models were able to adequately represent the complex behavior of the gray-box models error.

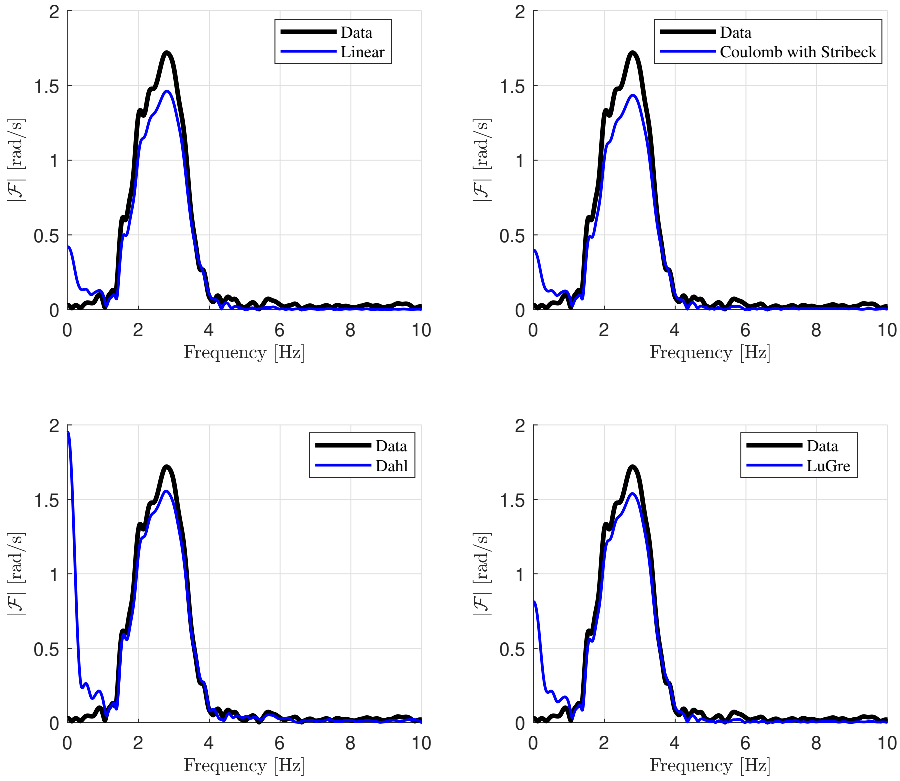

Figure 5.8: Frequency spectrum comparison between the gray-box simulation and the experimental data showing the frequencies which the models fit best.

The proposed hybrid identification approach is applied by combining the gray and black-box models as in Eq. 5-12. The comparison between both models simulations – the gray-box model and the hybrid model, for each case – and the eSEA data is presented in Figure 5.10. The results show that the hybrid model was able to reduce the amplitude and offset errors. The same conclusion was drawn from the analysis of the frequency spectrum comparison shown in Figure 5.11, where it was possible to observe that the hybrid model obtained a better fit throughout the range of frequencies analyzed. The metrics values for the hybrid models are presented in Table 5.4, which summarizes the metrics values obtained for each model for better analysis, and draws an accuracy comparison between the gray-box and the hybrid model by the analysis of MSE reduction. The results showed that the hybrid models present a MSE up to 89% smaller than the gray-box models.

Table 5.3: NARX neural network parameters values tested.

Parameter	Range of values
Model order	$1 \leq n_{\hat{e}}, n_{\tau}, n_{\dot{\theta}} \leq 10$
Number of hidden layers	$2 \leq n_{layers} \leq 6$
Number of neurons per layer	$8 \leq n_{neurons} \leq 1024$

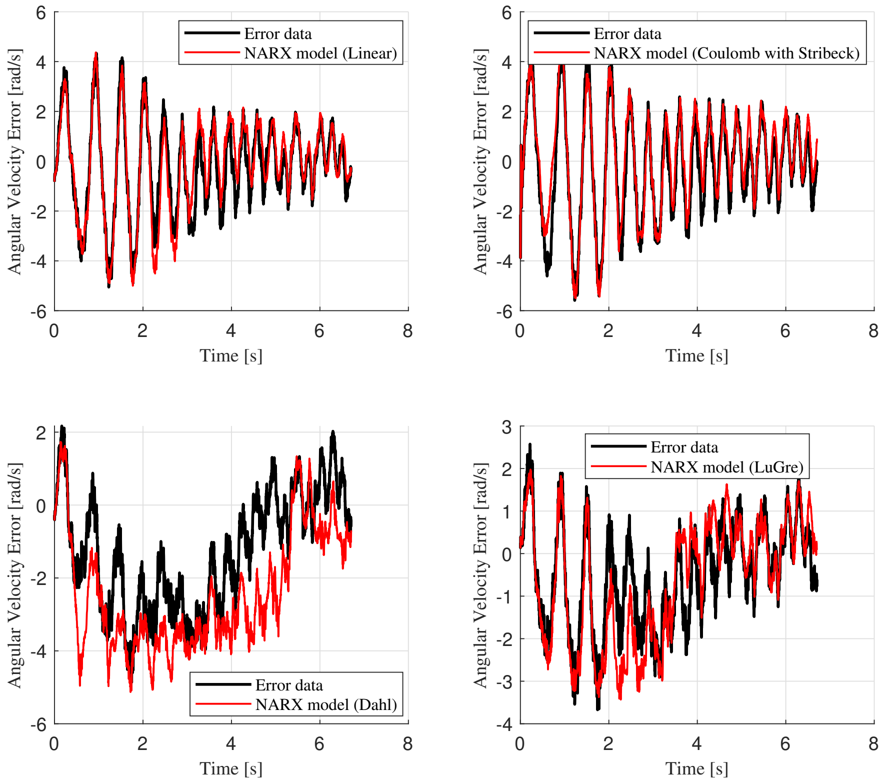

Figure 5.9: Comparison between the gray-box model error data and the NARX model free-run prediction demonstrating that NARX models were able to accurately predict the errors of the gray-box models.

Table 5.4: Model metrics comparison (Identification).

Model	MSE	R^2	MSE reduction
Linear	3.3253	0.8989	84.91%
hybrid model (Linear)	0.5018	0.9847	
Coulomb with Stribeck	4.5041	0.8630	89.42%
hybrid model (Coulomb)	0.4765	0.9855	
Dahl	4.1782	0.8729	47.30%
hybrid model (Dahl)	2.2018	0.9330	
LuGre	1.7023	0.9482	60.95%
hybrid model (LuGre)	0.6648	0.9798	

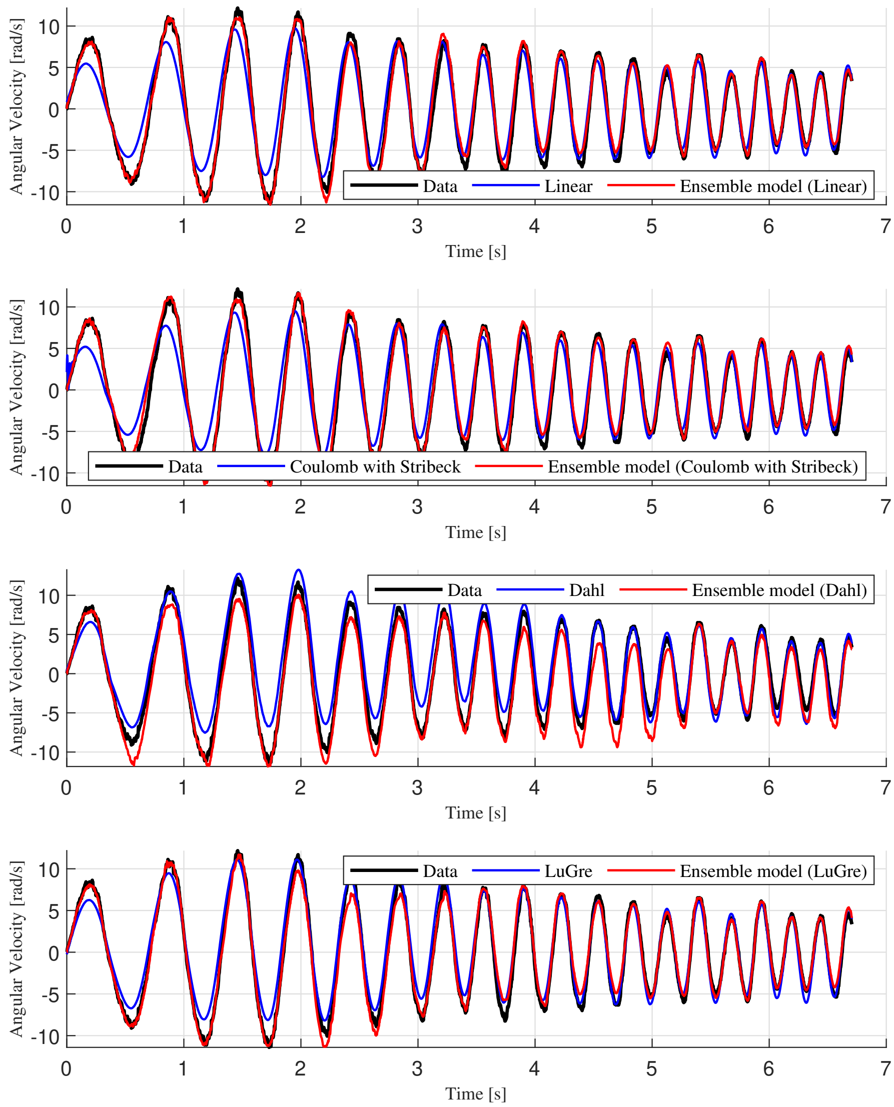

Figure 5.10: Result comparison between the gray-box simulations, hybrid model simulations, and the identification data showing the enhanced accuracy of the hybrid models.

5.4.3 Validation

In the validation process, the validation data is used to evaluate the performance of the models identified in the previous sections over a different data set. First, the performance of the gray-box models is evaluated, then, the black-box models are used to predict the gray-box models error. Finally, the results are combined to obtain the hybrid model simulations and then its performance is compared with the gray-box model.

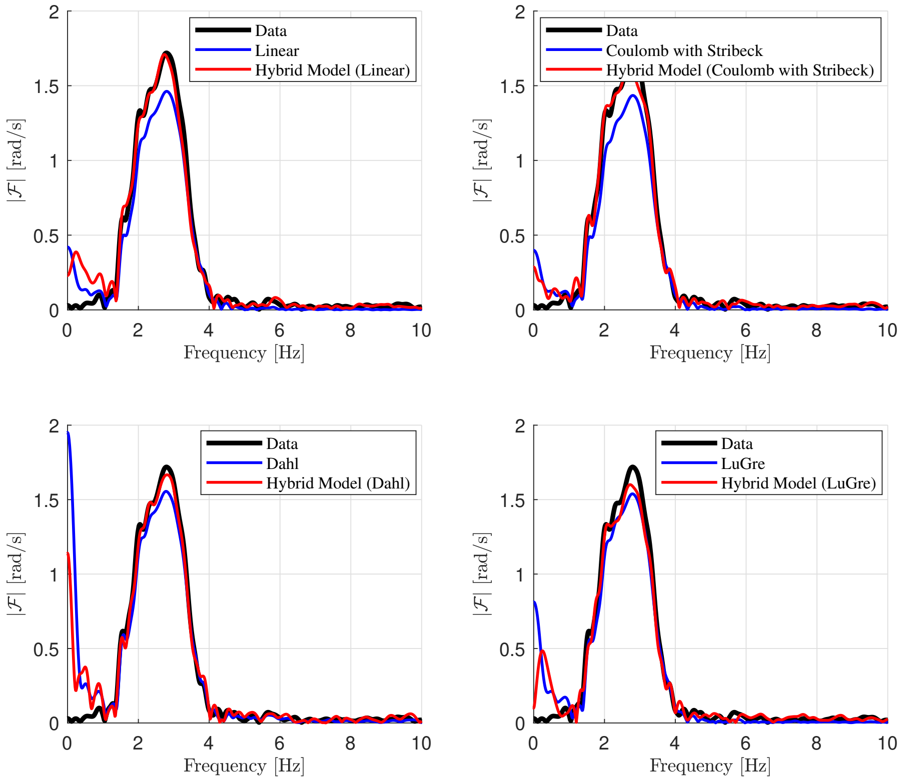

Figure 5.11: Frequency spectrum comparison between the gray-box simulation, hybrid model simulation and the identification data showing that the hybrid model results in a better fitting for all the frequencies considered.

Figures 5.12 and 5.13 contain the comparison between the gray-box model and the validation data in the time and frequency domain, respectively. These figures show that the models followed the system behavior with amplitude errors.

In the sequence, the NARX black-box models are used to predict the gray-box models error. Figure 5.14 presents the comparison between the error data and the NARX black-box model free-run simulation. Even though the results are not as good as the ones obtained in the identification process, the models were able to predict the error with considerable accuracy, except for the case of the Dahl model, where the NARX model did not present a good fitting.

Finally, both gray and black-box models are combined to obtain the hybrid models simulations, which are presented in time and frequency domain in Figures 5.15 and 5.16, respectively. These figures show that, even though the NARX predictions are not as accurate as the ones with the identification data, the hybrid model is still able to enhance the accuracy, except for the Dahl case, as verified by analyzing the model metrics in Table 5.5.

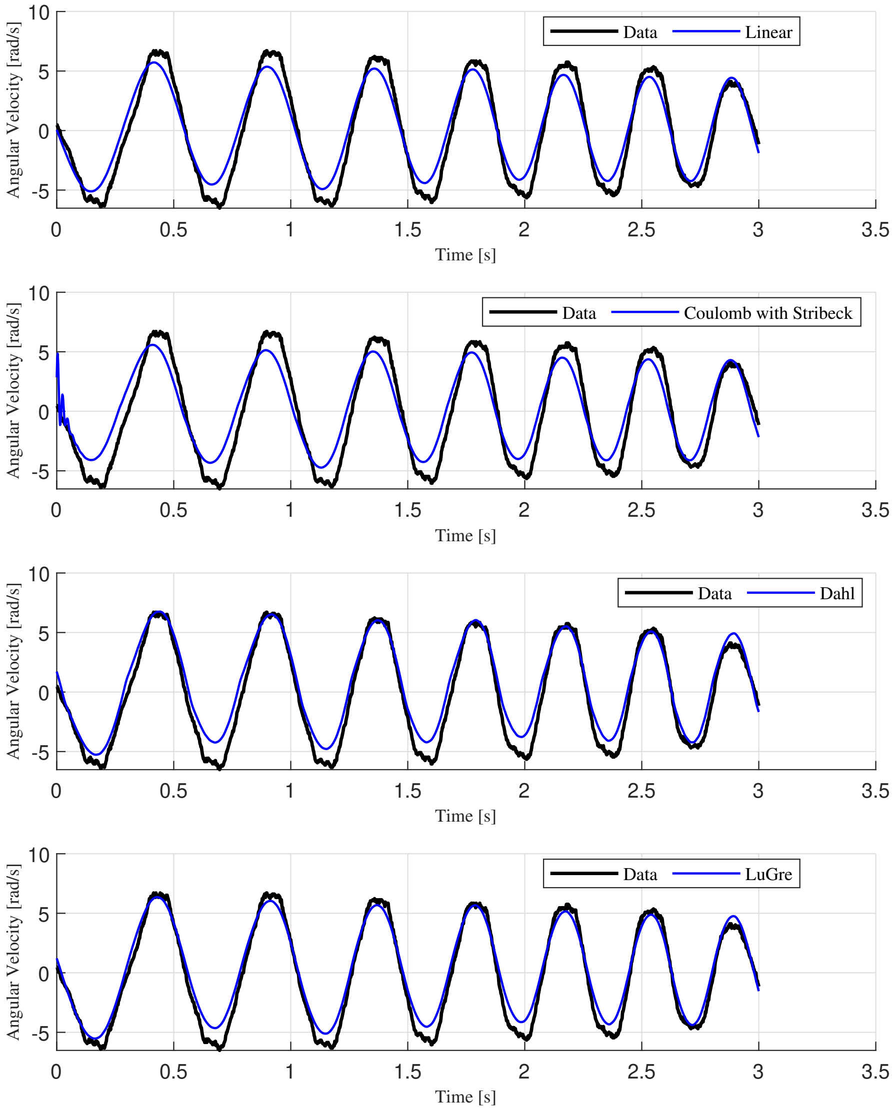

Figure 5.12: Result comparisons between the gray-box simulations and the validation data showing that the models are capable of describing the system behavior satisfactorily.

5.5 Results discussion

There are several advantages to using an elastomer-based compliant element, including cost reduction. However, due to the compliant material, some nonlinear behavior is expected under faster dynamics. This behavior was observed in the higher frequency region of the experimental data. Moreover, in addition to the compliant element nonlinear behavior, the eSEA may present other sources of nonlinearities, such as friction and assembly misalignment.

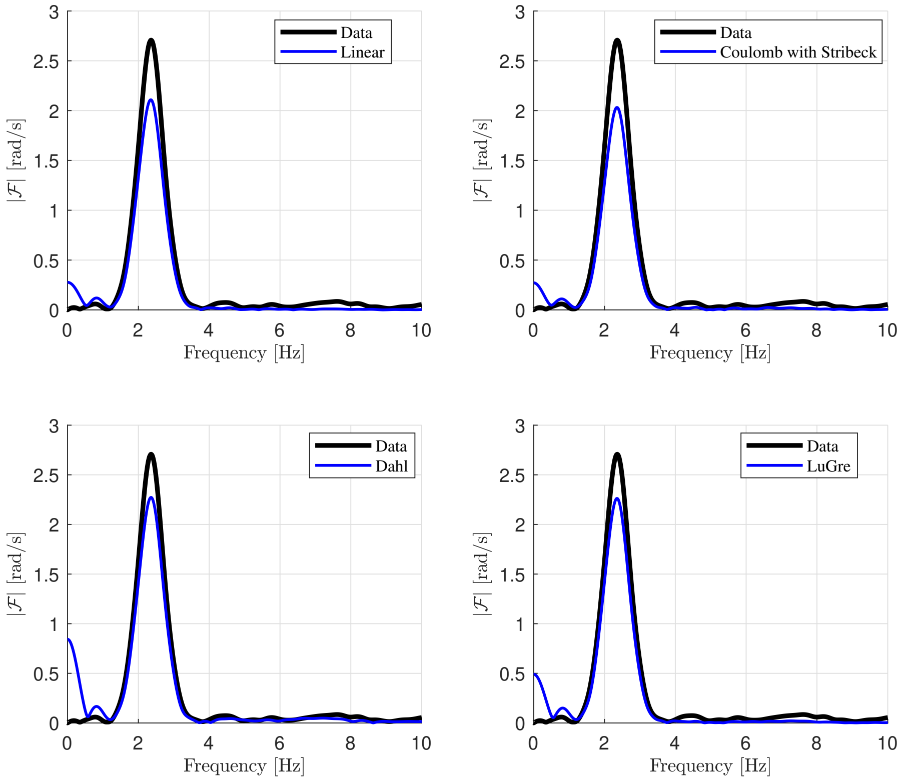

Figure 5.13: Frequency spectrum comparison between the gray-box simulation and the validation data showing the frequencies which the models fit best.

Table 5.5: Model metrics comparison (Validation).

Model	MSE	R^2	MSE reduction
Linear	1.3800	0.9229	61.26%
hybrid model (Linear)	0.5346	0.9701	
Coulomb with Stribeck	1.5279	0.8695	15.09%
hybrid model (Coulomb)	1.2974	0.9059	
Dahl	1.0859	0.9341	−27.20%
hybrid model (Dahl)	1.3813	0.8933	
LuGre	0.7609	0.9575	5.05%
hybrid model (LuGre)	0.7225	0.9596	

For the gray-box identification, the eSEA compliant element is considered a linear elastic material, and four different friction models are used to model the friction force acting in the system. Comparing the results in Figure 5.7, it is observed that all the gray-box models result in similar simulations, a fact also observed when comparing the results in the frequency domain in Figure 5.8. The metrics presented in Table 5.4 show that the LuGre gray-box model is the most accurate, followed by the Linear model, the Dahl model, and the Coulomb model. Nevertheless, all the models metrics values are close.

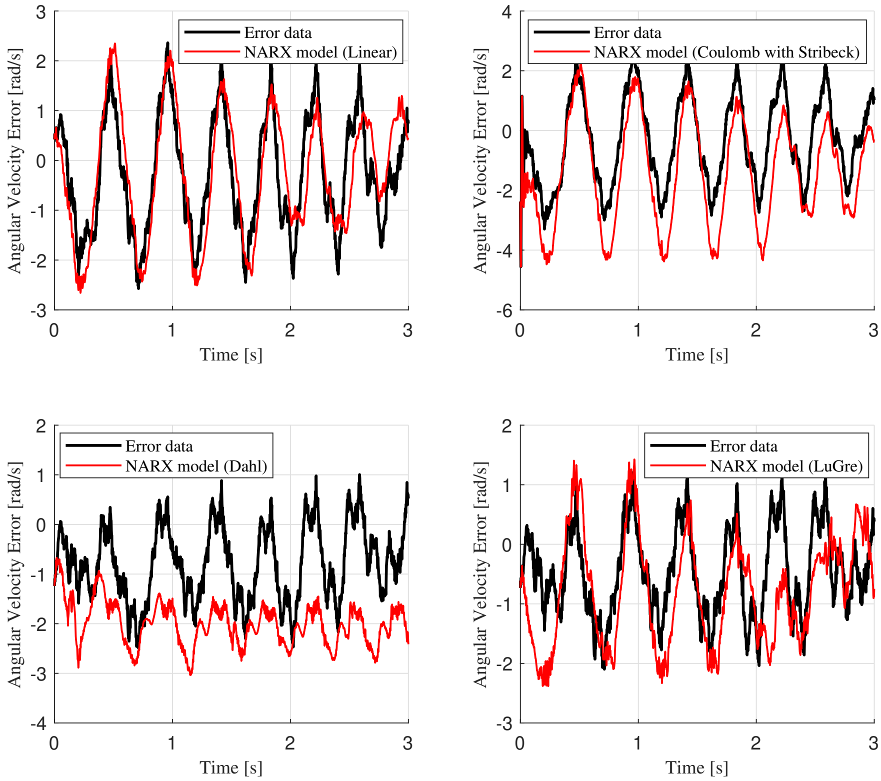

Figure 5.14: Comparison between the gray-box model error data and the NARX model free-run prediction considering the validation data.

Therefore, depending on the application, the linear gray-box box model would be a better choice for it is the simplest yet accurate, and may provide the necessary physical information about the system. Based on the results, it is possible to conclude that the error between the gray-box model and the experimental data is mostly due to unmodeled nonlinearities.

To deal with the system unmodelled nonlinearities, a black-box identification is performed in order to adjust a NARX model to predict the nonlinear error of the gray-box models. The results, presented in Figure 5.9, showed that the NARX model is capable of predicting the nonlinear error despite its complex behavior, however, for the Dahl case the fitting was not as good as the other cases.

Then, the proposed hybrid approach is applied by combining the models. The resulting hybrid models accurately predict the system behavior, including the nonlinearities associated with the compliant element behavior under fast dynamics, as seen in Figures 5.10 and 5.11. The models accuracy can also be evaluated from the analysis of the hybrid models metrics shown in Table 5.4, which indicates that the hybrid models are up to 89% more accurate than the respective gray-box models.

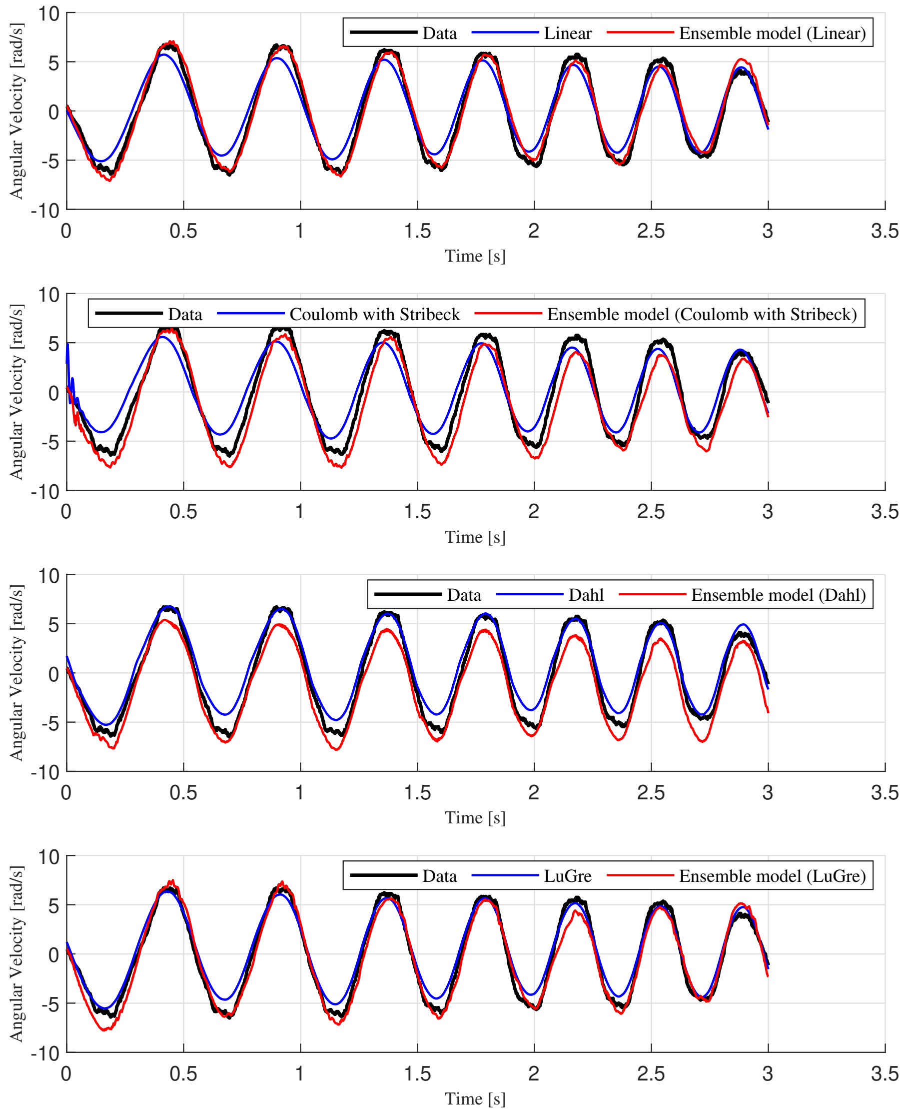

Figure 5.15: Result comparison between the gray-box simulations, hybrid model simulations, and the experimental data showing the enhanced accuracy of most of the hybrid models.

Finally, the identified models are tested using the validation data. The validation data consists of a swept-sine signal with different amplitude and frequency ranges. As expected, the results were not as good as the ones obtained with the identification data. However, the gray-box models were still able to follow the system behavior but with an amplitude error as seen in Figures 5.12 and 5.13. The metrics in Table 5.5 show that, for the validation data, the LuGre model is the most accurate, followed by the Dahl model, the Linear model, and the Coulomb model.

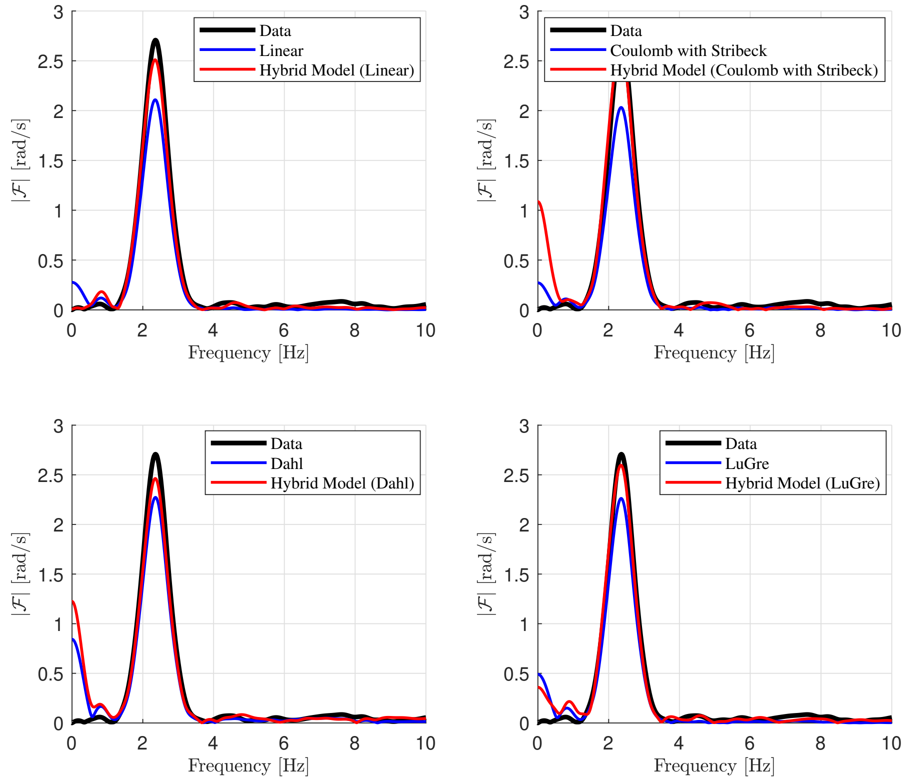

Figure 5.16: Frequency spectrum comparison between the gray-box simulation, hybrid model simulation and the experimental data showing that the hybrid model results in a better fitting for all the frequencies considered, with the exception of the Dahl model.

The NARX models free-run simulations were performed to predict the gray-box validation error. The NARX models were able to predict the validation error with considerable accuracy, as presented in Figure5.14. The exception is the case of the Dahl model for which the selected architecture was not able to satisfactorily predict the error. The hybrid simulations for the validation data are obtained by combining the gray and black-box simulations. The results presented in Figures 5.15 and 5.16 and Table 5.5 show that the hybrid model is able to increase the model accuracy in the majority of the cases. In fact, the Linear and LuGre models present an R^2 coefficient greater than 0.95, with a highlight for the linear model with $R^2 = 0.9701$, and 61.26% more accurate than the gray-box model. This level of accuracy and the physical information provided by the hybrid models make them suitable to be used in the construction of a digital twin of the eSEA.

The validation results showed that, when considering only the gray-box model, the more accurate model is the LuGre, followed by the Dahl, Linear, and Coulomb models. This indicates that the first two models are capable to address some of the nonlinearities of the system, and, therefore are more accurate. However, when the ensemble models are considered, the Linear model is the more accurate, followed by the LuGre, Dahl, and Coulomb models. The author interprets it as nonlinearities contained in the LuGre and Dahl models errors are not completely addressed by the black-box model as the nonlinearities in the Linear model error, i.e., the NARX model have better results in estimating the nonlinearities of the system than correcting the nonlinearities estimations of the gray-box model. Furthermore, the Author highlights the Dahl model case where the NARX model was not able to predict the error, causing an increase of the MSE value, as shown in Table 5.5.

It is important to notice that the proposed approach does not limit the choice of the model for the gray-box identification, i.e., any desired model can be used, including nonlinear models. The desired physical information of the system will bound the model choice. Moreover, another important characteristic of the proposed hybrid model is that most of the nonlinearities that are not considered in the gray-box model are addressed in the black-box model.

In fact, the main objective of this article is to prove the effectiveness of models that combine gray and black-box models and actually show, with original experimental data, that the proposed approach leads to better results in terms of predictive capability while maintaining model interpretability. The method proposed is focused on providing the necessary phenomenological information with enhanced accuracy. The choice of the black-box NARX neural network was based on the author's previous experience and its wide adoption by the system identification community since the 90s [119]. The results have shown the capabilities of the NARX-NN in predicting the errors of most of the models, despite the well-known artificial neural networks sensitivity to over-fitting. However, those results have also shown that there is room for improvements, i.e., probably there is an architecture that will provide better results, but the author could not find it considering the time-consuming process of training a neural network.

Moreover, despite the results obtained in this paper, it is not possible to affirm that the ANN is the best choice, nor other machine learning models as stated by the no-free lunch theorems [120, 121]. Testing these and other models applicable to identification problems could be the subject of future work.

5.6 Summary

This contribution aims to propose a novel hybrid model approach to be applied in the modeling of an eSEA. The proposed hybrid models combine a gray-box model with a black-box NARX model. The gray-box model provides phenomenological insights into the system, while the NARX model is responsible for dealing with unmodelled nonlinearities. The results showed that the obtained hybrid models are capable of accurately predicting the eSEA behavior, while providing the desired physical information, making them suitable to be used in the construction of a digital twin.

Furthermore, the proposed approach is flexible in a sense that it allows the choice of any desired model for the gray-box identification, including nonlinear models. The choice is only bounded by the required information of the system. Consequently, its application can be extended to other dynamic systems [122].

6
A hybrid gray and black-box artificial neural network friction identification of robotic actuators

There is a growing interest in data-driven models with machine learning for modeling and control in the context of system identification. Researchers have recently found ways to blend physical knowledge into purely data-driven modeling, in order to further improve model quality for analysis and simulation. The present work proposes a novel hybrid model that combines phenomenological gray-box models with black-box artificial neural networks in the context of viscous friction modeling for manipulators. It can provide desired physical insight while enhancing accuracy by addressing unknown nonlinearities in a two-stage procedure. Firstly the nonlinear state-space gray-box model is obtained, and later an artificial neural network is inserted into the state-space model to compensate for unknown friction terms. The proposed hybrid combined approach is successfully applied to real-world data, being up to 48% more accurate than the phenomenological model in terms of mean squared error considering the validation data.

6.1
Problem Definition

Dynamic models are crucial in most engineering applications, such as design optimization, control synthesis, fault detection, and other simulation applications. However, obtaining an accurate dynamical model can be a quite difficult task due to system nonlinearities and parameter uncertainties [123]. Hence, over the years, numerous works on system identification have been conducted to fulfill that need, as can be seen in [124].

This contribution proposes a novel hybrid identification method that combines a gray-box model with a black-box model. Specifically, a phenomenological model, which contains all the physical information desired about the system is combined with an RBFNN used to address the unmodeled nonlinearities, which are considered as a friction force. The resulting model can provide both physical insight and accuracy while maintaining interpretability, desirable characteristics for a DT. The proposed methodology is applied in the identification of an Electromechanical Positioning System (EMPS) [125].

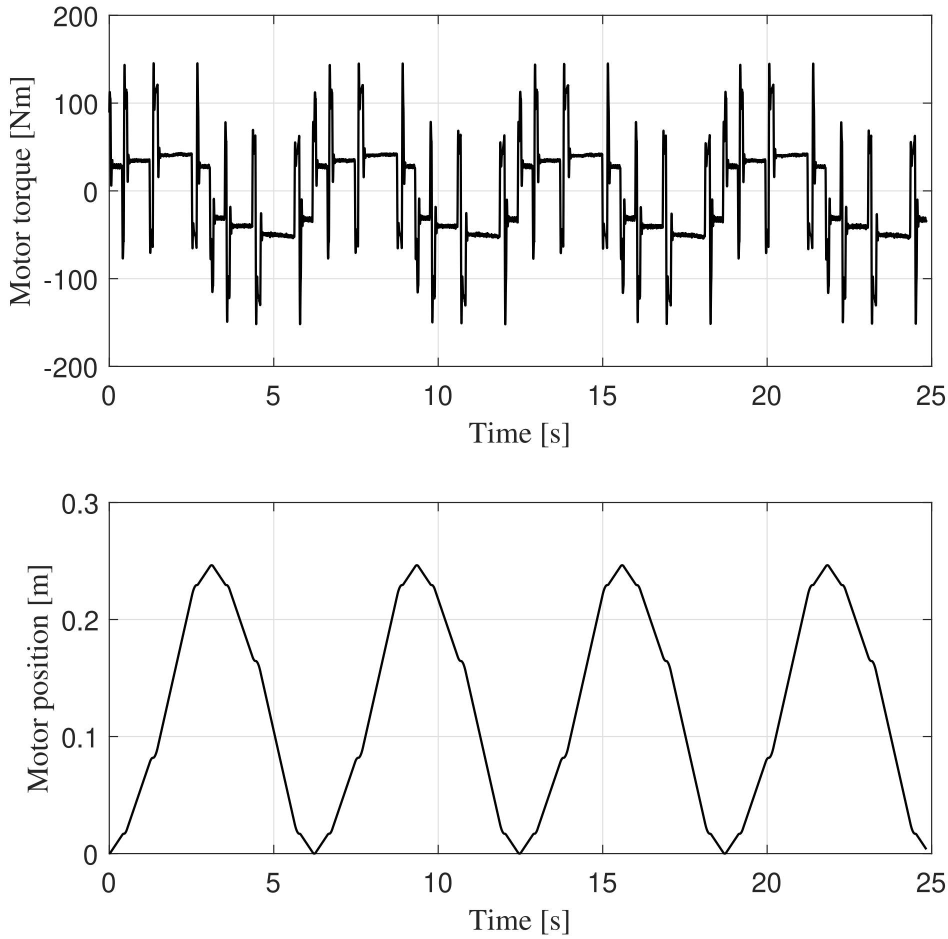

Figure 6.1: EMPS identification data [125].

6.2 Case Study

The EMPS is a standard actuator configuration commonly used in prismatic robotic joints and machine tools and it is described in detail in [125] whose authors kindly made the data available.

The system input signal is the motor torque τ and the output signal is the motor position expressed in the load side q_m. The datasets used in the identification and validation processes are the same ones presented in [125], and are shown in Figures 6.1 and 6.2, respectively. For more details about the system one shall recall to [125].

6.2.1 Electromechanical Positioning System

The EMPS is a relatively simple component and its dynamical equations can be obtained by applying Euler-Lagrange laws. Eq. (6-1) shows the dynamic

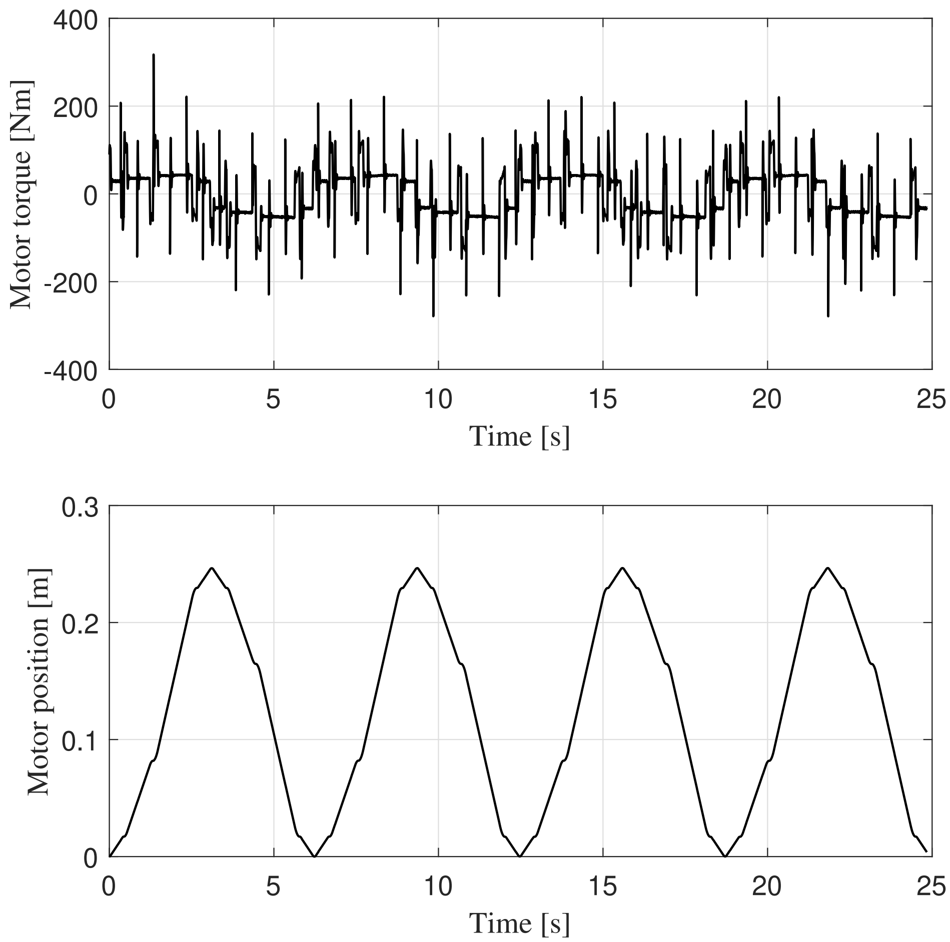

Figure 6.2: EMPS validation data [125].

equation of the EMPS, which takes into consideration the offset effect:

$$M\ddot{y} = \tau - F_f\left(\dot{y}\right) - offset \tag{6-1}$$

where M is the system mass; F_f is the friction force; and y, $\dot{y}$ and $\ddot{y}$ are the motor position, velocity, and acceleration, respectively.

For the friction force, it is considered that the system is subjected to a viscous friction force and a symmetrical Coulomb friction force. Therefore, the friction force equation is:

$$F_f\left(\dot{y}\right) = f_v\dot{y} + f_c sign\left(\dot{y}\right) \tag{6-2}$$

where f_v and f_c are, respectively, the viscous and the Coulomb friction coefficients. Defining the state vector as $\mathbf{y} = \left[y\ \dot{y}\right]^T$ and the input as $\mathbf{h} = [\tau]$, the dynamic equation (6-1) in the state-space form is $\dot{\mathbf{y}} = f\left(\mathbf{y}, \mathbf{h}\right)$ and is presented as follows:

$$\dot{\mathbf{y}} = \begin{bmatrix} \dot{y} \\ \frac{\tau - f_v \dot{y} - f_c sign(\dot{y}) - offset}{M} \end{bmatrix} \tag{6-3}$$

6.3 Proposed Approach

This contribution proposes a model with a hybrid architecture that combines a phenomenological gray-box model with a nonlinear friction RBFNN. The objective is to address the nonlinearities not modeled by the gray-box model as a nonlinear friction force modeled as an RBFNN. Therefore, the first step is to perform the gray-box identification to obtain the parameters of the phenomenological model. In this model, the unknown parameters are the system mass M, the viscous friction coefficient f_v, the Coulomb friction coefficient f_c, and the system offset.

In the sequence, The EMPS dynamic equations are modified to include the RBFNN, reminding that the parameters M, f_v, f_c, and $offset$ are determined in the gray-box identification process:

$$M\ddot{y} = \tau - F_f\left(\dot{y}\right) - F_{rbf}\left(\dot{y}\right) - offset \tag{6-4}$$

The RBFNN for the case study is presented in Figure 6.3. Thus, the nonlinear friction force F_{rbf} is calculated as follows:

$$F_{rbf} = \sum_{k=1}^{m} w_i \phi\left(\dot{y}\left(t\right), c_i, \sigma_i\right) \tag{6-5}$$

where c_i and σ_i are, respectively, the centers and the width of i^{th} hidden node, w_i is the output weight, and m is the number of hidden nodes. The Gaussian activation function is used as $\phi\left(\cdot\right)$:

$$\phi = exp\left[-\frac{\left(\dot{y}\left(t\right) - c_i\right)^2}{2\sigma_i^2}\right] \tag{6-6}$$

The black-box identification is performed in order to determine the RBFNN parameters, namely, c_i, σ_i, and w_i, given that different numbers of hidden nodes were tested. Notice that, the black-box identification is similar to the gray-box identification, thus, the same approach is used, i.e., to determine the network parameters, an optimization problem was solved using the method described in Section 3.1.

6.4 Results

In the following, the results obtained by applying the proposed approach to the EMPS are presented. Firstly, the gray-box identification is performed to obtain the phenomenological model, and then, using the parameters obtained

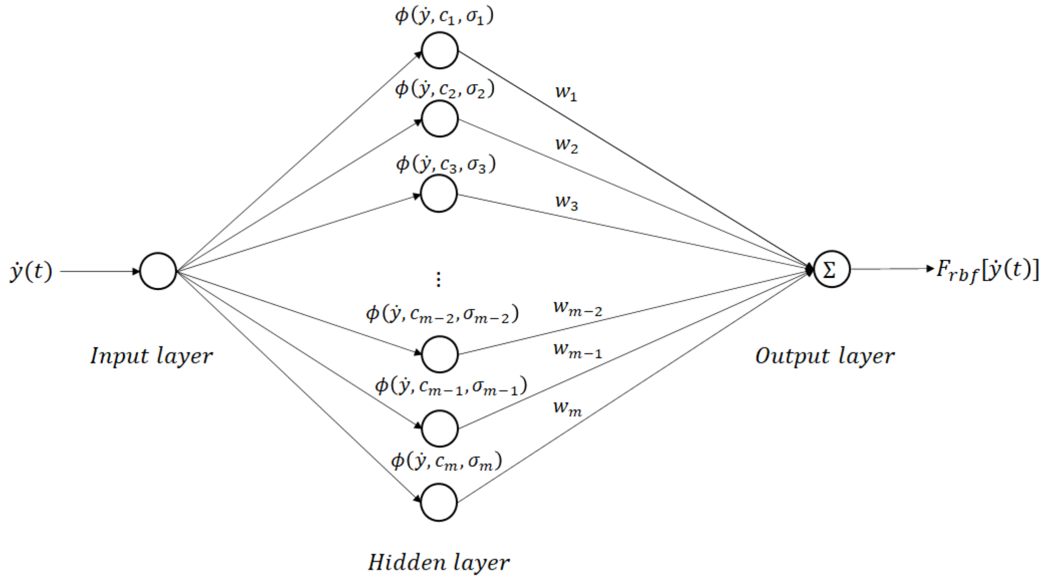

Figure 6.3: RBFNN schematics for the case study.

in the gray-box identification, the model shown in Eq. (6-4) is used to perform the black-box model identification where the RBFNN parameters are adjusted. With both models, it is possible to derive the hybrid model, whose metrics are compared with the gray-box model in order to assess the improvements that can be achieved. Finally, the models are evaluated using the validation data to verify the performance of the models using a different dataset. These steps are detailed in the following.

6.4.1 Identification

First, the gray-box identification was performed to obtain the unknown parameter of the model represented in Eq. 6-1. For the case study, the parameters searching intervals are presented in Table 6.1, which were based on the research presented in [125]. The unknown parameters obtained by this process are shown in Table 6.2 and the model metrics in Table 6.3.

Table 6.1: Models parameters searching interval.

	Searching interval
Gray-box	$30 \leq M \leq 150$
	$100 \leq f_v \leq 300$
	$0 \leq f_c \leq 40$
	$-15 \leq offset \leq 15$
RBFNN	$-1 \leq c_i \leq 1$
	$0.01 \leq \sigma_i \leq 1$
	$-100 \leq w_i \leq 100$

The gray-box model metrics show that the model can be considered accurate, considering its small value of MSE and the R^2 near 1. These results show that the gray-box identification method used was able to adjust the chosen dynamic model reasonably, which explains most of the EMPS physics. As shown next, it is still possible to further improve the model by adding more terms in the viscous friction terms.

Table 6.2: Gray-box model parameters.

Parameter	Values
M	$95.4520\ kg$
f_v	$214.9261\ N \cdot s/m$
f_c	$19.3607\ N \cdot s/m$
$offset$	$-3.2902\ N$

The proposed hybrid dynamic model is presented in Eq. (6-4) where an RBFNN is used to model a nonlinear friction force whose objective is to address the unmodeled nonlinearities. The black-box identification aims to adjust the RBFNN parameters bearing in mind that the gray-box parameters presented in Eq. (6-4) were already tuned. The black-box term in the model is added thus to improve the simulation capabilities of the model by adjusting the black-box model related parameters in an open-loop simulation using the nonlinear hybrid state-space model. The range of the model's free parameters is presented in Table 6.1. For the sake of comparison, several RBFNNs were identified, differing only by the number of nodes, for which the values $N_{neu} = 4, 8, 16, 32$ were tested.

The quantitative metrics for the hybrid model are presented in Table 6.3, where the hybrid model MSE reduction is also presented, in percentage, when compared to the gray-box model. The MSE reduction is used to evaluate the accuracy increase when adopting the strategy herein proposed.

Table 6.3: Model Metrics (Identification).

Model	MSE	R^2	MSE reduction
Gray-box	0.0049	0.9965	
Hybrid - 4 nodes RBFNN	0.0036	0.9981	26.3111%
Hybrid - 8 nodes RBFNN	0.0036	0.9981	26.7965%
Hybrid - 16 nodes RBFNN	0.0036	0.9981	26.4054%
Hybrid - 32 nodes RBFNN	0.0037	0.9980	25.4198%

Comparing the metrics presented in Table 6.3 for the identification process, it is possible to observe that the hybrid models show similar metrics, with the model with 8 nodes presenting the highest MSE reduction. This indicates that the RBFNN architecture has a limit to which extent it can improve the gray-box model quality, as increasing its complexity does not imply further increasing model quality in the validation phase. Moreover, even though the gray-box model is considered quite accurate, as the R^2 metrics show, the proposed hybrid models can further increase the accuracy by more than 26%.

Considering that a dynamic model should ideally present a compromise between complexity and accuracy, the suitable choice among the hybrid models is the one with 4 nodes, for it provides accuracy increasing with the simplest architecture.

6.4.2 Validation

The goal of the validation process is to test whether the identified model can predict the system's dynamic behavior using a different input/output dataset than the one used for training. All the models were tested, and their metrics are presented in Table 6.4 with the best hybrid model found in the previous section.

Table 6.4: Model Metrics (validation).

Model	MSE	R^2	MSE reduction
Gray-box	0.0069	0.9930	
Hybrid - 4 nodes RBFNN	0.0036	0.9982	48.5478%
Hybrid - 8 nodes RBFNN	0.0035	0.9982	48.8818%
Hybrid - 16 nodes RBFNN	0.0035	0.9982	48.6024%
Hybrid - 32 nodes RBFNN	0.0036	0.9980	47.9066%

From the analysis of the validation metrics, one can noticed that the gray-box model presents an MSE 40.82% greater, which also affects the value of the R^2 coefficient, even though it is still above 0.9. However, when the metrics of the hybrid models are analyzed, the values are similar to the ones obtained in the identification process. Once again, the metrics of the hybrid models have similar values. For all the hybrid models, the MSE reduction is around 48%, with the model with 8 nodes presenting the greatest MSE reduction. As in the identification stage, taking into consideration the necessary compromise between accuracy and complexity, one would choose the model with 4 nodes, for it presents both desired characteristics. The comparison between the EMPS data and the 4-node hybrid model simulations is presented in Figure 6.4.

The analysis of Figure 6.4 allows the verification of the model accuracy, which confirms the metrics shown before. An accuracy comparison between the gray-box and hybrid models can be drawn from Figure 6.5, which contains the absolute value of the models' errors. The more close to zero the error curve

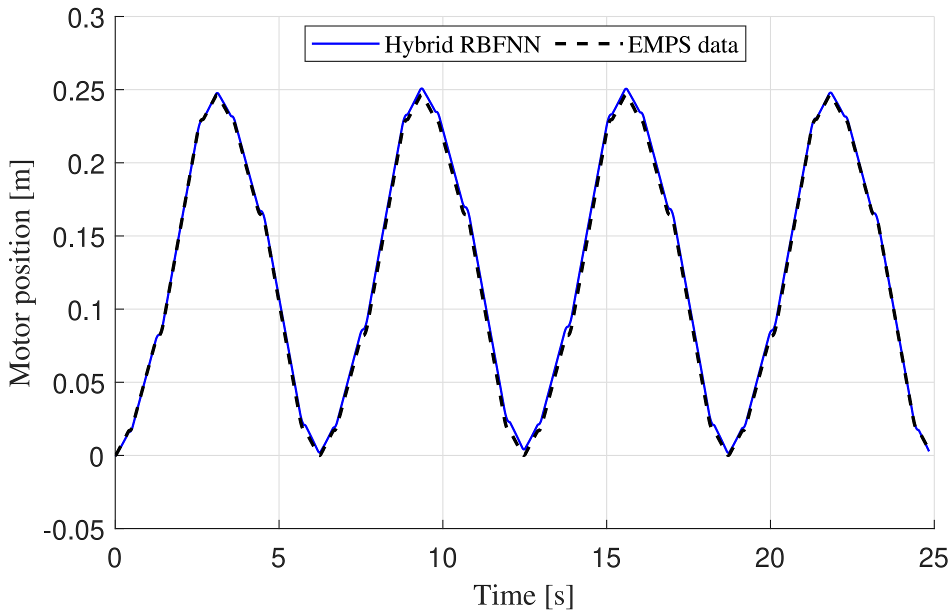

Figure 6.4: Result comparison between the hybrid model with 4 nodes and the EMPS validation data showing the model enhanced accuracy.

is, the more accurate the model is. In this figure, it is possible to observe that, on average, the hybrid model's absolute error is closer to zero, confirming its accuracy improvement. The same conclusion can be drawn by the raincloud plot of the error in Figure 6.6, where it is observed the distribution density of the hybrid model error is concentrated near zero. However, in Figure 6.6, notice that, even though the hybrid model has improved the error distribution, it is not a Gaussian distribution, which indicates that the dynamic model can still be refined.

In order to compare the influence of each model in the proposed hybrid model, the gray and black-box friction force curves were plotted in Figure 6.7, i.e., the curve of F_f, defined in Eq. (6-2), and F_{rbf}, defined in Eq. (6-5), are plotted over time. Figure 6.7 shows that the influence of the gray-box friction is greater than the black-box friction, though sufficient to considerably reduce the final error metric. It is interesting to note that, depending on the amplitude of the velocity, the RBFNN reduces or increases the final viscous friction.

The friction force curves of each model were also plotted over velocity, i.e., the gray-box model friction force (F_f) and the hybrid model friction force ($F_f + F_{rbf}$). Figure 6.8 shows this comparison, from which is possible to observe that the black-box friction influence is greater around $0m/s$, i.e., when the velocity changes its signal. It is also where the Coulomb friction discontinuity is placed. Although the black-box friction is smaller than the gray-box, and its influence is not limited to this region, it is sufficient to compensate for the

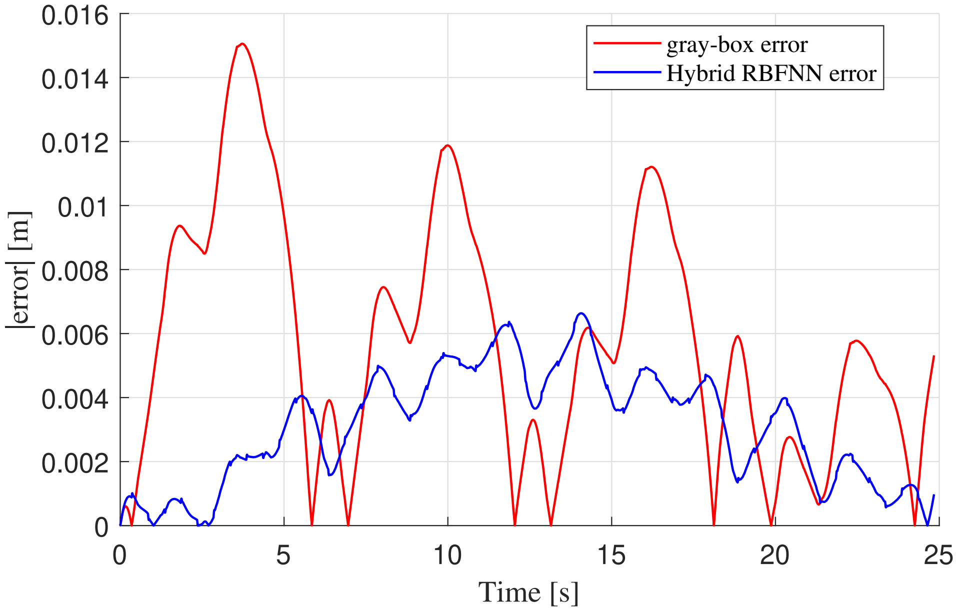

Figure 6.5: Comparison between the absolute value of the gray-box model and the hybrid model from which it is possible to observe the accuracy improvement.

effect of the Coulomb model's discontinuity. Furthermore, it is observed that the hybrid model friction force presents an unsymmetrical curvature, which indicates that there is a difference in friction depending on the velocity signal.

6.5 Discussion

The EMPS is a system extensively used in the industry in the construction of robotic manipulators and machine tools, which has challenging friction characteristics. It has been tested on other modeling approaches [126–129]. The dataset is thus used in this work as a benchmark for nonlinear systems, whose complexity may be extended to other case studies.

For the gray-box identification process, the model choice was based on the work of [125], which considers that the friction acting in the system can be modeled as a combination of viscous and Coulomb friction. The identification method based on the multiple shooting algorithm was able to adjust the model parameters, obtaining an accurate gray-box model with $R^2 = 0.9965$, which provides phenomenological insight into the EMPS.

On the basis of the parameters obtained in the gray-box identification, it is proposed a hybrid model, defined in Eq. (6-4), which contains a nonlinear friction force modeled as an RBFNN whose objective is to address the unmodeled nonlinearities. The black-box identification built with multiple shooting is performed for RBFNNs with varying complexity. The metrics in

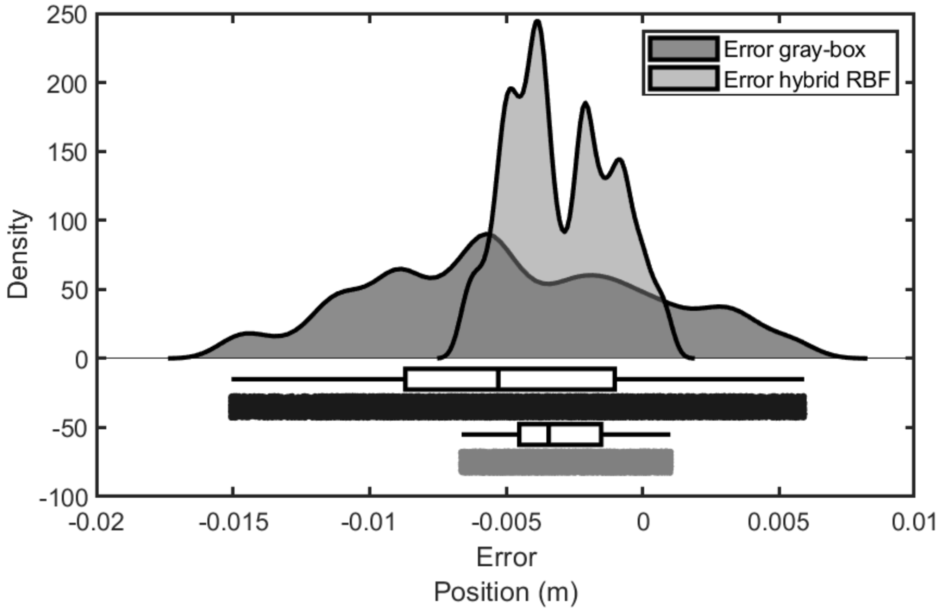

Figure 6.6: Raincloud plot of the gray-box and hybrid model errors.

Table 6.3 show that all the hybrid models presented an MSE reduction higher than 26%. This indicates that although the gray-box model is accurate, the proposed hybrid model was able to increase the accuracy.

The models were also validated using a different dataset. The metrics presented in Table 6.4 show that for the gray-box model, there is an increase in the MSE and consequently a reduction of the R^2 value when compared with the data on Table 6.3. However, the hybrid models present metrics with values similar to the ones obtained in the identification stage. Therefore, the hybrid models presented an MSE reduction higher than 48% when compared to the gray-box model for the validation data.

The aforementioned results showed that the gray-box method chosen was able to adjust a phenomenological model capable of describing most of the system physics, given its accuracy, which can be accessed from its metrics. The proposed hybrid model was able to increase the accuracy by over 26% in the identification process and 48% in the validation process. Moreover, the hybrid model's metrics do not show significant changes in values between identification and validation, thus indicating that the hybrid model in fact was able to generalize well the unmodelled nonlinearities, at least the ones excited by the used dataset.

Notice that, in the proposed hybrid identification method, the gray-box identification is performed first to guarantee the best fit between the system data and the gray-box model simulations, thus ensuring the model phenomenological insight. Then, to address the unmodelled nonlinearities,

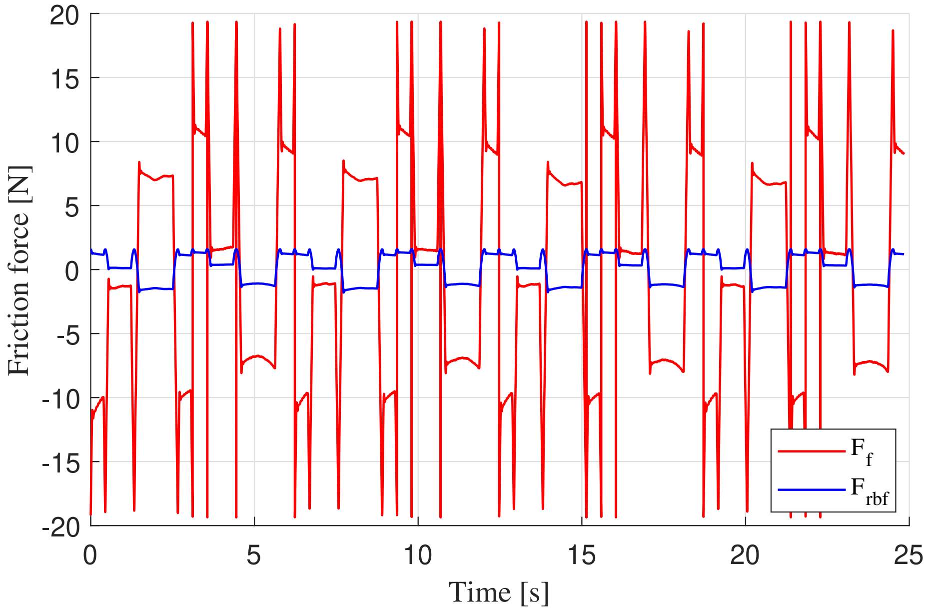

Figure 6.7: Comparison between the gray-box friction F_f and the black-box friction F_{rbf} from which is possible to infer their influence in the resulting hybrid model.

the black-box identification is performed. it is possible to verify this not only by the models' metrics in Tab 6.4 and Figures 6.5 and 6.6, but also by the friction force curves in Figures 6.7 and 6.8, where it is possible to evaluate the influence of each model in the system dynamics. Consequently, the proposed methodology provides a model with the characteristics of enhanced accuracy and interpretability that keeps a compromise with mathematical complexity. These are the desired characteristics of a dynamical model that would compose a DT. However, Figure 6.6 indicates that there is still a possibility for improvement. Several strategies can be employed to improve the model e.g. to use a richer signal that excites a wider range of frequency in the identification; and to use a different combination of models, i.e. gray-box models with different friction models and other black-box approaches such as SVM.

Additionally, the method herein presented may be further extended to other problems involving hybrid representations with machine learning and physics-based dynamic models. Such a concept is important, however, they are currently quite difficult to implement and simulate as done here. The use of modern deep or machine learning is still not straightforward to integrate with gray-box nonlinear state-space models as proposed. The reason is that, in order to create a physical model prior to model, one needs to encode such equations, which actually depend on the model characteristics. Yet, perhaps the greater difficulty is integrating modern black-box libraries to learn

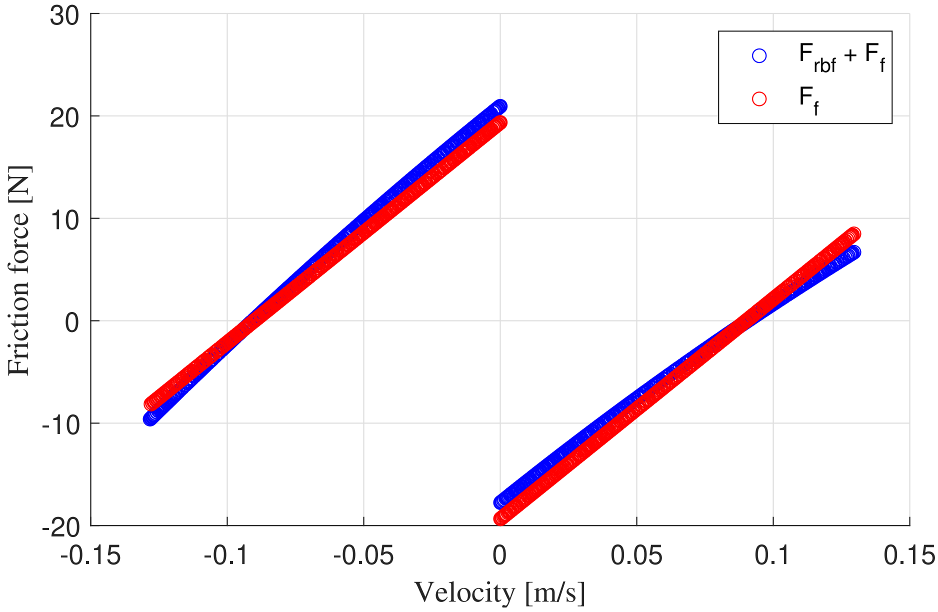

Figure 6.8: Friction force comparison over velocity, from which it is noticed the influence of the RBFNN friction over the region under influence of the Coulomb friction discontinuity.

unmodeled dynamics, as the learning process actually depends on a simulation. So the model should be built according to input and outputs that depend on each other due to the numerical integration, which turns the identification problem remarkably more difficult than a regular regression task.

Another aspect of the modeling paradigm that should be noted is that it is not always straightforward to define in which terms to add the black-box portion to the nonlinear state-space model. In the present example, the author knows that nonlinear friction is a disputed topic [130] and has thus decided to complement it by learning its shape directly from the data, which is nontrivial. However, that was forced by adding the black-box term to the acceleration equation and dependent on the velocity, which is quite typical in friction modeling. At the same time, some terms in the state-space should not be changed so as to maintain causality, as the equation related to the velocity, which is the derivative of position. Thus, it is necessary to add black-boxes where they might fit well in a complementary element to phenomenological modeling that does not create inconsistencies.

In spite of the difficulties and challenges discussed herein, the author hopes to motivate the use of hybrid models and the creation of toolboxes that are able to cope more easily with such problems, as the results show great improvement of the physics-based models by adding a black-box layer to the model without compromising interpretability.

6.6 Summary

Physics-based models have led to advances across engineering applications. However, numerical approximations or simplifications regarding a dynamic system may lead to a significant deviation from the measured data. Thus, the discrepancies between measured and predicted data occur even in systems where the mathematical representation is assumed to be well-known. Therefore, to cope with these problems, this paper proposes a novel hybrid identification approach combining a gray-box model with a black-box RBFNN. The gray-box model provides phenomenological information about the system in the proposed hybrid model. At the same time, the RBFNN architecture addresses the unmodeled nonlinearities.

The results demonstrated that the hybrid models have the potential to 1) accurately predict EMPS behavior while providing the desired physical information. These characteristics make the proposed approach suitable for constructing a DT; 2) be flexible, considering that it allows the choice of any desired model for the gray-box identification, bounded only by the required information of the system.

Part III

Final Remarks

7
Conclusions

This thesis aims to propose a hybrid identification approach where a gray-box model and black-box model are combined in order to obtain a dynamic model with the characteristics of enhanced accuracy and interpretability that keeps a compromise with mathematical complexity. These characteristics make such models interesting for the construction of a DT.

The results obtained from experimental data in all the contributions allow an overall conclusion that the obtained models hold the aforementioned characteristics, ergo, proving the efficiency of the proposed approach. Hereafter, the specific conclusions are addressed.

The first contribution aimed to model the vertical dynamics of a Toyota Hilux RWD using the data from the vehicle acquired during the transposition of a type-A bump. Therefore, a novel nonlinear hybrid half-car model for a vehicle's vertical dynamics is proposed through a hybrid identification technique that integrates gray-box and black-box identification. The proposed technique comprises three steps: firstly, adjusting the parameters of the half-car model through gray-box identification; secondly, obtaining a NARX model for the nonlinear error of the half-car model through black-box identification for each of the two chassis' degree of freedom; and finally, combining the models to form a hybrid model. The proposed method and resulting hybrid model are validated using experimental data, and the results demonstrate that the hybrid model fits the vehicle's data better than the linear half-car model, while remaining accurate and simple. Moreover, the proposed methodology successfully obtains a simple and accurate model for the vehicle's vertical dynamics using data from two chassis' degrees of freedom obtained by a single IMU. To this date, to the best of the knowledge of the author, there is no research on the application of hybrid models in vehicle vertical dynamics, and the results obtained encourage further research where other gray and black box combinations may be tested.

In the second contribution, the objective was to model an eSEA using experimental data. To fulfill this objective, a hybrid model approach for modeling an eSEA is proposed. The approach combines a gray-box model with a black-box NARX model, providing both phenomenological insights and the ability to handle unmodelled nonlinearities. The hybrid models accurately predict eSEA behavior and provide the desired physical information, with some models performing better than others. Additionally, the proposed approach is flexible and allows for the selection of any desired model for gray-box identification, including nonlinear models, limited only by the required information of the system. Therefore, the approach has the potential to be applied to other dynamic systems. Furthermore, the results have shown that there is still room for improvement and the approach flexibility should be tested over other machine learning techniques.

The third contribution objective was to model an EMPS system, which is a well-known benchmark for nonlinear modeling due to its challenging friction characteristics. Therefore, a hybrid modeling approach is applied to model the referred system. Physics-based models are the foundation stone of many advances in engineering applications, however, numerical approximations or simplifications of dynamic systems may result in significant deviations from measured data. To address this, we propose a novel hybrid identification approach that combines a gray-box model with a black-box RBFNN. The gray-box model provides phenomenological information about the system, while the RBFNN architecture addresses unmodelled nonlinearities. The results demonstrate that the proposed hybrid models have the potential to accurately predict EMPS behavior while providing the desired physical information. The approach is also flexible, allowing for the selection of any desired model for gray-box identification, limited only by the required information of the system. This approach differs from the other in a sense that the black-box model is inserted in the phenomenological model equations as nonlinear viscous friction, thus encouraging further research toward other hybrid model architectures.

Finally, regarding all the hybrid model structures proposed in this Thesis, notice that for the gray-box identification we have used an optimization approach based on the multiple shooting algorithm, which has shown to be able to deal with the ill-posed optimization problem defined by the gray-box identification. In addition, two different black-box models were used in this work, both based on artificial neural networks, namely, NARX neural network and RBFNN. The choice of neural network was based on the author's previous experience and its wide adoption by the system identification community, however, it may be sensible to overfit. Therefore, in the light of the herein obtained results, the method presented in this Thesis may be further extended to other problems involving hybrid representations with machine learning and physics-based dynamic models.

8
Future Works

From all results and discussions of each contribution, it is possible to suggest some future possible researches that may be conducted from those herein presented.

Regarding the application of hybrid models in vehicle systems, future research possibilities may include applying the proposed method in vehicles with more complex suspension systems, such as magnetorheological suspension, evaluating the hybrid model's performance, and applying it to the control synthesis of an active suspension system. Furthermore, currently, the method is focused on the half-car model, therefore, a possible expansion for a full-car model would consider more degrees of freedom, expanding the applicability of the method. In addition, in this work, the application of the methodology was focused on the vehicle vertical dynamics, therefore, future research may address the application of the methodology in the lateral dynamics, similarly to what was done in [131]. From lateral dynamics, it is possible to expand the applications to trajectory control.

Related to the second contribution, considering its application in robotics, future research can be focused on the application of the proposed methodology in SEA manipulators with more degrees of freedom, which can lead to the use of the hybrid model in the synthesis of an MPC trajectory control. Furthermore, different combinations of models can be tested, as the black-box approach enables different modeling paradigms than the ones proposed here [132].

The third contribution is also related to the field of robotics. Therefore, future work may focus on the application of the proposed methodology in other types of actuators with challenging friction characteristics such as hydraulic actuators. Moreover, the method proposed in the third contribution may also be used in the modeling of eSEA, however, focused on the compliant element nonlinear elasticity.

Bibliography

[1] NELLES, O.. **Nonlinear dynamic system identification**. In: NONLINEAR SYSTEM IDENTIFICATION, p. 547–577. Springer, Berlin, Heidelberg, 2001.

[2] VODYAHO, A. I.; ZHUKOVA, N. A.; SHICHKINA, Y. A.; ANAAM, F. ; ABBAS, S.. **About one approach to using dynamic models to build digital twins**. Designs, 6(2):25, 2022.

[3] JUAREZ, M. G.; BOTTI, V. J. ; GIRET, A. S.. **Digital twins: Review and challenges**. Journal of Computing and Information Science in Engineering, 21(3), 04 2021.

[4] GUO, J.; LV, Z.. **Application of digital twins in multiple fields**. Multimedia Tools and Applications, 81:26941–26967, 2022.

[5] BOTÍN-SANABRIA, D. M.; MIHAITA, A.-S.; PEIMBERT-GARCÍA, R. E.; RAMÍREZ-MORENO, M. A.; RAMÍREZ-MENDOZA, R. A. ; LOZOYA-SANTOS, J. D. J.. **Digital twin technology challenges and applications: A comprehensive review**. Remote Sensing, 14(6):1335, 2022.

[6] PAWAR, S.; AHMED, S. E.; SAN, O. ; RASHEED, A.. **Hybrid analysis and modeling for next generation of digital twins**. Journal of Physics: Conference Series, 2018(1):012031, 2021.

[7] LJUNG, L.. **Perspectives on system identification**. Annual Reviews in Control, 34(1):1–12, 2010.

[8] LEE, S.-D.; JUNG, S.. **Real-time rls-based joint model identification and state observer design for robot manipulators: Experimental studies**. International Journal of Control, Automation and Systems, 19(12):4025–4033, 2021.

[9] SINGH, K. B.; ARAT, M. A. ; TAHERI, S.. **Literature review and fundamental approaches for vehicle and tire state estimation**. Vehicle System Dynamics, 57(11):1643–1665, 2019.

[10] AHMEID, M.; ARMSTRONG, M.; GADOUE, S.; AL-GREER, M. ; MISSAILIDIS, P.. **Real-time parameter estimation of DC–DC converters using a self-tuned Kalman filter**. IEEE Transactions on Power Electronics, 32(7):5666–5674, 2016.

[11] GUIHAL, J.-M.; AUGER, F.; BERNARD, N. ; SCHAEFFER, E.. **Efficient implementation of continuous-discrete extended Kalman filters for state and parameter estimation of nonlinear dynamic systems**. IEEE Transactions on Industrial Informatics, 18(5):3077–3085, 2021.

[12] DAUM, F.. **Nonlinear filters: beyond the Kalman filter**. IEEE Aerospace and Electronic Systems Magazine, 20(8):57–69, 2005.

[13] FU, Z.; HAN, B. ; CHEN, Y.. **Levenberg–marquardt method with general convex penalty for nonlinear inverse problems**. Journal of Computational and Applied Mathematics, 404:113771, 2022.

[14] LUENGO, D.; MARTINO, L.; BUGALLO, M.; ELVIRA, V. ; SÄRKKÄ, S.. **A survey of monte carlo methods for parameter estimation**. EURASIP Journal on Advances in Signal Processing, 2020(1):1–62, 2020.

[15] RABIEYAN, H.; ARASTOU, A.; KARRARI, H. ; KARRARI, M.. **Mathematical modeling and parameter estimation of a coordinated turbine-boiler controlled steam power plant**. In: 2021 31^{st} AUSTRALASIAN UNIVERSITIES POWER ENGINEERING CONFERENCE, p. 1–6, Perth, Australia, 2021. IEEE.

[16] CORTEZ, R.; GARRIDO, R. ; MEZURA-MONTES, E.. **Spectral richness pso algorithm for parameter identification of dynamical systems under non-ideal excitation conditions**. Applied Soft Computing, p. 109490, 2022.

[17] DOKEROGLU, T.; SEVINC, E.; KUCUKYILMAZ, T. ; COSAR, A.. **A survey on new generation metaheuristic algorithms**. Computers & Industrial Engineering, 137:106040, 2019.

[18] HUSSAIN, K.; MOHD SALLEH, M. N.; CHENG, S. ; SHI, Y.. **Metaheuristic research: a comprehensive survey**. Artificial intelligence review, 52:2191–2233, 2019.

[19] MOLINA, D.; POYATOS, J.; SER, J. D.; GARCÍA, S.; HUSSAIN, A. ; HERRERA, F.. **Comprehensive taxonomies of nature-and bio-inspired optimization: Inspiration versus algorithmic behavior,**

critical analysis recommendations. Cognitive Computation, 12:897–939, 2020.

[20] SJÖBERG, J.; ZHANG, Q.; LJUNG, L.; BENVENISTE, A.; DELYON, B.; GLORENNEC, P.-Y.; HJALMARSSON, H. ; JUDITSKY, A.. **Nonlinear black-box modeling in system identification: a unified overview**. Automatica, 31(12):1691–1724, 1995.

[21] AYALA, H. V. H.; HABINEZA, D.; RAKOTONDRABE, M. ; DOS SANTOS COELHO, L.. **Nonlinear black-box system identification through coevolutionary algorithms and radial basis function artificial neural networks**. Applied Soft Computing, 87:105990, 2020.

[22] CHIUSO, A.; PILLONETTO, G.. **System identification: A machine learning perspective**. Annual Review of Control, Robotics, and Autonomous Systems, 2:281–304, 2019.

[23] GHADAMI, A.; EPUREANU, B. I.. **Data-driven prediction in dynamical systems: recent developments**. Philosophical Transactions of the Royal Society A, 380(2229):20210213, 2022.

[24] FAROUGHI, S. A.; PAWAR, N.; FERNANDES, C.; DAS, S.; KALANTARI, N. K. ; MAHJOUR, S. K.. **Physics-guided, physics-informed, and physics-encoded neural networks in scientific computing**. arXiv preprint arXiv:2211.07377, 2022.

[25] HAO, Z.; LIU, S.; ZHANG, Y.; YING, C.; FENG, Y.; SU, H. ; ZHU, J.. **Physics-informed machine learning: A survey on problems, methods and applications**. arXiv preprint arXiv:2211.08064, 2022.

[26] WICHARD, J. D.; OGORZAŁEK, M.. **Time series prediction with ensemble models applied to the cats benchmark**. Neurocomputing, 70(13-15):2371–2378, 2007.

[27] KOTU, V.; DESHPANDE, B.. **Data science: concepts and practice**. Morgan Kaufmann, 2018.

[28] BRACAMONTE, L. F.; FONTAINE, R. G.. **Vehicle test facilities at aberdeen test center and yuma test center**. Technical report, US Army Aberdeen Test Center Aberdeen Proving Ground United States, 2017.

[29] SANDU, C.; ANDERSEN, E. R. ; SOUTHWARD, S.. **Multibody dynamics modelling and system identification of a quarter-car test rig**

with mcpherson strut suspension. Vehicle System Dynamics, 49(1-2):153–179, 2011.

[30] FALLAH, M.; BHAT, R. ; XIE, W.. **New model and simulation of macpherson suspension system for ride control applications**. Vehicle System Dynamics, 47(2):195–220, 2009.

[31] HUREL, J.; PERALTA, J.; AMAYA, J.; FLORES, B. ; FLORES, F.. **Determination of the equivalent parameters for modelling a mcpherson suspension with a quarter-car model**. In: 2017 IEEE 26th INTERNATIONAL SYMPOSIUM ON INDUSTRIAL ELECTRONICS, p. 454–459, Edinburgh, UK, 2017. IEEE.

[32] NIU, Z.; JIN, S.; WANG, R. ; ZHANG, Y.. **Geometry optimization of a planar double wishbone suspension based on whole-range nonlinear dynamic model**. Proceedings of the Institution of Mechanical Engineers, Part D: Journal of Automobile Engineering, 236(4):569–581, 2022.

[33] FERNANDES, J.; GONÇALVES, P. ; SILVEIRA, M.. **Interaction between asymmetrical damping and geometrical nonlinearity in vehicle suspension systems improves comfort**. Nonlinear Dynamics, 99(2):1561–1576, 2020.

[34] CHIANG, H.-H.; LEE, L.-W.. **Optimized virtual model reference control for ride and handling performance-oriented semiactive suspension systems**. IEEE Transactions on Vehicular Technology, 64(5):1679–1690, 2014.

[35] ZHOU, G.; KIM, H. S. ; CHOI, Y. J.. **A new method of identification of equivalent suspension and damping rates of full-vehicle model**. Vehicle System Dynamics, 57(11):1573–1600, 2018.

[36] KANCHWALA, H.. **Vehicle suspension model development using test track measurements**. Proceedings of the Institution of Mechanical Engineers, Part D: Journal of Automobile Engineering, 234(5):1442–1459, 2020.

[37] REITERER, F.; GAMPER, H.; THALLER, S.; SCHRANGL, P.; KOKAL, H. ; DEL RE, L.. **Fast parametrization of vehicle suspension models**. In: 2018 ANNUAL AMERICAN CONTROL CONFERENCE, p. 3263–3268, Milwaukee, WI, USA, 2018. IEEE.

[38] ATTIA, T.; VAMVOUDAKIS, K. G.; KOCHERSBERGER, K.; BIRD, J. ; FURUKAWA, T.. **Simultaneous dynamic system estimation and optimal control of vehicle active suspension**. Vehicle System Dynamics, 57(10):1467–1493, 2019.

[39] CUI, Y.; KURFESS, T. ; MESSMAN, M.. **A methodology to integrate a nonlinear shock absorber dynamics into a vehicle model for system identification**. SAE International Journal of Materials and Manufacturing, 4(1):527–534, 2011.

[40] THALLER, S.; REITERER, F.; SCHMIED, R.; WASCHL, H.; KOKAL, H. ; DEL RE, L.. **Fast determination of vehicle suspension parameters via continuous time system identification**. IFAC-PapersOnLine, 49(11):448–453, 2016.

[41] PEDRO, J. O.; NHLAPO, S. M. ; MPANZA, L. J.. **Model predictive control of half-car active suspension systems using particle swarm optimisation**. IFAC-PapersOnLine, 53(2):14438–14443, 2020.

[42] IMINE, H.; MADANI, T.. **Heavy vehicle suspension parameters identification and estimation of vertical forces: experimental results**. International Journal of Control, 88(2):324–334, 2015.

[43] HERNANDEZ-ALCANTARA, D.; MORALES-MENENDEZ, R.; AMEZQUITA-BROOKS, L.; SENAME, O. ; DUGARD, L.. **Fault estimation methods for semi-active suspension systems**. In: 2015 IEEE INTERNATIONAL AUTUMN MEETING ON POWER, ELECTRONICS AND COMPUTING, p. 1–5, Ixtapa, Mexico, 2015. IEEE.

[44] ANTONOV, S.; FEHN, A. ; KUGI, A.. **Unscented Kalman filter for vehicle state estimation**. Vehicle System Dynamics, 49(9):1497–1520, 2011.

[45] WENZEL, T. A.; BURNHAM, K.; BLUNDELL, M. ; WILLIAMS, R.. **Dual extended Kalman filter for vehicle state and parameter estimation**. Vehicle System Dynamics, 44(2):153–171, 2006.

[46] HONG, S.; LEE, C.; BORRELLI, F. ; HEDRICK, J. K.. **A novel approach for vehicle inertial parameter identification using a dual Kalman filter**. IEEE Transactions on Intelligent Transportation Systems, 16(1):151–161, 2014.

[47] LIU, Y.-J.; DOU, C.-H.; SHEN, F. ; SUN, Q.-Y.. **Vehicle state estimation based on unscented Kalman filtering and a genetic-particle**

swarm algorithm. Journal of The Institution of Engineers (India): Series C, 102(2):447–469, 2021.

[48] REINA, G.; MESSINA, A.. **Vehicle dynamics estimation via augmented extended Kalman filtering**. Measurement, 133:383–395, 2019.

[49] YAO, S.; XU, D.. **An application of a progressive neural network technique in the identification of suspension properties of tracked vehicles**. In: PROCEEDINGS OF THE 9^{th} INTERNATIONAL CONFERENCE ON NEURAL INFORMATION PROCESSING, volume 2, p. 542–546, Singapore, 2002. IEEE.

[50] WITTERS, M.; SWEVERS, J.. **Black-box model identification for a continuously variable, electro-hydraulic semi-active damper**. Mechanical Systems and Signal Processing, 24(1):4–18, 2010.

[51] LIU, Y.; CUI, D.. **Research on road roughness based on NARX neural network**. Mathematical Problems in Engineering, 2021:9173870, 2021.

[52] JIN, G.; SAIN, M. K.; PHAM, K. D.; BILLIE, F. ; RAMALLO, J.. **Modeling mr-dampers: a nonlinear blackbox approach**. In: PROCEEDINGS OF THE 2001 AMERICAN CONTROL CONFERENCE, volume 1, p. 429–434, Arlington, VA, USA, 2001. IEEE.

[53] WEI, S.; WANG, J. ; OU, J.. **Method for improving the neural network model of the magnetorheological damper**. Mechanical Systems and Signal Processing, 149:107316, 2021.

[54] DAI, L.; CHI, M.; XU, C.; GAO, H.; SUN, J.; WU, X. ; LIANG, S.. **A hybrid neural network model based modelling methodology for the rubber bushing**. Vehicle System Dynamics, p. 1–22, 2021.

[55] LIN, J.; LI, H.; HUANG, Y.; HUANG, Z. ; LUO, Z.. **Adaptive artificial neural network surrogate model of nonlinear hydraulic adjustable damper for automotive semi-active suspension system**. IEEE Access, 8:118673–118686, 2020.

[56] TJAHJOWIDODO, T.; AL-BENDER, F. ; VAN BRUSSEL, H.. **Quantifying chaotic responses of mechanical systems with backlash component**. Mechanical systems and signal processing, 21(2):973–993, 2007.

[57] DO, T.; TJAHJOWIDODO, T.; LAU, M. W. S. ; PHEE, S. J.. **An investigation of friction-based tendon sheath model appropriate for control purposes**. Mechanical Systems and Signal Processing, 42(1-2):97–114, 2014.

[58] TJAHJOWIDODO, T.; ZHU, K.; DAILEY, W.; BURDET, E. ; CAMPOLO, D.. **Multi-source micro-friction identification for a class of cable-driven robots with passive backbone**. Mechanical Systems and Signal Processing, 80:152–165, 2016.

[59] DO, T.; TJAHJOWIDODO, T.; LAU, M. ; PHEE, S.. **Nonlinear friction modelling and compensation control of hysteresis phenomena for a pair of tendon-sheath actuated surgical robots**. Mechanical Systems and Signal Processing, 60:770–784, 2015.

[60] YILDIRIM, M. C.; SENDUR, P.; KANSIZOGLU, A. T.; URAS, U.; BILGIN, O.; EMRE, S.; YAPICI, G. G.; ARIK, M. ; UGURLU, B.. **Design and development of a durable series elastic actuator with an optimized spring topology**. Proceedings of the Institution of Mechanical Engineers, Part C: Journal of Mechanical Engineering Science, 235(24):7848–7858, 2021.

[61] IRMSCHER, C.; WOSCHKE, E.; MAY, E. ; DANIEL, C.. **Design, optimisation and testing of a compact, inexpensive elastic element for series elastic actuators**. Medical engineering & physics, 52:84–89, 2018.

[62] LIU, H.; CUI, S.; LIU, Y.; REN, Y. ; SUN, Y.. **Design and vibration suppression control of a modular elastic joint**. Sensors, 18(6):1869, 2018.

[63] WANG, T.; ZHENG, T.; ZHAO, S.; SUI, D.; ZHAO, J. ; ZHU, Y.. **Design and control of a series–parallel elastic actuator for a weight-bearing exoskeleton robot**. Sensors, 22(3):1055, 2022.

[64] WANG, T.; ZHU, Y.; ZHENG, T.; SUI, D.; ZHAO, S. ; ZHAO, J.. **Palexo: A parallel actuated lower limb exoskeleton for high-load carrying**. IEEE Access, 8:67250–67262, 2020.

[65] JARRETT, C.; MCDAID, A.. **Modeling and feasibility of an elastomer-based series elastic actuator as a haptic interaction sensor for exoskeleton robotics**. IEEE/ASME Transactions on mechatronics, 24(3):1325–1333, 2019.

[66] CAO, P.; GAN, Y. ; DAI, X.. **Model-based sensorless robot collision detection under model uncertainties with a fast dynamics identification**. International Journal of Advanced Robotic Systems, 16(3):1729881419853713, 2019.

[67] BRIOT, S.; GAUTIER, M.. **Global identification of joint drive gains and dynamic parameters of parallel robots**. Multibody System Dynamics, 33(1):3–26, 2015.

[68] URREA, C.; PASCAL, J.. **Design and validation of a dynamic parameter identification model for industrial manipulator robots**. Archive of Applied Mechanics, 91(5):1981–2007, 2021.

[69] LIU, S.-P.; MA, Z.-Y.; CHEN, J.-L.; CAO, J.-F.; FU, Y. ; LI, S.-Q.. **An improved parameter identification method of redundant manipulator**. International Journal of Advanced Robotic Systems, 18(2):17298814211002118, 2021.

[70] VANTILT, J.; AERTBELIËN, E.; DE GROOTE, F. ; DE SCHUTTER, J.. **Optimal excitation and identification of the dynamic model of robotic systems with compliant actuators**. In: 2015 IEEE INTERNATIONAL CONFERENCE ON ROBOTICS AND AUTOMATION, p. 2117–2124, Seattle, WA, USA, 2015. IEEE.

[71] MADSEN, E.; ROSENLUND, O. S.; BRANDT, D. ; ZHANG, X.. **Model-based on-line estimation of time-varying nonlinear joint stiffness on an e-series universal robots manipulator**. In: 2019 INTERNATIONAL CONFERENCE ON ROBOTICS AND AUTOMATION, p. 8408–8414, Montreal, QC, Canada, 2019. IEEE.

[72] GAUTIER, M.; JANOT, A. ; VANDANJON, P.-O.. **A new closed-loop output error method for parameter identification of robot dynamics**. IEEE Transactions on Control Systems Technology, 21(2):428–444, 2012.

[73] JIA, J.; ZHANG, M.; LI, C.; GAO, C.; ZANG, X. ; ZHAO, J.. **Improved dynamic parameter identification method relying on proprioception for manipulators**. Nonlinear Dynamics, 105(2):1373–1388, 2021.

[74] SARIYILDIZ, E.; MUTLU, R. ; YU, H.. **A sliding mode force and position controller synthesis for series elastic actuators**. Robotica, 38(1):15–28, 2020.

[75] LEE, H.; OH, S.. **Design of reduced order disturbance observer of series elastic actuator for robust force control**. In: 2018 IEEE 15th INTERNATIONAL WORKSHOP ON ADVANCED MOTION CONTROL, p. 663–668, Tokyo, Japan, 2018. IEEE.

[76] HAN, S.; WANG, H. ; YU, H.. **Nonlinear disturbance observer-based robust motion control for multi-joint series elastic actuator-driven robots**. In: 2021 IEEE INTERNATIONAL CONFERENCE ON ROBOTICS AND AUTOMATION, p. 10469–10475, Xi'an, China, 2021. IEEE.

[77] DE SOUZA, D. A.; BATISTA, J. G.; VASCONCELOS, F. J.; DOS REIS, L. L.; MACHADO, G. F.; COSTA, J. R.; JUNIOR, J. N.; SILVA, J. L.; RIOS, C. S. ; JÚNIOR, A. B.. **Identification by recursive least squares with Kalman filter (RLS-KF) applied to a robotic manipulator**. IEEE Access, 9:63779–63789, 2021.

[78] NGUYEN, Q.-C.; VU, V.-H. ; THOMAS, M.. **A Kalman filter based ARX time series modeling for force identification on flexible manipulators**. Mechanical Systems and Signal Processing, 169:108743, 2022.

[79] MOAFI, S. A.; NAJAFI, F.. **Force control of an uncertain series elastic actuator system via a fuzzy sliding mode controller and a nonlinear state estimator**. Proceedings of the Institution of Mechanical Engineers, Part I: Journal of Systems and Control Engineering, 234(4):462–471, 2020.

[80] LEBOUTET, Q.; ROUX, J.; JANOT, A.; GUADARRAMA-OLVERA, J. R. ; CHENG, G.. **Inertial parameter identification in robotics: A survey**. Applied Sciences, 11(9):4303, 2021.

[81] BANKA, N.; PIASKOWY, W. T.; GARBINI, J. ; DEVASIA, S.. **Iterative machine learning for precision trajectory tracking with series elastic actuators**. In: 2018 IEEE 15th INTERNATIONAL WORKSHOP ON ADVANCED MOTION CONTROL, p. 234–239, Tokyo, Japan, 2018. IEEE.

[82] MUKHOPADHYAY, R.; CHAKI, R.; SUTRADHAR, A. ; CHATTOPADHYAY, P.. **Model learning for robotic manipulators using recurrent neural networks**. In: PREMIER INTERNATIONAL TECHNICAL CONFERENCE OF IEEE REGION 10, p. 2251–2256, Kochi, India, 2019. IEEE.

[83] ZHANG, Y.; LIU, H.; MA, T.; HAO, L. ; LI, Z.. **A comprehensive dynamic model for pneumatic artificial muscles considering different input frequencies and mechanical loads**. Mechanical Systems and Signal Processing, 148:107133, 2021.

[84] SHAO, N.; ZHOU, Q.; SHAO, C. ; ZHAO, Y.. **Adaptive control of robot series elastic drive joint based on optimized radial basis function neural network**. International Journal of Social Robotics, 13(7):1823–1832, 2021.

[85] WANG, Y.; CHEN, Z.; ZU, H. ; ZHANG, X.. **An optimized rbf neural network based on beetle antennae search algorithm for modeling the static friction in a robotic manipulator joint**. Mathematical Problems in Engineering, 2020, 2020.

[86] SEO, H.-T.; PARK, J.-I. ; PARK, J.. **A compact series elastic element using a rubber compression mechanism**. Review of Scientific Instruments, 92(6):065004, 2021.

[87] SUN, N.; CHENG, L. ; XIA, X.. **Design and hysteresis modeling of a miniaturized elastomer-based clutched torque sensor**. IEEE Transactions on Instrumentation and Measurement, 71:1–9, 2022.

[88] KIM, D.-H.; OH, J.-H.. **Hysteresis modeling for torque control of an elastomer series elastic actuator**. IEEE/ASME Transactions on Mechatronics, 24(3):1316–1324, 2019.

[89] AUSTIN, J.; SCHEPELMANN, A. ; GEYER, H.. **Control and evaluation of series elastic actuators with nonlinear rubber springs**. In: 2015 IEEE/RSJ INTERNATIONAL CONFERENCE ON INTELLIGENT ROBOTS AND SYSTEMS, p. 6563–6568, Hamburg, Germany, 2015. IEEE.

[90] WEI, H.; XIANG, K.; CHEN, H.; TANG, B. ; PANG, M.. **Improvement of torque estimation for series viscoelastic actuator based on dual extended Kalman filter**. Actuators, 10(10):258, 2021.

[91] KARNIADAKIS, G. E.; KEVREKIDIS, I. G.; LU, L.; PERDIKARIS, P.; WANG, S. ; YANG, L.. **Physics-informed machine learning**. Nature Reviews Physics, 3(6):422–440, 2021.

[92] BOCK, H. G.; PLITT, K.-J.. **A multiple shooting algorithm for direct solution of optimal control problems**. IFAC Proceedings Volumes, 17(2):1603–1608, 1984.

[93] RAWLINGS, J. B.; MAYNE, D. Q. ; DIEHL, M.. **Model predictive control: theory, computation, and design**. Nob Hill Publishing Madison, WI, Santa Barbara, California, 2 edition, 2017.

[94] ANDERSSON, J. A. E.; GILLIS, J.; HORN, G.; RAWLINGS, J. B. ; DIEHL, M.. **CasADi – A software framework for nonlinear optimization and optimal control**. Mathematical Programming Computation, 11(1):1–36, 2019.

[95] ANDERSSON, J. A.; GILLIS, J.; HORN, G.; RAWLINGS, J. B. ; DIEHL, M.. **Casadi: a software framework for nonlinear optimization and optimal control**. Mathematical Programming Computation, 11(1):1–36, 2019.

[96] GRÜNE, L.; PANNEK, J.. **Nonlinear model predictive control**. In: NONLINEAR MODEL PREDICTIVE CONTROL, p. 45–69. Springer, Cham, 2017.

[97] RETZLER, A.; SWEVERS, J.; GILLIS, J. ; KOLLÁR, Z.. **Shooting methods for identification of nonlinear state-space grey-box models**. In: 2022 IEEE 17^{th} INTERNATIONAL CONFERENCE ON ADVANCED MOTION CONTROL, p. 207–212, Padova, Italy, 2022. IEEE.

[98] IZMAILOV, A.; SOLODOV, M.. **Otimização, volume 1: condições de otimalidade, elementos de análise convexa e de dualidade**. IMPA, Brazil, 2005.

[99] NOCEDAL, J.; WRIGHT, S. J.. **Numerical optimization**. Springer, New York, NY, 2006.

[100] UGALDE, H. M. R.; CARMONA, J.-C.; ALVARADO, V. M. ; REYES-REYES, J.. **Neural network design and model reduction approach for black box nonlinear system identification with reduced number of parameters**. Neurocomputing, 101:170–180, 2013.

[101] MORALES, E. F.; MURRIETA-CID, R.; BECERRA, I. ; ESQUIVEL-BASALDUA, M. A.. **A survey on deep learning and deep reinforcement learning in robotics with a tutorial on deep reinforcement learning**. Intelligent Service Robotics, 14(5):773–805, 2021.

[102] KINGMA, D. P.; BA, J.. **Adam: A method for stochastic optimization**. In: 3^{rd} INTERNATIONAL CONFERENCE ON LEARNING REPRESENTATIONS, San Diego, CA, USA, 5 2015.

[103] CLEVERT, D.-A.; UNTERTHINER, T. ; HOCHREITER, S.. **Fast and accurate deep network learning by exponential linear units (ELUs)**. In: 4^{th} INTERNATIONAL CONFERENCE ON LEARNING REPRESENTATIONS, San Juan, Puerto Rico, 2016.

[104] ABADI, M.; BARHAM, P.; CHEN, J.; CHEN, Z.; DAVIS, A.; DEAN, J.; DEVIN, M.; GHEMAWAT, S.; IRVING, G.; ISARD, M. ; OTHERS. **Tensorflow: a system for large-scale machine learning.** In: 12^{th} USENIX SYMPOSIUM ON OPERATING SYSTEMS DESIGN AND IMPLEMENTATION, volume 16, p. 265–283, Savannah, GA, USA, 2016. USENIX.

[105] DE OLIVEIRA, P. D.; BRAGA, A. P. D. S.; DOS REIS, L. L.; NOGUEIRA, F. G. ; JÚNIOR, A. B. D. S.. **System identification through rbf neural networks: Improving accuracy by a numerical approximation method for the centroids and widths adjustment**. In: XIII BRAZILIAN CONGRESS ON COMPUTATIONAL INTELLIGENCE, Rio de Janeiro, Brazil, 2017.

[106] GHOSH, J.; NAG, A.. **An Overview of Radial Basis Function Networks**, p. 1–36. Physica-Verlag HD, Heidelberg, 2001.

[107] SCHAIBLE, B.; XIE, H. ; LEE, Y.-C.. **Fuzzy logic models for ranking process effects**. IEEE Transactions on Fuzzy Systems, 5(4):545–556, 1997.

[108] ALLEN, R. W.; ROSENTHAL, T. J.. **Requirements for vehicle dynamics simulation models**. Technical report, SAE Technical Paper, 1994.

[109] PINTELON, R.; SCHOUKENS, J.. **System identification: a frequency domain approach**. John Wiley & Sons, Hoboken, NJ, USA, 2012.

[110] JAZAR, R. N.. **Vehicle Dynamics Theory and Applications**. Springer, New York, NY, USA, 2nd edition edition, 2013.

[111] ZHOU, M.; WANG, S.. **A method to determine the topology of custom torsional elastic element for the lightweight rotary series elastic actuator**. Journal of Physics: Conference Series, 1939:012080, 2021.

[112] SUN, L.; LI, M.; WANG, M.; YIN, W.; SUN, N. ; LIU, J.. **Continuous finite-time output torque control approach for series elastic actuator**. Mechanical Systems and Signal Processing, 139:105853, 2020.

[113] LOPES, F.; MEGGIOLARO, M.. **Design of a low-cost series elastic actuator for application in robotic manipulators.** In: 26^{th} INTERNATIONAL CONGRESS OF MECHANICAL ENGINEERING, Online, 11 2021. ABCM.

[114] LOPES, F. R.. **Desenvolvimento e controle de um acoplador elástico baseado em elastômeros para SEA.** PhD thesis, Pontifícia Universidade Católica do Rio de Janeiro, 2022.

[115] MARQUES, F.; FLORES, P.; PIMENTA CLARO, J. ; LANKARANI, H. M.. **A survey and comparison of several friction force models for dynamic analysis of multibody mechanical systems.** Nonlinear Dynamics, 86(3):1407–1443, 2016.

[116] DAHL, P. R.. **A solid friction model.** Technical report, Aerospace Corporation, El Segundo-CA, 1968.

[117] DE WIT, C. C.; OLSSON, H.; ASTROM, K. J. ; LISCHINSKY, P.. **A new model for control of systems with friction.** IEEE Transactions on automatic control, 40(3):419–425, 1995.

[118] LIU, D.-P.. **Parameter identification for lugre friction model using genetic algorithms.** In: 2006 INTERNATIONAL CONFERENCE ON MACHINE LEARNING AND CYBERNETICS, p. 3419–3422, Dalian, China, 2006. IEEE.

[119] NARENDRA, K.; PARTHASARATHY, K.. **Identification and control of dynamical systems using neural networks.** IEEE Transactions on neural networks, 1:4–27, 1990.

[120] KUHN, M.; JOHNSON, K. ; OTHERS. **Applied predictive modeling,** volume 26. Springer, New York, NY, 2013.

[121] STERKENBURG, T. F.; GRÜNWALD, P. D.. **The no-free-lunch theorems of supervised learning.** Synthese, 199(3):9979–10015, 2021.

[122] PIRES, I.; AYALA, H. V. H. ; WEBER, H. I.. **Nonlinear ensemble gray and black-box system identification of friction induced vibrations in slender rotating structures.** Mechanical Systems and Signal Processing, 186:109815, 2023.

[123] ZHANG, R.; TAO, J.. **A nonlinear fuzzy neural network modeling approach using an improved genetic algorithm.** IEEE Transactions on Industrial Electronics, 65(7):5882–5892, 2017.

[124] GEVERS, M.. **A personal view of the development of system identification: A 30-year journey through an exciting field.** IEEE Control Systems Magazine, 26(6):93–105, 2006.

[125] JANOT, A.; GAUTIER, M. ; BRUNOT, M.. **Data set and reference models of emps.** In: NONLINEAR SYSTEM IDENTIFICATION BENCHMARKS, Eindhoven, Netherlands, 2019.

[126] PINTO, W. C. F.; AYALA, H. V. H.. **Ensemble grey and black-box nonlinear system identification of a positioning system.** In: CONGRESSO BRASILEIRO DE AUTOMÁTICA, volume 2, Online, 2020. Sociedade Brasileira de Automática.

[127] FUENTES, R.; NAYEK, R.; GARDNER, P.; DERVILIS, N.; ROGERS, T.; WORDEN, K. ; CROSS, E.. **Equation discovery for nonlinear dynamical systems: A bayesian viewpoint.** Mechanical Systems and Signal Processing, 154:107528, 2021.

[128] WEIGAND, J.; DEFLORIAN, M. ; RUSKOWSKI, M.. **Input-to-state stability for system identification with continuous-time runge–kutta neural networks.** International Journal of Control, 96(1):24–40, 2021.

[129] SUN, J.; HUANG, Y.; YU, W. ; GARCIA-ORTIZ, A.. **Nonlinear system identification: Prediction error method vs neural network.** In: 2021 10^{th} INTERNATIONAL CONFERENCE ON MODERN CIRCUITS AND SYSTEMS TECHNOLOGIES, p. 1–4, Thessaloniki, Greece, 2021. IEEE.

[130] PENNESTRI, E.; ROSSI, V.; SALVINI, P. ; VALENTINI, P. P.. **Review and comparison of dry friction force models.** Nonlinear Dynamics, 83(4):1785 – 1801, 2016.

[131] PEREIRA, C. L.; SOUSA, D. H. B. ; AYALA, H. V. H.. **Three-axle vehicle lateral dynamics identification using double lane change maneuvers data.** In: 2021 29^{th} MEDITERRANEAN CONFERENCE ON CONTROL AND AUTOMATION, p. 910–915, Puglia, Italy, 2021. IEEE.

[132] WORDEN, K.; BARTHORPE, R.; CROSS, E.; DERVILIS, N.; HOLMES, G.; MANSON, G. ; ROGERS, T.. **On evolutionary system identification with applications to nonlinear benchmarks.** Mechanical Systems and Signal Processing, 112:194–232, 2018.